



A STUDY OF SOLAR NEAR INFRARED GLOBAL AND DIFFUSE RADIATION
IN THAILAND FROM GROUND AND SATELLITE-BASED DATA



A Thesis Submitted in Partial Fulfillment of the Requirements
for Doctor of Philosophy (PHYSICS)
Department of PHYSICS
Graduate School, Silpakorn University
Academic Year 2018
Copyright of Graduate School, Silpakorn University

การศึกษารังสีรวมและรังสีกระจายของรังสีอินฟราเรดจากดวงอาทิตย์ในประเทศไทย
จากข้อมูลภาคพื้นดินและข้อมูลดาวเทียม



วิทยานิพนธ์นี้เป็นส่วนหนึ่งของการศึกษาตามหลักสูตรปรัชญาดุษฎีบัณฑิต
สาขาวิชาฟิสิกส์ แบบ 1.1 ปรัชญาดุษฎีบัณฑิต
ภาควิชาฟิสิกส์
บัณฑิตวิทยาลัย มหาวิทยาลัยศิลปากร
ปีการศึกษา 2561
ลิขสิทธิ์ของบัณฑิตวิทยาลัย มหาวิทยาลัยศิลปากร

A STUDY OF SOLAR NEAR INFRARED GLOBAL AND DIFFUSE
RADIATION IN THAILAND FROM GROUND AND SATELLITE-
BASED DATA



A Thesis Submitted in Partial Fulfillment of the Requirements
for Doctor of Philosophy (PHYSICS)
Department of PHYSICS
Graduate School, Silpakorn University
Academic Year 2018
Copyright of Graduate School, Silpakorn University

Title A study of solar near infrared global and diffuse radiation in Thailand from ground and satellite-based data
By Warangkana THONGRASMEE
Field of Study (PHYSICS)
Advisor Serm Janjai

Graduate School Silpakorn University in Partial Fulfillment of the Requirements for the Doctor of Philosophy

..... Dean of graduate school
(Associate Professor Jurairat Nunthanid, Ph.D.)

Approved by

..... Chair person
(Assistant Professor Itsara Masiri , Ph.D.)

..... Advisor
(Professor Serm Janjai , Ph.D.)

..... External Examiner
(Associate Professor Sirichai Thepa , Ph.D.)



59306802 : Major (PHYSICS)

Keyword : solar near infrared radiation, satellite data, diffuse radiation, global radiation

MISS WARANGKANA THONGRASMEE : A STUDY OF SOLAR NEAR INFRARED GLOBAL AND DIFFUSE RADIATION IN THAILAND FROM GROUND AND SATELLITE-BASED DATA THESIS ADVISOR : PROFESSOR SERM JANJAI, Ph.D.

In this work, global and diffuse solar near infrared radiation (SNIR) were measured at four stations in Thailand namely, the Meteorological Center in Chiang Mai (18.78°N, 98.98°E), the Meteorological Center in Ubon Ratchathani (15.25°N, 104.87°E), Silpakorn University in Nakhon Pathom (13.82°N 100.04°E) and the Meteorological Center in Songkhla (7.2°N, 100.6°E). A semi-empirical model for estimating monthly average hourly diffuse solar near infrared radiation in Thailand using ground- and satellite-based data was developed. Cloud, precipitable water and cosine of solar zenith angle were related to diffuse SNIR in form of an exponential function. The model was validated against independent diffuse SNIR measurements. The result showed that diffuse SNIR radiation from the model and that from the measurements were in reasonable agreement with root mean square difference (RMSD) and mean bias difference (MBD) of 16.7% and 1.5%, respectively. This model was employed to estimate the monthly average hourly diffuse SNIR over Thailand and presented as maps showing the geographical distribution of diffuse SNIR. For global SNIR, a technique for mapping hourly global SNIR was developed using MTSAT-1R satellite data. A simple radiative balance model is used to relate an atmospheric reflectance as seen by the satellite to an equivalent reflectance obtained from pyranometer measurements in the SNIR band. The tuned and calibrated atmospheric reflectance from satellite data is then used to estimate surface SNIR irradiance and the results are shown as SNIR maps. Statistics for monthly average of hourly SNIR irradiance are presented for Thailand using five years (2009-2013) of satellite data. In order to utilize more widely measured solar broadband radiation (BR) for estimating SNIR, hourly, daily, and monthly average daily model of SNIR-to-BR ratio were proposed. The models are expressed as functions of precipitable water (w), aerosol optical depth (AOD) ozone(O_3) and cloud index (n). Results from these models validation revealed that global SNIR calculated from the models and that from the measurements were in good agreement. Finally, measured global and diffuse SNIR data from four sites were analyzed. Diurnal and seasonal variations of global and diffuse SNIR were examined. Monthly averages of SNIR at these sites are relatively high over year.

ACKNOWLEDGEMENTS

This thesis is submitted in partial fulfillment for the degree of Doctor of Philosophy (Physics), Graduate school, Silpakorn University.

I would like to express my deep gratitude to Professor Dr.Serm Jaijan, my academic advisor, for their patient helpful guidance, enthusiastic encouragement and useful critiques of this research work.

Besides my advisor, I would like to thank the rest of my thesis committee: Asst. Prof. Dr. Itsara Masiri and Assoc. Prof. Dr.Sirichai Thepa for their insightful comments.

I am also grateful to Solar Laboratory of Silpakorn University for funding my Ph.D. research.

My research would have been impossible without the help and support of all teachers and researchers of Solar Laboratory of Silpakorn University, especially Asst. Prof. Dr. Korntip Tohsing.

Finally, I wish to thank my family and friends for their support and encouragement throughout my life.

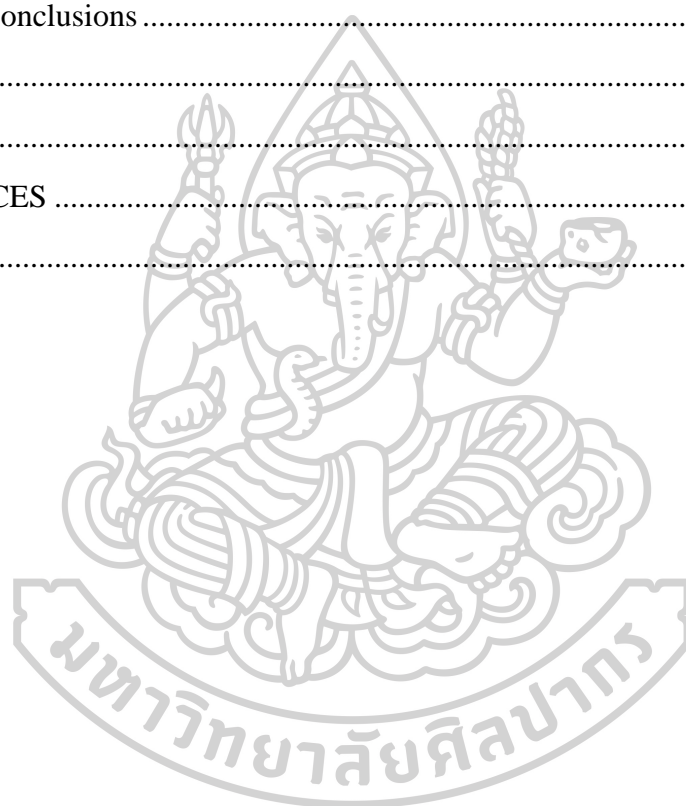
Warangkana THONGRASMEE



TABLE OF CONTENTS

	Page
ABSTRACT.....	D
ACKNOWLEDGEMENTS.....	E
TABLE OF CONTENTS.....	F
LIST OF TABLES.....	H
LIST OF FIGURES.....	I
Chapter 1 Introduction.....	1
1.1 Rationale of this work.....	1
1.2 Objectives.....	2
1.3 Organization of the thesis.....	2
Chapter 2 A semi-empirical model for estimating diffuse solar near infrared radiation in Thailand.....	3
2.1 Introduction.....	3
2.2 Data and Instruments.....	3
2.3 Results and discussion.....	6
2.4 Conclusions.....	18
Chapter 3 A technique for mapping hourly global solar near infrared radiation from satellite data.....	19
3.1 Introduction.....	19
3.2 Methodology.....	19
3.3. Results.....	27
3.4 Conclusions.....	32
Chapter 4 The ratio of solar near infrared radiation to broadband global solar radiation	33
4.1 Introduction.....	33
4.2 Measurements and data.....	33
4.3 Results and discussions.....	35

4.4 Conclusions.....	42
Chapter 5 The statistical characteristics of solar near infrared radiation in Thailand .	43
5.1 Introduction.....	43
5.2 Diurnal variation.....	43
5.2 Seasonal variation.....	53
5.3 Distributions of hourly solar near infrared radiation	59
5.4 Distributions of daily solar near infrared radiation.....	71
Chapter 6 Conclusions	83
Appendix 1.....	85
Appendix 2.....	86
REFERENCES	88
VITA.....	92



LIST OF TABLES

	Page
Table 1 Period of the data at the four stations for model validation.....	6
Table 2 Result of statistics for non-linear regression $I_{dSNIR} = a_0 \exp(a_1 \rho'_{EA})$	8
Table 3 The coefficient values of Eq. (2.2) from a non-linear regression method	10
Table 4 Instrument details and data acquired in the study.	20
Table 5 Values of coefficients of Eq. (4.2) and the corresponding t-statistic.....	36
Table 6 Comparison between hourly SNIR ratio from measurement and those from hourly SNIR ratio model.....	38
Table 7 Values of coefficients of Eq. (4.3) and the corresponding t-statistic.....	38
Table 8 Comparison between daily SNIR ratio from measurement and those from daily SNIR ratio model	40
Table 9 Values of coefficients of eq. (4.4) and the corresponding t-statistic.	41



LIST OF FIGURES

	Page
Fig. 1 Installations feature of SNIR instruments at the four sites in Thailand.....	4
Fig. 2 An example of a rectified image over Thailand	5
Fig. 3 Relationship between diffuse SNIR (I_{dSNIR}) and satellite-derived earth-atmospheric reflectivity (ρ'_{EA}) for the interval solar zenith angle (θ_z). The data used for this analysis are from the first group.....	7
Fig. 4 Relationship between diffuse SNIR (I_{dSNIR}) and cosine of solar zenith angle ($\cos(\theta_z)$).....	9
Fig. 5 Relationship between diffuse SNIR (I_{dSNIR}) and precipitable water (w)	9
Fig. 6 Comparison between monthly average hourly diffuse SNIR from measurement ($I_{dSNIR,meas}$) and those from the semi-empirical model ($I_{dSNIR,mod}$) at Nakhon Pathom (NP), Chiang Mai (CM), Ubon Ratchathani (UB) and Songkhla (SK).....	11
Fig. 7 Geographical distribution maps of long-term monthly average hourly diffuse SNIR irradiance over Thailand during January to June (2006-2016).....	13
Fig. 8 Geographical distribution maps of long-term monthly average hourly diffuse SNIR irradiance over Thailand during July to December (2006-2016)	14
Fig. 9 Monthly average daily diffuse SNIR variations at four stations in Thailand....	16
Fig. 10 Geographical distribution maps of long-term monthly average daily diffuse SNIR over Thailand.	17
Fig. 11 Position of SNIR measurements and pictorial view of SNIR pyranometers. A, B, C and D indicate the northern, northeastern, central and the southern regions, respectively.	20
Fig. 12 Procedure for mapping SNIR from satellite data. a) Development of the relation between atmospheric reflectivity in satellite band (ρ'_A) and SNIR band (ρ_{SNIR}). b) The calculation process of surface SNIR covering the entire country.....	23
Fig. 13 Earth-atmosphere reflected solar radiation as detected by a satellite sensor. Greek symbols ρ and α represent scattering and absorption respectively while subscripts A and G refer to the atmosphere and ground, respectively. Primes refer to the satellite band. The first reflection represents radiation reflected from the	

atmosphere (ρ'_A), while the second represents radiation escaping to space after one reflection by the surface $((1-\rho'_A)^2(1-\alpha'_A)^2\rho'_G)$. All data is normalized to an incoming solar irradiance of 1.	24
Fig. 14 Relationship between monthly average ρ'_A from the satellite estimates and ρ_{SNIR} obtained from the ground-based measurement at the four stations.....	27
Fig. 15 Comparison between hourly average SNIR obtained from the measurement ($I_{SNIR,meas}$) and that calculated from the model ($I_{SNIR,model}$).	28
Fig. 16 The monthly average hourly SNIR maps for all months at 9:30 h.....	29
Fig. 17 The monthly average hourly SNIR maps for all months at 12:30 h.....	30
Fig. 18 The monthly average hourly SNIR maps for all months at 15:30 h.....	31
Fig. 19 Installations feature of instruments at 4 sites in Thailand. (a) pyranometer measuring BR, (b) pyranometer measuring SNIR and (c) Sunphotometer.	34
Fig. 20 Example of a satellite image and the position of the pixels selected for calculating cloud index.	35
Fig. 21 Comparison between hourly SNIR from the model and that from the measurement.	37
Fig. 22 Comparison between daily SNIR from the model and that from the measurement.	39
Fig. 23 Comparison between monthly average daily SNIR from the model and that from the measurement.....	41
Fig. 24 The variation of monthly average hourly global solar near infrared radiation under all sky condition at Chiang Mai station. [error bar ± 1 standard deviation, SD] 44	44
Fig. 25 The variation of monthly average hourly global solar near infrared radiation under all sky condition at Ubon Ratchathani station. [error bar ± 1 standard deviation, SD]	45
Fig. 26 The variation of monthly average hourly global solar near infrared radiation under all sky condition at Nakhon Pathom station. [error bar ± 1 standard deviation, SD]	46
Fig. 27 The variation of monthly average hourly global solar near infrared radiation under all sky condition at Songkhla station. [error bar ± 1 standard deviation, SD]....	47
Fig. 28 The variation of monthly average hourly diffuse solar near infrared radiation under all sky condition at Chiang Mai station. [error bar ± 1 standard deviation, SD] 49	49

Fig. 29 The variation of monthly average hourly diffuse solar near infrared radiation under all sky condition at Ubon Ratchathani station. [error bar ± 1 standard deviation, SD]	50
Fig. 30 The variation of monthly average hourly diffuse solar near infrared radiation under all sky condition at Nakhon Pathom station. [error bar ± 1 standard deviation, SD]	51
Fig. 31 The variation of monthly average hourly diffuse solar near infrared radiation under all sky condition at Songkhla station. [error bar ± 1 standard deviation, SD]....	52
Fig. 32 Variation of global SNIR (\bar{H}_{SNIR}) during the year at Chiang Mai station.....	54
Fig. 33 Variation of global SNIR (\bar{H}_{SNIR}) during the year at Ubon Ratchathani station.....	54
Fig. 34 Variation of global SNIR (\bar{H}_{SNIR}) during the year at Nakhon Pathom station.	55
Fig. 35 Variation of global SNIR (\bar{H}_{SNIR}) during the year at Songkhla station.....	55
Fig. 36 Variation of diffuse SNIR (\bar{H}_{dSNIR}) during the year at Chiang Mai station....	57
Fig. 37 Variation of diffuse SNIR (\bar{H}_{dSNIR}) during the year at Ubon Ratchathani station.....	57
Fig. 38 Variation of diffuse SNIR (\bar{H}_{dSNIR}) during the year at Nakhom Pathom station.....	58
Fig. 39 Variation of diffuse SNIR (\bar{H}_{dSNIR}) during the year at Songkhla station.....	58
Fig. 40 The statistical distributions of hourly global SNIR for each month at Chiang Mai station.	60
Fig. 41 The statistical distributions of hourly global SNIR for each month at Ubon Rathethani station.....	61
Fig. 42 The statistical distributions of hourly global SNIR for each month at Nakhon Pathom station.....	62
Fig. 43 The statistical distributions of hourly global SNIR for each month at Songkhla station.....	63
Fig. 44 The statistical distributions of hourly global SNIR for all month at Chiang Mai, Ubon Ratchathani, Nakhon Pathom and Songkhla station.....	64
Fig. 45 The statistical distribution of hourly diffuse SNIR for each month at Chiang Mai station.	66

Fig. 46 The statistical distribution of hourly diffuse SNIR for each month at Ubon Rathethani station.....	67
Fig. 47 The statistical distribution of hourly diffuse SNIR for each month at Nakhon Pathom station.....	68
Fig. 48 The statistical distribution of hourly diffuse SNIR for each month at Songkhla station.....	69
Fig. 49 The statistical distributions of hourly diffuse SNIR for all month at Chiang Mai, Ubon Ratchathani, Nakhon Pathom and Songkhla station.....	70
Fig. 50 The statistical distributions of daily global SNIR for each month at Chiang Mai station.	72
Fig. 51 The statistical distributions of daily global SNIR for each month at Ubon Rathethani station.....	73
Fig. 52 The statistical distributions of daily global SNIR for each month at Nakhon Pathom station.....	74
Fig. 53 The statistical distributions of daily global SNIR for each month at Songkhla station.....	75
Fig. 54 The statistical distributions of daily global SNIR for all month at Chiang Mai, Ubon Ratchathani, Nakhon Pathom and Songkhla station.	76
Fig. 55 The statistical distribution of daily diffuse SNIR for each month at Chiang Mai station.	78
Fig. 56 The statistical distribution of daily diffuse SNIR for each month at Ubon Ratchathani station.....	79
Fig. 57 The statistical distribution of daily diffuse SNIR for each month at Nakhon Pathom station.....	80
Fig. 58 The statistical distribution of daily diffuse SNIR for each month at Songkhla station.....	81
Fig. 59 The statistical distributions of daily diffuse SNIR for all month at Chiang Mai, Ubon Ratchathani, Nakhon Pathom and Songkhla station.	82

Chapter 1

Introduction

1.1 Rationale of this work

Broadband solar radiation or BR (0.3 - 3.0 μm) at the earth's surface consists of ultraviolet radiation (0.29-0.40 μm), visible (0.4-0.7 μm) and near infrared radiation (0.7-3.0 μm). Solar near infrared radiation (SNIR) contributes about 52% of total energy from the sun (Petty, 2006) and it affects temperature of the earth's atmosphere and surface. Thus, SNIR is important to solar energy applications and climate change studies. The studies on the amount of water vapor in the atmosphere and physical properties of clouds are usually required SNIR information.

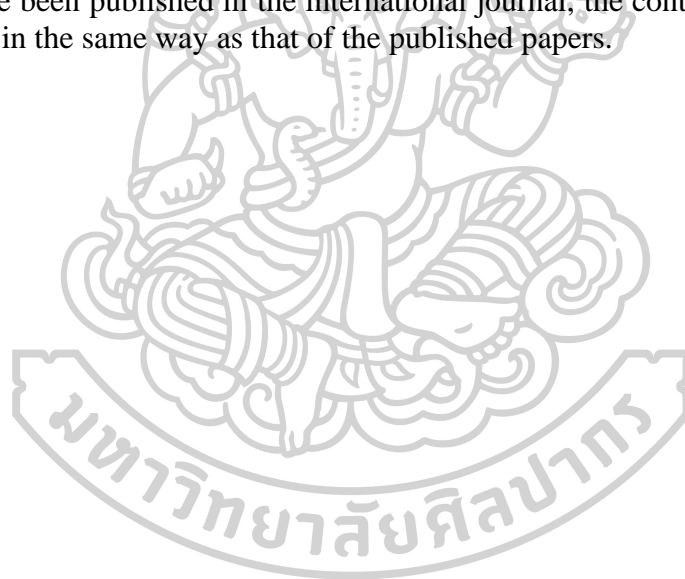
Generally, the amount of SNIR incident on the earth's surface should be obtained from the measurements. Gate et al.(1958) successfully measured SNIR for the first time in Mexico. However, measured SNIR data is too sparse, as compared to other parts of the solar spectrum. An alternative to obtain SNIR data is to use modeling approach. In the past decade, some researchers have proposed models for estimating SNIR. For example, Escobedo et al.(2009) developed models to estimate SNIR from BR under various sky conditions using ground-based measurements at Botucatu in Brazil. Additionally, they also carried out the statistical analysis of hourly and daily SNIR at this site in a later study (Escobedo et al., 2011) . Recently, Rossi et al. (2018) was proposed linear regression equation for estimating daily global, diffuse and direct SNIR as function of daily global diffuse and direct BR, respectively by considering the seasonal and cloudy effect. Most of previous models expressed the ratio of SNIR-to-BR as constant values, making their applications being limited. In addition, these models are mostly developed from measurement data in different climate from Thailand. In this work, global and diffuse SNIR were measured in main regions of Thailand namely, Chiang Mai Ubon Rathcathani, Nakhon Pathom and Songkhla in order to develop global and diffuse SNIR models. Firstly, the semi-empirical model for calculating diffuse SNIR was developed using ground and satellite-based data as input. Additionally, we considered radiative transfer model to determine physical model for mapping global SNIR. To investigate the spatial distribution of global and diffuse SNIR covered Thailand regions, diffuse and global SNIR were calculated over Thailand using the developed models. We also proposed ratio model of SNIR-to-BR for estimating SNIR in Thailand as function of corresponding atmospheric parameters namely, cloud index, total ozone column, precipitable water and aerosol optical depth. Finally, we studied the statistical characteristics of global and diffuse SNIR by analyzing diurnal variation, seasonal variation and distribution from measured data at the four stations in Thailand.

1.2 Objectives

- 1) To study the distribution of diffuse SNIR in Thailand.
- 2) To investigate the distribution of global SNIR in Thailand.
- 3) To develop the ratio of SNIR-to-BR models.
- 4) To analyze the statistical characteristics of diffuse and global SNIR in Thailand.

1.3 Organization of the thesis

This thesis composes of 6 chapters. Chapter 1 presents the rationale of the work and its objectives. Chapter 2 explains a method for developing a semi-empirical model for estimating diffuse SNIR in Thailand. Chapter 3 describes a technique for mapping global SNIR from satellite imagery data. Chapter 4 presents the ratio of solar near infrared radiation to broadband global solar radiation. Chapter 5 presents the statistical characteristics of measured diffuse and global SNIR data in Thailand. Finally, Chapter 6 is the conclusion. The related modelling work is presented in Appendix. As chapter 2 and 3 have been published in the international journal, the content of these chapters was written in the same way as that of the published papers.



Chapter 2

A semi-empirical model for estimating diffuse solar near infrared radiation in Thailand

2.1 Introduction

The solar near infrared radiation (SNIR) that reaches the earth's surface is partitioned into direct and diffuse radiation, with their sum denotes as global SNIR. The amount of the radiation depends on latitude, longitude, geographic, local climatology as well as cloud, aerosol, water vapor, ozone and gases. The atmospheric parameters have different effects on the components of the radiation. Cloud and aerosol are main parameters which can increase visible and near infrared radiation while decrease visible. Moreover, precipitable water is also an important absorption parameter in the near infrared band (Iqbal, 1983).

In the past, there have been few studies that examined the SNIR part of the solar spectrum. Weiss and Norman (1985) used direct and diffuse data in the visible and broadband region from ground-based measurements to derive the fraction of direct to global radiation in the visible and SNIR regions of the solar spectrum. Escobedo et al., (2009) developed models to estimate hourly and daily SNIR irradiance from broadband radiation under various sky conditions. They showed that hourly and daily SNIR irradiance were linear functions of broadband radiation for various cloud conditions. They developed the model further in a later study (Escobedo et al., 2011) which estimated seasonal variability of SNIR irradiance in Botucatu, Brazil.

As may be noted in the above paragraph, SNIR radiation and particularly diffuse SNIR radiation has not been studied in detail in most regions of the world. Therefore, the objectives of this study are to develop a semi-empirical model for calculating diffuse solar near infrared radiation for Thailand and to map this component of solar infrared radiation over this country.

2.2 Data and Instruments

2.2.1 Diffuse near infrared measurement

A precision spectral pyranometer (Eppley, model PSP) with an RG695 filter was used to measure diffuse near infrared radiation in a spectral band covering the region 0.695-2.80 μm . The instrument was installed on a sun tracker (Kipp&Zonen, model 2AP) attached with a shaded ball and therefore providing obstruction from the sun at all times. Uncertainty in the measurement of the radiometer is approximately 9 $\mu\text{V}/\text{W}\cdot\text{m}^{-2}$, temperature dependence is 1% in the range -20°C to $+40^{\circ}\text{C}$ and the cosine response is about 1% for 0 to 70 degrees from zenith and 3% from 70 to 80 degrees. Voltage signals from the pyranometer were recorded every second using a Yokogawa data logger, model DX2000. All voltages were converted to diffuse near infrared irradiance using the calibration sensitivity of the pyranometer. Then the data were averaged to hourly data.

The instrument was installed at four sites in Thailand during different periods covering various environments and climatic regimes. The first deployment was in the

* This chapter has been published in Journal of Renewable energy, Volume 117, 175-183, 2018.

center of the country at Silpakorn University, Nakhon Pathom (13.82°N, 100.04°E) from May, 2012 to January, 2014. The second deployment was in the northeast, in Ubon Ratchathani (15.25°N, 104.87°E) from February, 2014 to February, 2015. The third deployment was in the north, in Chiang Mai (18.78°N, 98.98°E) from March, 2015 to February, 2016 and the fourth site deployment was in the south, in Songkhla (7.20°N, 100.60°E) from May to November, 2016. The locations and instruments at all sites are shown in Fig. 1.

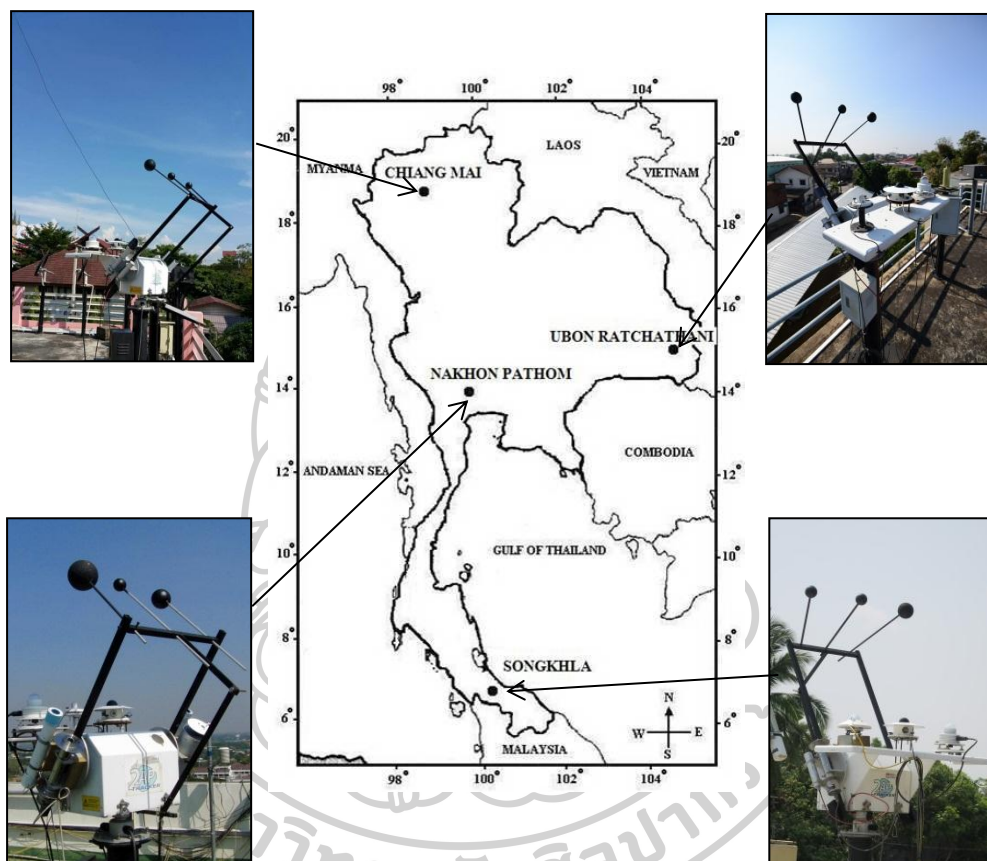


Fig. 1 Installations feature of SNIR instruments at the four sites in Thailand

2.2.2 Satellite data

Geostationary satellite data offers distinct advantages in mapping regional cloud cover as it scans the areas of interest in a timely and regular fashion with a single sensor, therefore avoiding errors arising from use of multiple cloud-observing platforms (Liu et al., 2012). In this study, hourly data from the Multifunctional Transport Satellite (Himawari-6) and Himawari-8 in the visible channel were used. The data from Himawari-6 encompassing 2006-2015 and the data from Himawari-8 covering 2016 were also employed in this work. Raw images from both satellites were transformed into a cylindrical projection and navigated. The navigation process is as follows.

In the first step, the satellite data were displayed as image using an Interactive Data Language (IDL) computer program. In the second step, a digital map of Thailand was overlaid on each image and this map was adjusted to fit the image using the coastline and islands as references. The fitting was carried out using the IDL program.

Finally, the fitted image was sectorized to obtain the navigated image covering Thailand (Fig. 2).

Each navigated image consists of the matrix of 550 pixels×850 pixels and each pixel contains the information in terms of digital gray levels varying between 0-255. This digital gray level was further converted to pseudo-reflectivity by using a calibration table (JMA, 2009) and turned into an earth-atmospheric reflectivity (ρ_{EA}) by division with the cosine of the local solar zenith angle (Janjai et al., 2009). This parameter was related to cloud cover, with high reflectivity representing high cloud cover and vice-versa.

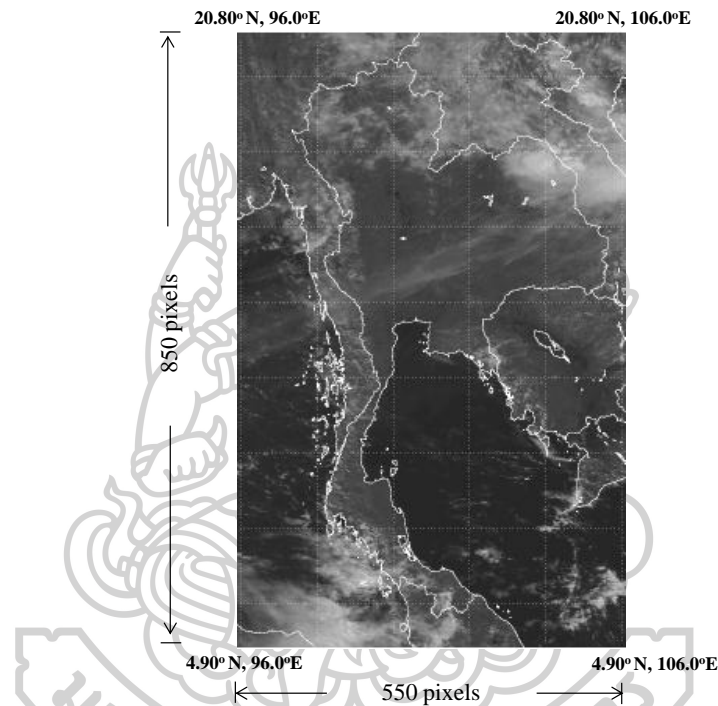


Fig. 2 An example of a rectified image over Thailand

In this work, the earth-atmospheric reflectivity data were processed on an hourly basis between 8:30 to 16:30 over an eleven-year period of 2006 – 2016.

2.2.3 Meteorological parameters

Precipitable water is a main parameter which can absorb near infrared radiation at the earth's surface and also affects diffuse near infrared radiation. Thus, this parameter was used as an input in the proposed model. Precipitable water covering the country can be calculated by using relative humidity and air temperature measured at 84 meteorological stations in Thailand followed a model suggested by Janjai et al. (2005) as shown in Eq. (2.1).

$$w = 0.8933 \exp\left(0.1715 \frac{rh p_s}{T}\right) \quad (2.1)$$

where w is precipitable water (cm), rh is relative humidity in decimal, p_s is saturated vapour pressure (mbar) and T is air temperature (K). The precipitable water of the 84

stations were interpolated for obtaining precipitable water covering the country on a monthly basis of the year 2006 - 2016. The thin plate splines method was used for the interpolation (Li & Heap, 2008).

2.3 Results and discussion

In this study, diffuse SNIR radiation data were separated into two groups. The first group was used for model formulation and the second group was employed for model validation. The first group is composed of the data from two stations namely Nakhon Pathom (NP) and Ubon Ratchathani (UB). The periods of data from NP and UB are January-December, 2013 and February, 2014-January, 2015, respectively. The periods of the data of the second group are shown in Table 1. Based on these data, the following research activities were carried out.

Table 1 Period of the data at the four stations for model validation

Station	Model validation
Nakhon Pathom (NP)	May – December, 2012 and January, 2014
Ubon Ratchathani (UB)	February, 2015
Chiang Mai (CM)	March, 2015 – February, 2016
Songkhla (SK)	May – November, 2016

2.3.1 Analysis of the dependence on cloud effect

Many research works have studied cloud effects on solar radiation (Chou et al., 1995; Butt et al., 2010; Pecenek et al., 2016; Watanabe et al., 2016). Clouds are complex in nature and have the potential to generate more diffuse radiation at the surface, although very thick clouds with high optical depth may actually diminish diffuse radiation compared to the cloudless case. It is useful in our analysis to examine the relationship between satellite-derived earth-atmospheric reflectivity (ρ'_{EA}) vs diffuse SNIR, and grouped accordingly to solar zenith angle as shown in Fig. 3.

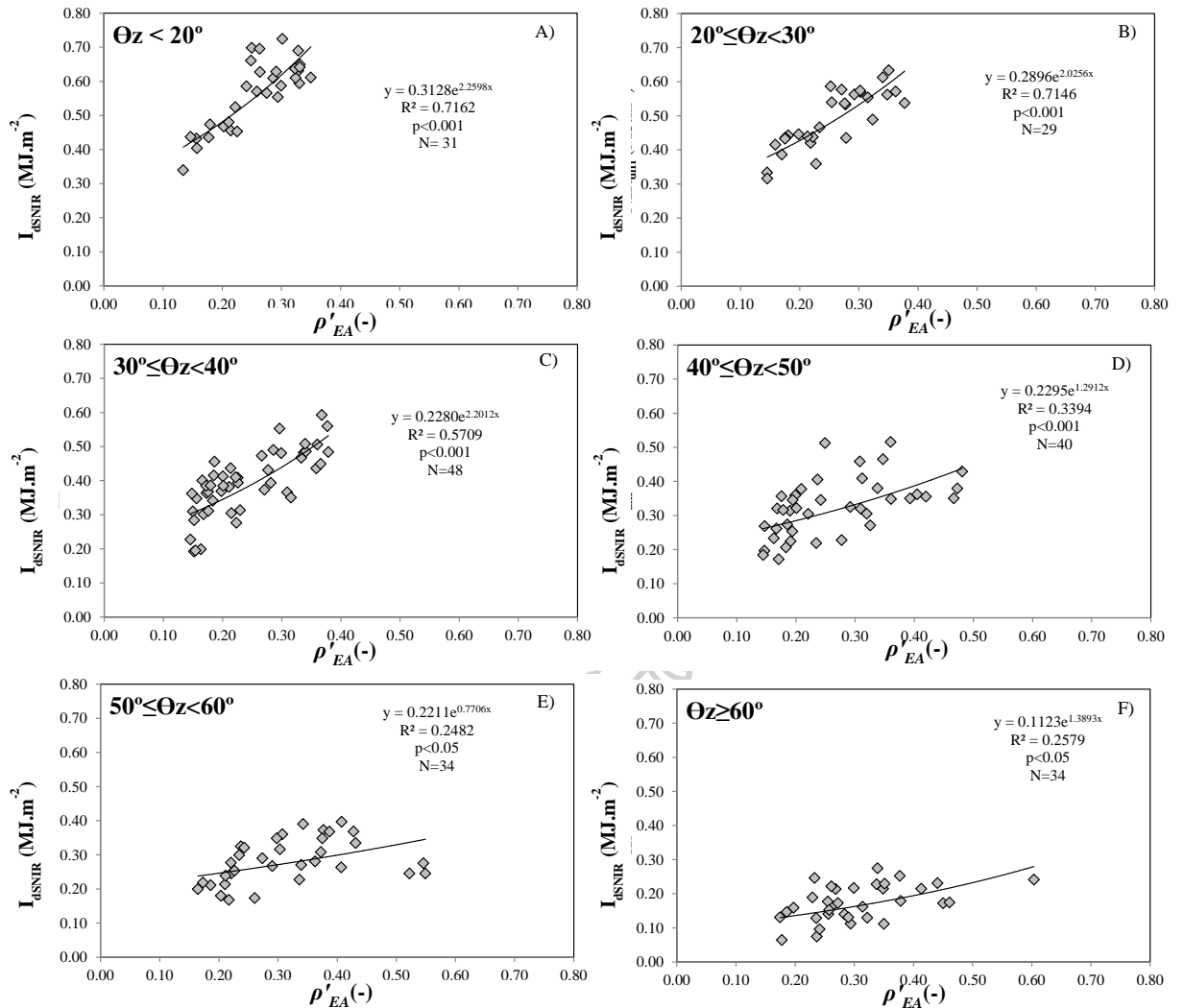


Fig. 3 Relationship between diffuse SNIR (I_{dSNIR}) and satellite-derived earth-atmospheric reflectivity (ρ'_{EA}) for the interval solar zenith angle (θ_z). The data used for this analysis are from the first group.

From Fig. 3, it is clear that diffuse SNIR has a non-linear behavior which may be represented by an exponential function of earth-atmospheric reflectivity for each interval of solar zenith angle. However, as may be observed, the span of possible values decrease as solar zenith angle interval increases, possibly a result of non-Lambertian reflection from cloud tops (Liu et al., 2004). This process will affect the coefficient of variance R^2 , decreasing its value with increasing solar zenith angle range. Nevertheless, the regression for all zenith angle ranges is significant at the 95% level of confidence. Statistics for each solar zenith angle range are shown in Table 2.

Table 2 Result of statistics for non-linear regression $I_{dSNIR} = a_0 \exp(a_1 \rho_{EA}')$

Solar zenith angle	Coef.	Value of coef.	R ²	Std. error	t-statistic	p-value	n
$\theta_z < 20^\circ$	a ₀	0.3128	0.7162	0.0287	10.9183	<0.0001	31
	a ₁	2.2598		0.3282	6.88448	<0.0001	
$20^\circ \leq \theta_z < 30^\circ$	a ₀	0.2896	0.7146	0.0232	12.5015	<0.0001	29
	a ₁	2.0256		0.2840	7.13295	<0.001	
$30^\circ \leq \theta_z < 40^\circ$	a ₀	0.2280	0.5709	0.0185	12.2954	<0.001	48
	a ₁	2.2012		0.2933	7.50372	<0.001	
$40^\circ \leq \theta_z < 50^\circ$	a ₀	0.2295	0.3394	0.0239	9.6129	<0.001	40
	a ₁	1.2912		0.3364	3.8387	<0.001	
$50^\circ \leq \theta_z < 60^\circ$	a ₀	0.2211	0.2482	0.0259	8.5292	<0.001	34
	a ₁	0.7706		0.3364	2.2907	<0.05	
$60^\circ \geq \theta_z$	a ₀	0.1123	0.2579	0.0174	6.4670	<0.001	34
	a ₁	1.3893		0.4438	3.1304	<0.05	

2.3.2 Analysis of dependence on solar zenith angle

The ratio of diffuse to global SNIR increases with solar zenith angle due to the longer path length of the direct beam and increased scattering. A plot of diffuse SNIR vs cosine of the solar zenith angle is depicted in Fig. 4. From the figure, the relationship is non-linear, and may be described by an exponential function. It is significant at the 99% level of confidence. Therefore, this parameter was included in the model.

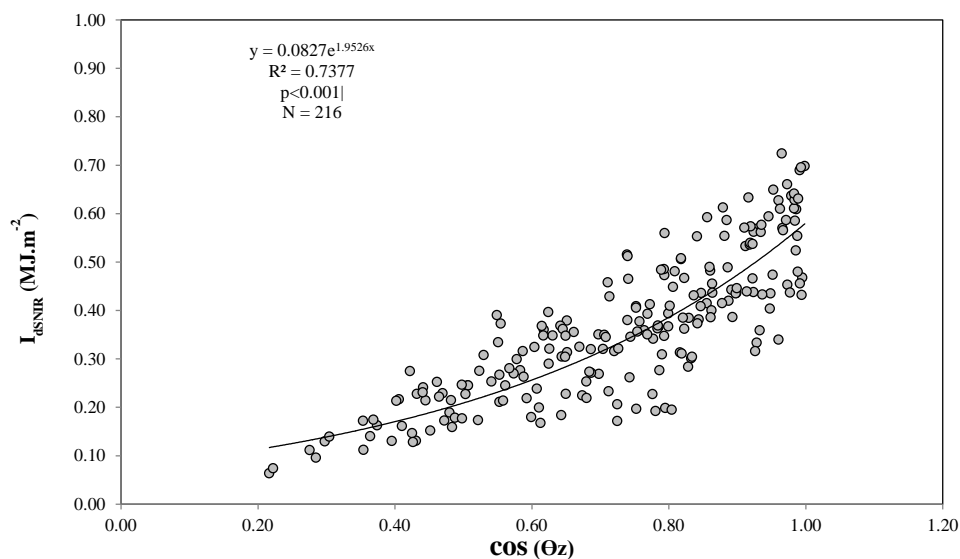


Fig. 4 Relationship between diffuse SNIR (I_{dSNIR}) and cosine of solar zenith angle ($\cos(\theta_z)$)

2.3.3 Analysis of dependence on precipitable water

This section will consider precipitable water as SNIR is strongly absorbed by precipitable water in the atmosphere. Absorption by precipitable water is high in Thailand as it is in the tropics and therefore this term is important affecting the magnitude of diffuse SNIR at the surface.

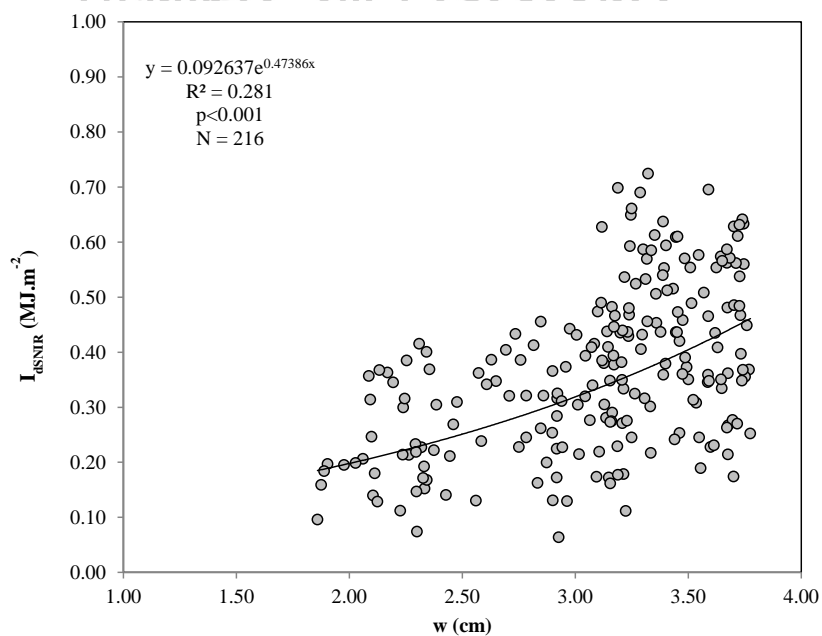


Fig. 5 Relationship between diffuse SNIR (I_{dSNIR}) and precipitable water (w)

Fig. 5 shows a correlation between diffuse SNIR and precipitable water. Scattering of data is large as other factors such as cloud cover, zenith angle and aerosol depletion are also acting. However, the trend may be described as an exponential function, with a 99% level of confidence.

2.3.4 Formulation and validation of model

Given the non-linear behavior between diffuse SNIR and ρ'_{EA} , w and $\cos\theta_Z$, a semi-empirical model for estimating diffuse SNIR was proposed as follows:

$$I_{dSNIR} = A_o I_{oSNIR} \exp^{(A_1 \rho'_{EA} + A_2 w + A_3 \cos\theta_Z)} \quad (2.2)$$

where I_{oSNIR} is extraterrestrial SNIR in $MJ.m^{-2}$ (Iqbal, 1983), w is precipitable water in cm, ρ'_{EA} is satellite-derived earth-atmospheric reflectivity, θ_Z is solar zenith angle, and A_o, A_1, A_2 and A_3 are regression coefficients. To obtain the values of these coefficients, the diffuse SNIR data from the first group together with the corresponding data of precipitable water, the reflectivity and cosine of solar zenith angle were fitted to the model using a non-linear regression approach (Dougherty, 2011) and the results are shown in Table 3. As all input data used for the fitting were based on monthly average hourly values, the values of coefficients are for the calculation of monthly average hourly diffuse SNIR radiation.

Table 3 The coefficient values of Eq. (2.2) from a non-linear regression method

Coefficient	Value of coefficient	Standard error	t-statistic	p-value	R ²	N
A _o	0.0515847073	0.00447828578	11.5188512	<0.05	0.86	216
A ₁	1.65346393	0.169901074	9.73192161	<0.05		
A ₂	0.10125271	0.0340973911	2.96951488	<0.05		
A ₃	0.735786364	0.0811338362	9.06879791	<0.05		

All regression coefficients are significant at 95% with absolute of t-statistic more than 2. Therefore, the semi-empirical model was used for estimating monthly average hourly diffuse SNIR and then compared with those from the ground-based measurements. In this work, root mean square difference (RMSD) and mean bias difference (MBD) were used for an evaluation of the model's performance as described in Eq. (2.3) and (2.4).

$$RMSD(\%) = \frac{\sqrt{\frac{\sum_{i=1}^n (I_{i,dSNIR,mod} - I_{i,dSNIR,meas})^2}{N}}}{\frac{\sum_{i=1}^n I_{i,dSNIR,meas}}{N}} \times 100 \quad (2.3)$$

$$\text{MBD}(\%) = \frac{\frac{\sum_{i=1}^n (I_{i,\text{dSNIR,mod}} - I_{i,\text{dSNIR,meas}})}{N}}{\frac{\sum_{i=1}^n I_{i,\text{dSNIR,meas}}}{N}} \times 100 \quad (2.4)$$

where $I_{i,\text{dSNIR,mod}}$ is diffuse SNIR from the semi-empirical model, $I_{i,\text{dSNIR,meas}}$ is diffuse SNIR from ground-based measurements and N is total number of the data. The result of the model validation is shown in Fig. 6.

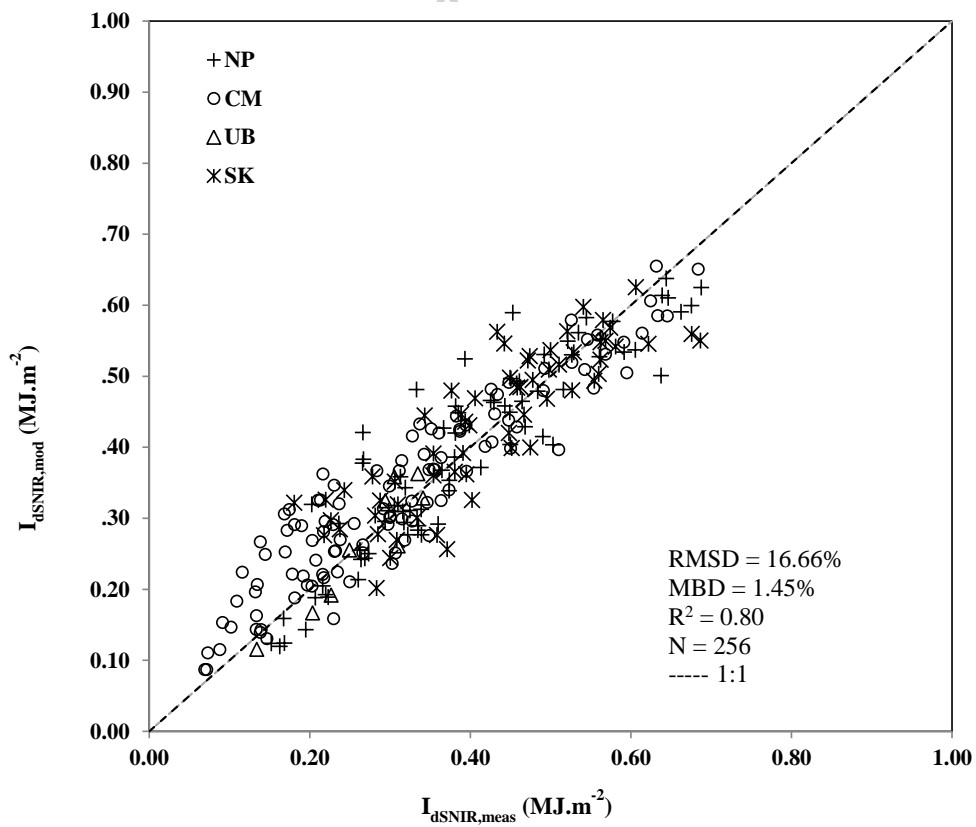


Fig. 6 Comparison between monthly average hourly diffuse SNIR from measurement ($I_{\text{dSNIR,meas}}$) and those from the semi-empirical model ($I_{\text{dSNIR,mod}}$) at Nakhon Pathom (NP), Chiang Mai (CM), Ubon Ratchathani (UB) and Songkhla (SK)

The results show that the semi-empirical model can be used to estimate monthly average hourly diffuse SNIR with an RMSD and MBD of 16.7% and 1.5%, respectively. This satisfactory model performance provided a means to generate monthly average hourly diffuse SNIR covering the country, with emphasis on diurnal and seasonal variations.

2.3.5 Implementation of diffuse SNIR Mapping

To produce the diffuse SNIR maps, input data of all parameters of the model (Eq. (2.2)) are needed for the entire areas corresponding to the satellite pixels. For each hour of a given month, the values of reflectivity were averaged to obtain monthly average hourly reflectivity. The same procedure was carried out for precipitable water and cosine of solar zenith angle. The average values of these parameters were used as input of the model (Eq. (2.2)) to obtain monthly average hourly diffuse SNIR. This monthly average hourly diffuse SNIR was further averaged over the long-term period (2006-2016) and the results are shown as maps (Figs. 7 - 8).



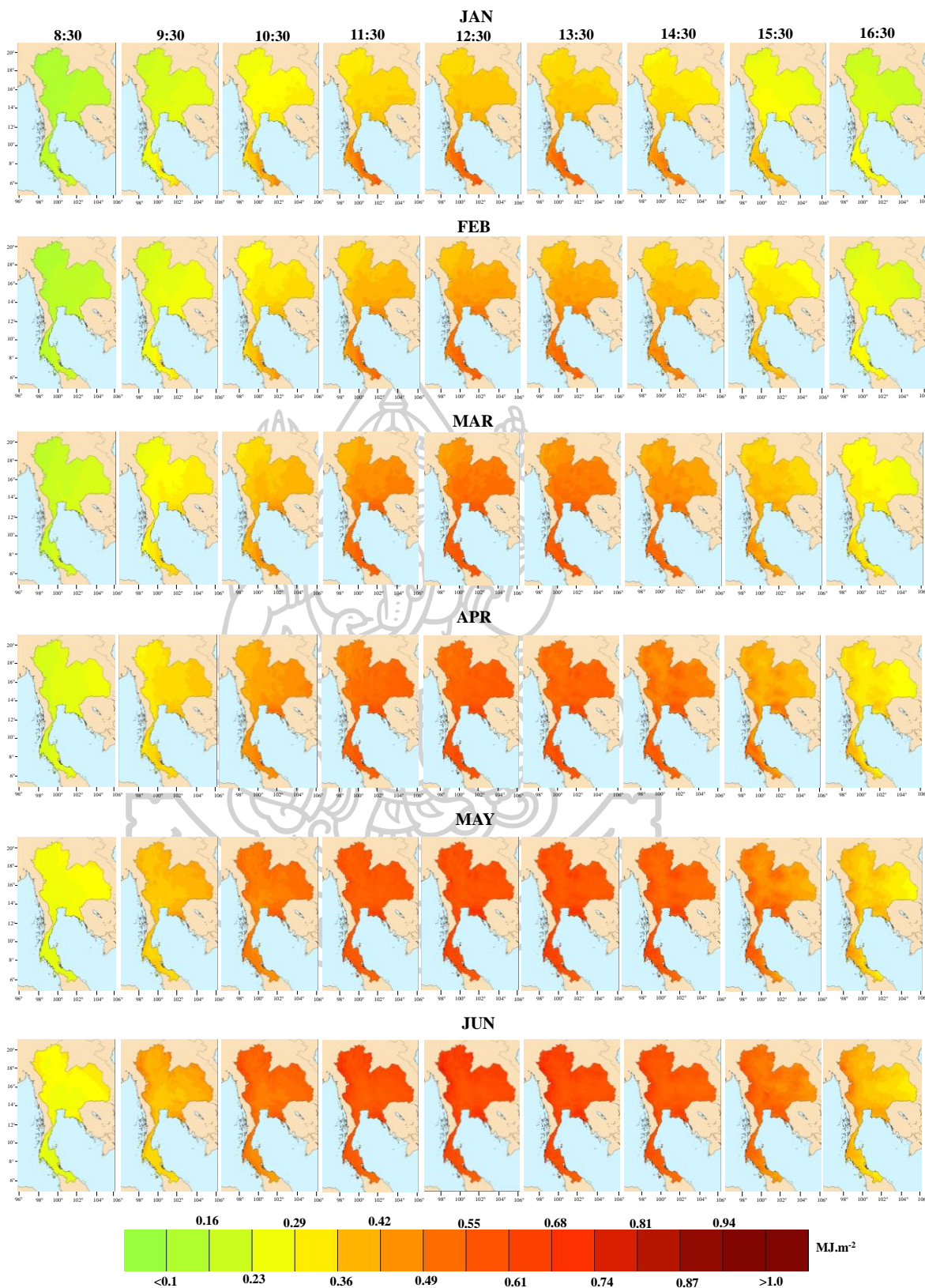


Fig. 7 Geographical distribution maps of long-term monthly average hourly diffuse SNIR irradiance over Thailand during January to June (2006-2016)

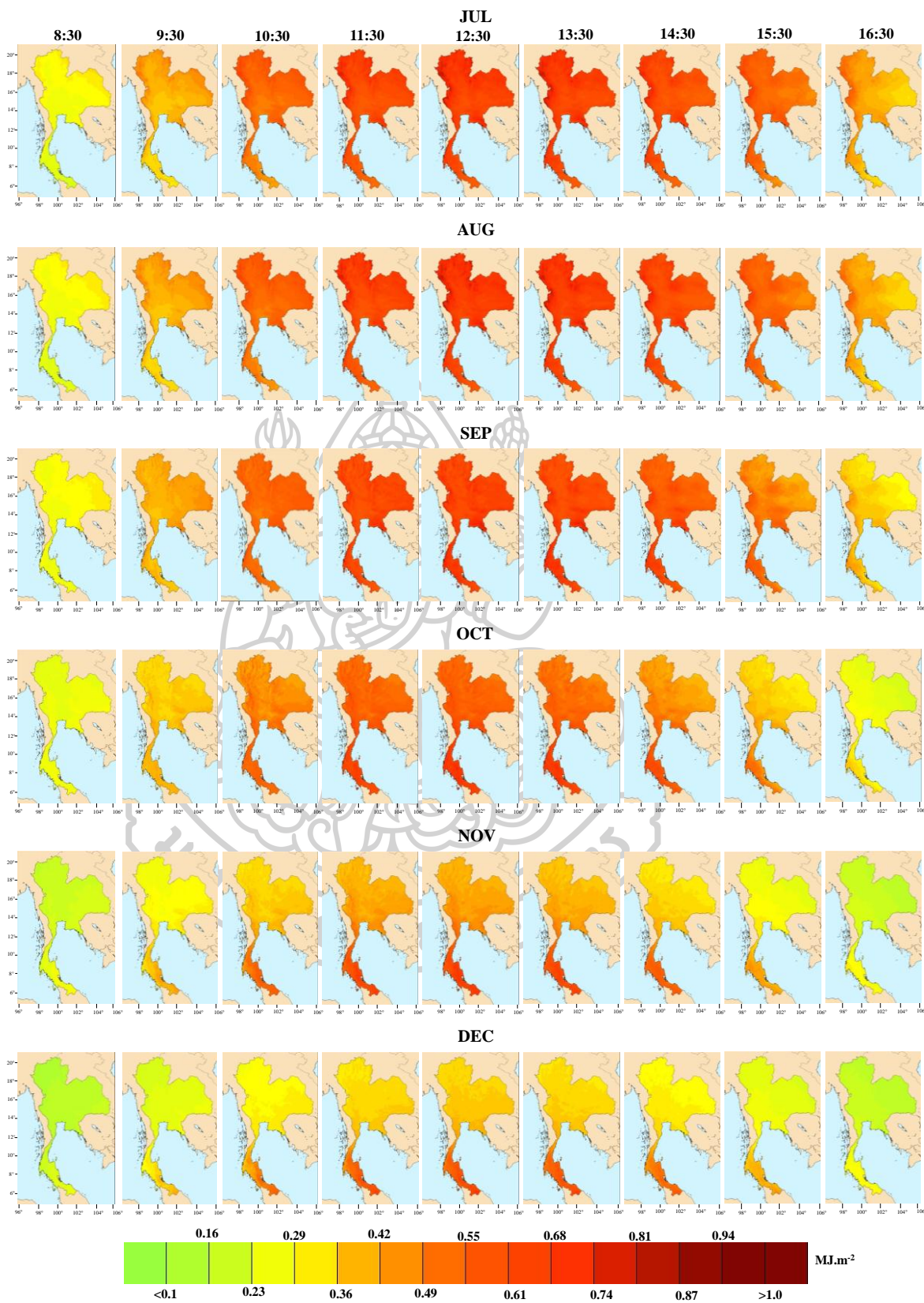


Fig. 8 Geographical distribution maps of long-term monthly average hourly diffuse SNIR irradiance over Thailand during July to December (2006-2016)

From Fig. 7 - 8, the maps reveal diurnal and seasonal diffuse SNIR variability in the region. For diurnal variation, diffuse SNIR exhibits a maximum at noon, and decreasing towards sunrise and sunset. Maximum diffuse SNIR are in range 0.43 – 0.90 MJ.m⁻². Diffuse SNIR increases seasonally from January to August. In January and February, the Northeast monsoon is active, bringing dry air to the North and Northeast of the country. The lack of cloud cover creates a lower diffuse SNIR environment compared to other regions of the country. This process is enhanced by a negative solar declination at this time of year, bringing high solar zenith angles, increasing solar pathlengths and lower solar irradiance at the surface, especially in the north of the country.

During the summer season of March and April, declination angles are small and the sun is nearly overhead at local noon. Diffuse SNIR irradiance increases compared to January and February but moderately, as there is little cloud cover. In later months, Thailand is under the influence of the Southwest monsoon, bringing more clouds and rainfall especially in the southern part of the country. Diffuse SNIR will increase as a result of increased cloudiness during this time. From August onward, diffuse SNIR will gradually decrease as the Southwest monsoon wanes and the dry Northeast monsoon begins to influence the region.

2.3.6 Monthly average daily diffuse SNIR in Thailand

In order to utilize diffuse SNIR in solar energy applications, monthly average daily diffuse SNIR was generally required. A semi-empirical model for estimating diffuse SNIR from Eq. (2.2) is used to calculate monthly average hourly diffuse SNIR. These data are summed to obtain monthly average daily diffuse SNIR in each month and averaged over the long-term encompassing 2006 - 2016. The results from four stations are shown in Fig. 9. The variation of Chiang Mai, Ubon Ratchathani and Nakhon Pathom station have similar trend with the high diffuse SNIR in the rainy season during May – October and maximum value is found in August due to the highest amount of clouds. Afterward, the upper part of Thailand is influenced by the northeast monsoon, which causes a decrease in diffuse SNIR during November - April. For Songkhla station, diffuse SNIR was quite high through the year because of high clouds covers in this part of Thailand. The distributions of monthly average daily diffuse SNIR are shown as maps in Fig.10.

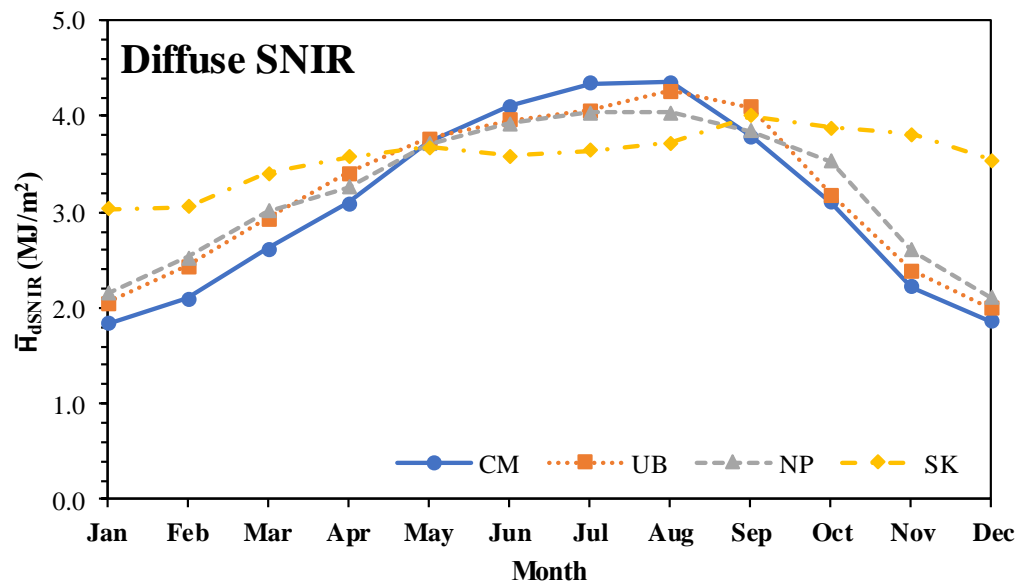
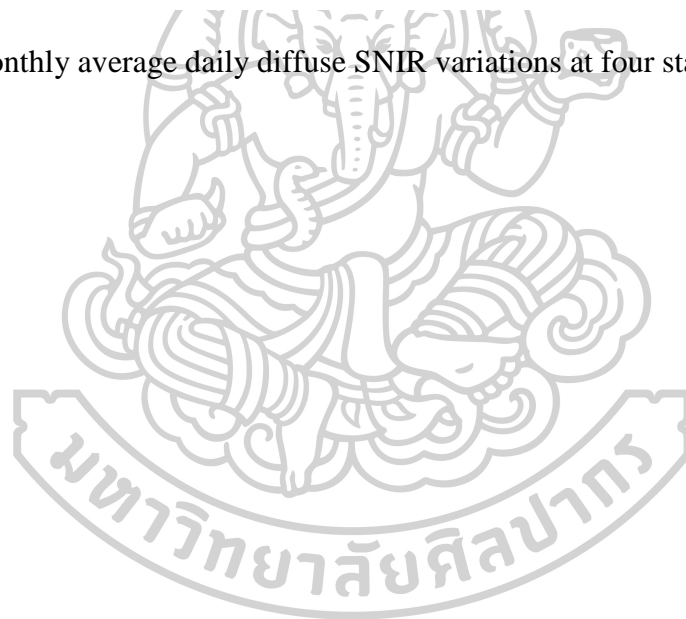


Fig. 9 Monthly average daily diffuse SNIR variations at four stations in Thailand.



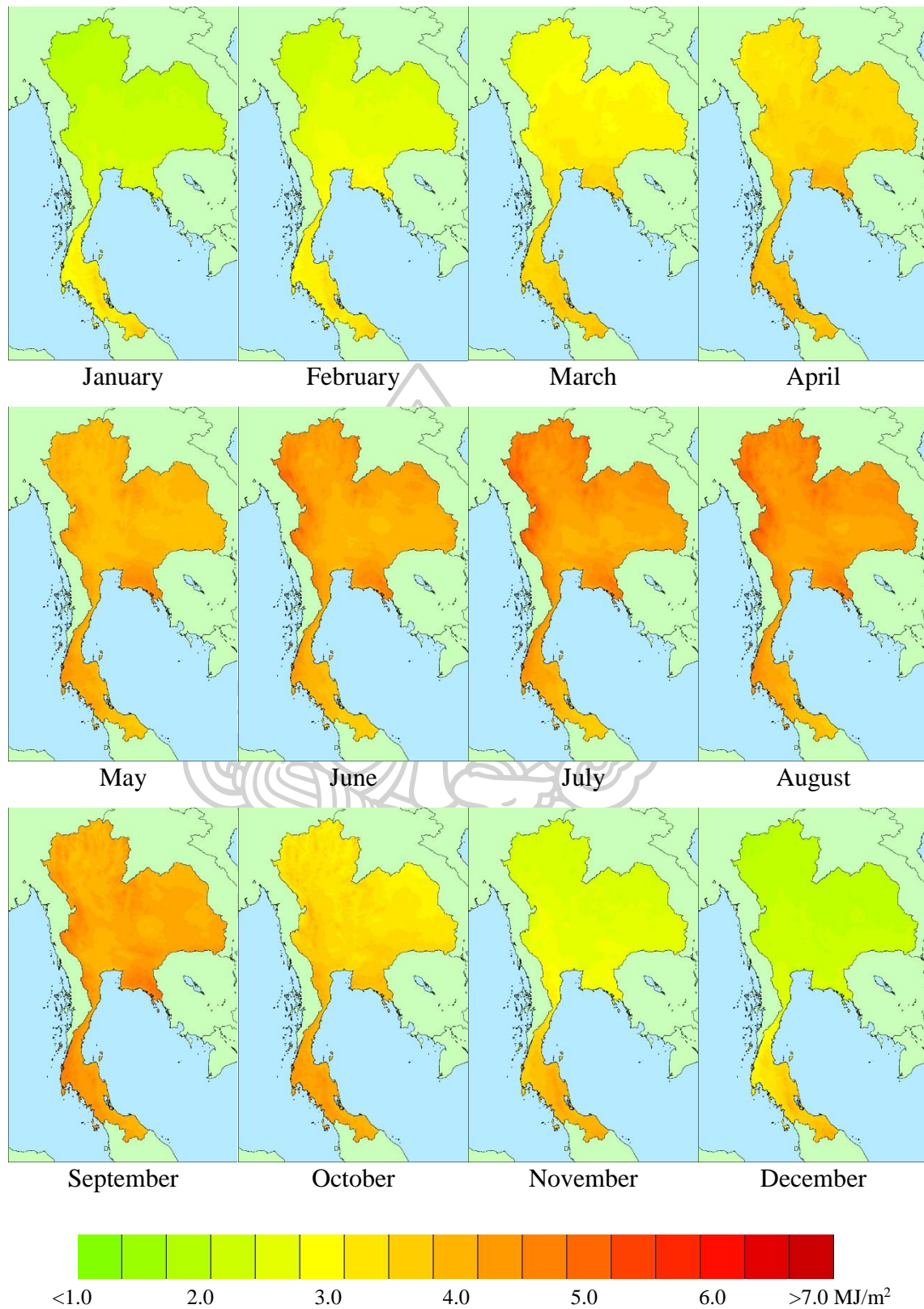
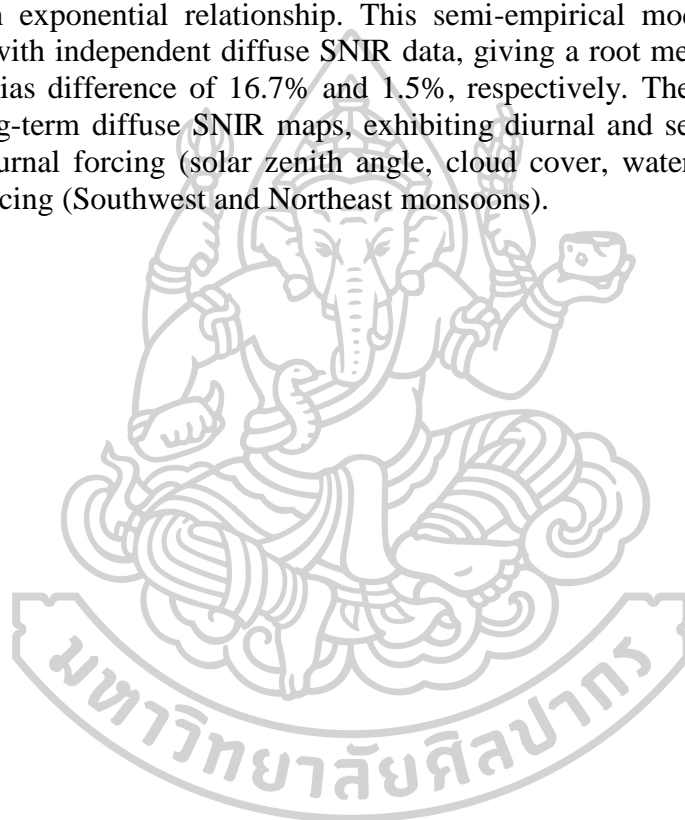


Fig. 10 Geographical distribution maps of long-term monthly average daily diffuse SNIR over Thailand.

2.4 Conclusions

From the problem of insufficient diffuse SNIR data, a semi-empirical model for estimating such data has been developed for Thailand. In developing the model, diffuse SNIR radiation in this country was acquired. The data was analyzed and the results were incorporated into a semi-empirical model. Diffuse SNIR was influenced primarily by the optical path length and to a lesser degree, by cloud cover depletion and water vapour absorption. The earth-atmospheric reflectivity from satellite data was used as a surrogate for cloud cover, while relative humidity and air temperature data from surface stations were used to estimate precipitable water.

Diffuse SNIR was best modelled using the above three variables as independent terms in an exponential relationship. This semi-empirical model is in reasonable agreement with independent diffuse SNIR data, giving a root mean square difference and mean bias difference of 16.7% and 1.5%, respectively. The model was used to provide long-term diffuse SNIR maps, exhibiting diurnal and seasonal variability in response diurnal forcing (solar zenith angle, cloud cover, water vapour) as well as seasonal forcing (Southwest and Northeast monsoons).



Chapter 3

A technique for mapping hourly global solar near infrared radiation from satellite data

3.1 Introduction

Solar near infrared radiation (SNIR) at the earth surface, occupying mainly a spectral region between 0.695 μm to 2.80 μm , represents approximately half of the total solar spectrum (Muneer, 2007; Petty, 2006). As a result, SNIR contributes significantly the total radiant flux utilized by solar thermal energy systems in such activities as solar hot water systems and solar drying systems. It is also an important component of heat input of buildings, with consequences to their heating and cooling loads. Like broadband (0.3 μm -3.0 μm) solar radiation, SNIR is influenced by cloud and water vapor, which vary with location and time. Consequently, SNIR varies with location and time.

SNIR has not been investigated, to the same degree as other wavelength bands of the solar spectrum such as the UV or visible regions. A pioneering study by Gates et al. (1958) measured the spectrum of SNIR at various altitudes up to 10,000 ft using an infrared spectrometer attached to a balloon. A later work by Bolsenga (1967) investigated SNIR in northern Greenland employing an Eppley pyranometer with Schott RG-8 filters. Some studies have attempted to partition SNIR as a fraction of broadband radiation for cloudless skies (Weiss & Norman, 1985) and in South America in more general conditions (Escobedo et al., 2009; Rossi et al., 2018).

Information on SNIR is best obtained using a modelling approach as studies covering the tropical region are scarce compared to other parts of the solar spectrum, for example the ultraviolet and photosynthetically active radiation (Janjai et al., 2010, Choosri et al., 2017), and ground observations are few. In this study, we address the problem by developing an algorithm to estimate SNIR from satellite data, therefore providing a comprehensive regional coverage.

3.2 Methodology

3.2.1 Data acquisition and processing

Table 4 provides details of the data used. Surface irradiance in the SNIR (0.695 μm - 2.80 μm) was acquired using pyranometers (Eppley, model PSP) fitted with Schott glass filters RG-695 at four locations in Thailand: Chiang Mai (18.78°N; 98.98°E), Ubon Ratchathani (15.25°N; 104.87°E), Nakhon Pathom (13.82°N; 100.04°E) and Songkhla (7.20°N; 100.60°E) (Fig. 11). On a yearly basis the pyranometers are calibrated against a travelling standard which has been calibrated at the manufacturer and is traceable to the National Institute of Standard and Technology (NIST). Data is acquired every second by a data logger (Yokogawa, model DC100) and processed to hourly irradiation ($\text{J. m}^{-2}. \text{h}^{-1}$).

* This chapter has been published in Journal of Renewable Energy and Smart Grid Technology. Volume 14, No. 2, 2019.



Fig. 11 Position of SNIR measurements and pictorial view of SNIR pyranometers. A, B, C and D indicate the northern, northeastern, central and the southern regions, respectively.

Table 4 Instrument details and data acquired in the study.

Source	Instrument	Duration	Acquisition Frequency	Area
Near infrared irradiance (0.695 μm - 2.80 μm)	Eppley PSP pyranometer equipped with RG-695 filter	1/1/2009-31/12/2013	Every second integrated to hourly	4 locations: Chiang Mai (18.78°N; 98.98°E), Ubon Ratchathani (15.25°N; 104.87°E), Nakhon Pathom (13.82°N; 100.04°E) and Songkla (7.20°N; 100.60°E)
Reflectance of the earth atmospheric system (0.55 μm – 0.90 μm)	MTSAT-1R satellite	1/1/2009-31/12/2013	Hourly (8:30-16:30 local time)	5°N-21°N 96°E-106°E

Visible reflectance data was acquired on an hourly basis from the Japanese geostationary satellite MTSAT-1R. The raw signal in counts is converted into the earth-atmospheric reflectivity (ρ'_{EA}) using a conversion table provided by the satellite agency (JMA, 2009). Each satellite image is then sectorised into a geographical area bounded by latitude: 5°N-21°N and longitude 96°-106°E, navigated using the local coastlines and transformed into the cylindrical projection linear in latitude and longitude. The final image has a pixel resolution of 3 km x 3 km.

Precipitable water data is needed for the satellite model and it was developed from relative humidity and air temperature data recorded at 85 meteorological stations throughout the country. Then the spline interpolation technique was applied to obtain precipitable water over the country (Cole, 1976; Janjai et al., 2005; Janjai et al., 2009).

A radiative transfer model from Tanre et al. (1986) was used to derive a relationship between aerosol depletion and visibility and applied to visibility data recorded at 85 stations throughout the country. These estimations of depletion at discrete points were fitted with a minimum curve surface using the spline interpolation approach and therefore providing a monthly estimate of aerosol depletion (Janjai et al., 2009). The final step involved partitioning aerosol depletion into scattering and absorption which was done using the single scattering albedo from the AERONET data in the regions of East and Southeast Asia. Details of the expression are shown in Eqs. (3.4c) and (3.6) in the next section.

All data were acquired over a five-year period (1 January, 2009 – 31 December, 2013) and these were partitioned into two data sets. The period between 1 January, 2009 to 31 December, 2012 was used to build up a radiative model regression, essentially linking a satellite atmospheric reflectance to surface-derived reflectance as discussed in the next section. The resultant regression model was validated using an independent data set (1 January – 31 December, 2013).

After the validation, all data sets were turned into monthly averages for hourly values covering individual years. Therefore, a total of 60 individual months (5 years x 12 months) were processed. Each individual month was characterized by averages for 9 hours (8:00-9:00, 9:00-10:00, etc.). All model development, validation and statistics are performed with these hourly averages over the month. The reason being that this approach provides information on cloud-related diurnal changes, while at the same time removing random noise that may be caused by an individual cloud process at one specific hour.

3.2.2 Satellite model

Numerous studies have used satellite data to derive surface solar radiation using various approaches (Exell, 1984, Schillings et al., 2004, Tarpley, 1979, Gautier et al. 1980, Nunez, 1993, Polo et al., 2008, Martins et al., 2007, Vonder et al., 1973). They range from simple regressions between satellite-derived reflectivity and pyranometer data to one dimensional radiative transfer model which use look-up tables (Pinker & Laszlo, 1992; Masiri et al., 2008).

Much of the error in the satellite technique revolves around establishing a true cloud optical depth and reflectance from a single satellite view. One alternative used here is to relate, at a given location, the satellite-derived reflectivity to an atmosphere reflectivity needed to produce the required SNIR at the surface. Fig. 12 shows the various steps involved. In Fig. 12a the satellite-derived earth-atmospheric reflectivity

(ρ'_{EA}) is changed into an atmosphere reflectivity (ρ'_A) using a radiation balance model. These data are subsequently compared with an atmosphere reflectivity determined from the SNIR (ρ_{SNIR}) at the same location. In the second step (Fig. 12b) all the satellite data set is transformed into an atmosphere reflectivity which is then used to estimate SNIR.



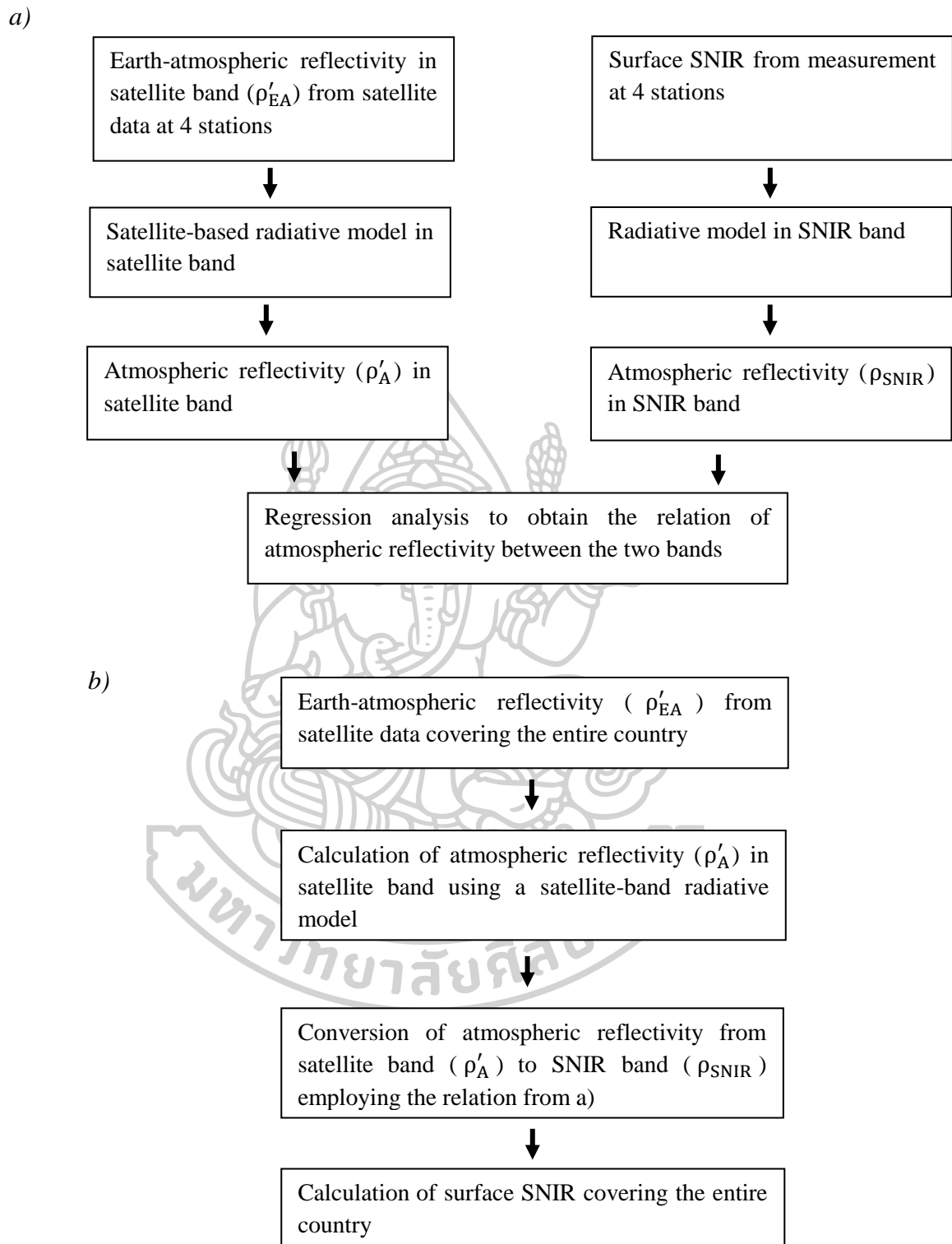


Fig. 12 Procedure for mapping SNIR from satellite data. a) Development of the relation between atmospheric reflectivity in satellite band (ρ'_A) and SNIR band (ρ_{SNIR}). b) The calculation process of surface SNIR covering the entire country.

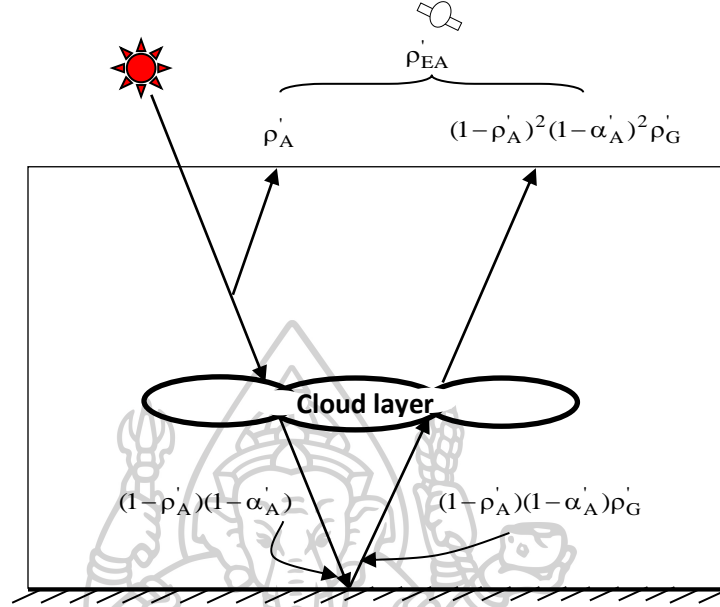


Fig. 13 Earth-atmosphere reflected solar radiation as detected by a satellite sensor. Greek symbols ρ and α represent scattering and absorption respectively while subscripts A and G refer to the atmosphere and ground, respectively. Primes refer to the satellite band. The first reflection represents radiation reflected from the atmosphere (ρ'_A), while the second represents radiation escaping to space after one reflection by the surface $((1-\rho'_A)^2(1-\alpha'_A)^2\rho'_G)$. All data is normalized to an incoming solar irradiance of 1.

Fig. 13 provides a schematic diagram of the satellite-derived reflectivity when the incoming solar irradiance is one. In this simple model, all scattering and absorption terms are taken as equal in both the downwelling and upwelling directions. The radiation scheme adds all the outgoing radiation to space after reflection from the atmosphere only (ρ'_A), and one reflection by the surface $(1-\rho'_A)^2(1-\alpha'_A)^2\rho'_G$. Here ρ and α represent scattering and absorption, respectively, while subscripts A and G refer to the atmosphere and ground respectively and primes refer to the satellite viewing band ($0.55\mu\text{m} - 0.90\mu\text{m}$). The outgoing radiation to space (ρ'_{EA}) can be written as:

$$\rho'_{EA} = \rho'_A + (1-\rho'_A)^2(1-\alpha'_A)^2\rho'_G \quad (3.1)$$

Eq. (3.1) has one unknown, ρ'_A describing the reflection by the atmosphere, while the other terms are known: ρ'_{EA} is the satellite-derived reflectivity, ρ'_G is the surface reflectance and α'_A is the atmospheric absorption which includes water vapour, gasses, and aerosols. Therefore, Eq. (3.1) may be solved as a quadratic in ρ'_A :

$$\rho'_A = \frac{-B \pm (B^2 - 4AC)^{1/2}}{2A}$$

$$A = (1 - 2\alpha'_A + (\alpha'_A)^2)\rho'_G$$

$$B = (1 - 2\rho'_G + 4\alpha'_A\rho'_G - 2\rho'_G(\alpha'_A)^2)$$

$$C = (1 + (\alpha'_A)^2 - 2\alpha'_A)\rho'_G - \rho'_{EA}$$
(3.2)

The atmospheric absorption term may be expanded into its component terms:

$$\alpha'_A = \alpha'_{\text{gas}} + \alpha'_w + \alpha'_{\text{aer}}$$

$$\alpha'_i = 1 - \frac{\int_{0.55}^{0.90} I_\lambda \tau_{i\lambda} d\lambda}{\int_{0.55}^{0.90} I_\lambda d\lambda}$$
(3.3)

where the subscripts “gas”, “w” and “aer” refer to the absorption by atmospheric gases, water vapour and aerosol, respectively. Any of these terms may be expressed as a transmission (τ'_i) integrated over the satellite band and normalized by the extra-terrestrial irradiance in the satellite band (Eq. 3.3). Expressions for α'_{gas} and α'_w may be readily obtained from Leckner (1978) as discussed in Iqbal (1983) (Eqs. (3.4a) and (3.4b)), while the relationship for α'_{aer} is best described by the relationship from Janjai et al. (2009) for the Thailand region (Eq. (3.4c)):

$$\tau'_{\text{gas}}(\lambda) = 1 - \alpha'_{\text{gas}}(\lambda) = \exp[(-1.41k_{a\lambda} m)/(1 + 118.93k_{a\lambda} m)]$$
(3.4a)

$$\tau'_w(\lambda) = 1 - \alpha'_w(\lambda) = \exp(-0.2385k_{w\lambda} w m/(1 + 20.07k_{w\lambda} w m))$$
(3.4b)

$$\alpha'_{\text{aer}} = [1 - (1.0358 - 0.3293(\text{VIS})^{-0.66})m^{0.9}](1 - \omega_0)$$
(3.4c)

where $k_{a\lambda}$ is an absorption coefficient for mixed gases in the atmosphere (dimensionless), $k_{w\lambda}$ is an absorption coefficient for precipitable water vapour (cm^{-1}), w is precipitable water vapour (cm), m is air mass (dimensionless), VIS is visibility in km and ω_0 is aerosol single scattering albedo. The term in the square brackets in Eq. (4c) represents the aerosol depletion for the Thailand region. It is multiplied by ω_0 which by definition is the ratio of the scattering to the total aerosol depletion. The ω_0 term was obtained as a yearly average figure from the four Cimel sunphotometers located at each of the experimental sites which forms part of AERONET (Holben et al., 1998). Precipitable water vapour for the Thailand region may be described in terms of a monthly average surface climatology (Janjai et al., 2005):

$$w = 0.893 \exp(0.1715 \times rh \times p_s / T)$$
(3.5)

where rh is relative humidity in decimal unit, p_s is saturated pressure in mbar and T is air temperature in K.

The scattering term ρ'_A is the sum of two terms $\rho'_A = \rho'_C + \rho'_{aer}$ where ρ'_C represents the contribution from clouds and the atmosphere via Rayleigh scattering, and ρ'_{aer} is the scattering contribution by aerosol depletion, described as (Janjai et al., 2009):

$$\rho'_{aer} = [1 - (1.0358 - 0.3293(\text{VIS})^{-0.66})^{m^{0.9}}] \omega_0 \quad (3.6)$$

where VIS is visibility in km.

The final term in the solution involves surface albedo. This term is high in the infrared spectrum but relatively low in the band covered by the satellite sensor (0.55 μm – 0.90 μm). We have used the IGBP spectral albedos as described by Moody et al., (2007) for a mixture of evergreen broad forest and cropland with a 50% contribution from each. The authors provide spectral albedos at four wavelengths for a diffuse white sky. These were then linearly interpolated and a weighted average albedo was obtained using the LIBRADTRAN (Mayer & Kylling, 2005) radiative transfer package:

$$\rho'_G = \frac{\int_{0.55}^{0.90} \rho'_G(\lambda) I_\lambda d\lambda}{\int_{0.55}^{0.90} I_\lambda d\lambda} \quad (3.7)$$

The global SNIR radiation as measured by a pyranometer sensor at the surface (τ_{SNIR}) may be expressed in a normalized form:

$$\tau_{\text{SNIR}} = \frac{I_{\text{SNIR}}}{I_{\text{OSNIR}}} = \frac{(1 - \rho_{\text{SNIR}})(1 - \alpha_{\text{SNIR}})}{1 - \rho_{\text{SNIR}}\rho_{\text{GSNIR}}} \quad (3.8a)$$

$$\rho_{\text{SNIR}} = \frac{\tau_{\text{SNIR}} + \alpha_{\text{SNIR}} - 1}{\tau_{\text{SNIR}}\rho_{\text{GSNIR}} + \alpha_{\text{SNIR}} - 1} \quad (3.8b)$$

where I_{SNIR} is the measured SNIR, I_{OSNIR} is the extra-terrestrial SNIR and all other terms are as defined in Eq.(3.1) with the exception that the integration is performed over all the SNIR wavelengths (0.695 μm to 2.80 μm). The transmission τ_{SNIR} is given as the product of a loss by scattering ($1 - \rho_{\text{SNIR}}$) times loss by absorption ($1 - \alpha_{\text{SNIR}}$) but enhanced by multiple scattering between the surface albedo (ρ_{GSNIR}) and the atmosphere albedo (ρ_{SNIR}): $[1/(1 - \rho_{\text{SNIR}}\rho_{\text{GSNIR}})]$.

We require a solution to ρ_{SNIR} as sensed by the pyranometer and it is given by Eq. (3.8b). All terms to the right of Eq. (3.8b) are known and may be estimated as in Eqs. (3.3) to (3.7) with a longer integration for SNIR wavelengths. The final step relates the satellite-determined monthly-averaged ρ'_A to the pyranometer estimate of monthly average ρ_{SNIR} at the four surface stations. Knowing the transformation, Eq. (3.8a) may be applied to estimate τ_{SNIR} at every pixel in the satellite image. Absolute irradiance is

readily obtained by multiplying τ_{SNIR} by the extra-terrestrial irradiance ($I_{0\text{SNIR}}$) at a particular location.

3.3. Results

3.3.1 Model performance

Fig. 14 shows monthly average ρ'_A from the satellite data at the four station locations vs estimates of ρ_{SNIR} for the period 1 January, 2009 to 31 December, 2012. A least square linear regression fit to the data gave the following statistics:

$$\rho_{\text{SNIR}} = 0.7142\rho'_A + 0.0863 \quad (3.9)$$

$$R^2 = 0.71; \text{ SE} = 0.061; \text{ N} = 1146$$

with a highly significant R^2 at a level of confidence greater than 95%. SE is standard error and N is total number of data. Cloud reflection is largely independent of wavelength (Iqbal, 1983; Stephens, 1994) and this difference is likely to be a result of a decreasing Rayleigh scattering efficiency in the SNIR bands compared to the band occupied by the satellite sensor.

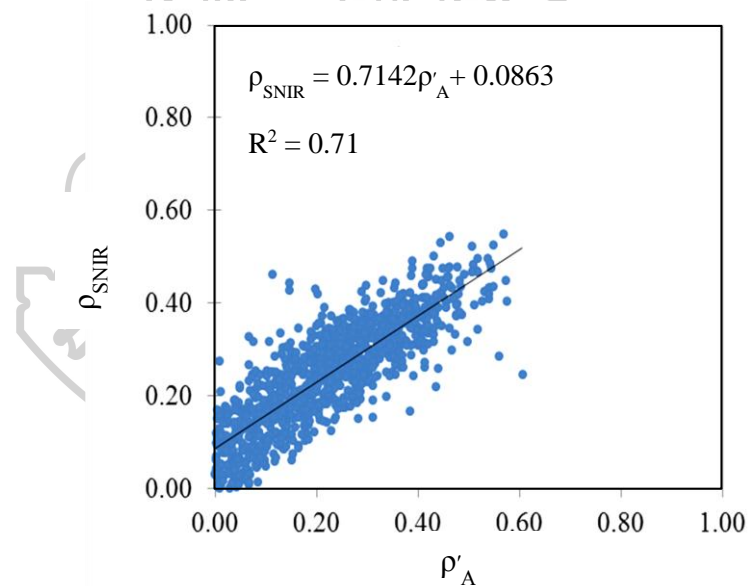


Fig. 14 Relationship between monthly average ρ'_A from the satellite estimates and ρ_{SNIR} obtained from the ground-based measurement at the four stations.

The normalized SNIR (τ_{SNIR}) may be obtained by applying the transformation in Eq. (3.9) to the normalized SNIR in Eq. (3.8a). Hourly average satellite-derived irradiances are plotted vs measured irradiances for the independent period of January – December, 2013 (Fig. 15). Irradiance for all four stations is used, involving a total of 432 data pairs (4 stations x 12 months x 1 year x 9 hours). The independent validation is satisfactory with a mean bias difference (MBD) of 3.7% which approaches instrumental errors of 2% and a root mean square difference (RMSD) of 16.0%.

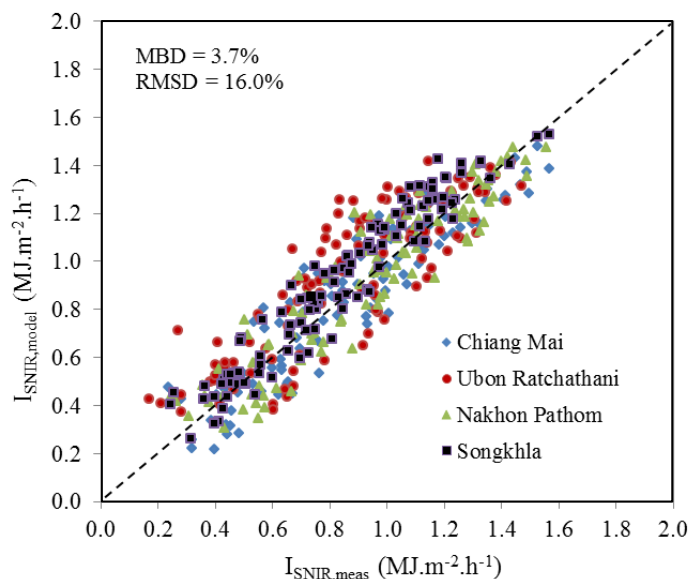


Fig. 15 Comparison between hourly average SNIR obtained from the measurement ($I_{\text{SNIR,meas}}$) and that calculated from the model ($I_{\text{SNIR,model}}$).

3.3.2 Statistics of monthly average hourly SNIR

Fig. 16 – 18 present hourly average maps for each month at representative times 9:30, 12:30 and 15:30 local time. Each hourly map is an average of 1825 images (365 days x 5 years) and is therefore a robust statistic. Examining the morning images (Fig. 16) there is a yearly signal with low values at the start and end of the year, and high values during mid-year. In addition, there are pronounced regional maxima in the eastern section of the country, with the highest readings ($0.8 - 0.9 \text{ MJ.m}^{-2}.\text{h}^{-1}$) occurring in the dry months before the full onset of the Southwest monsoon, April, May and June. The pattern is likely to be a result of two factors. Firstly, the solar zenith angle in the early morning is lower in the eastern part of the country, which is also characterized by a less frequent cloud cover.

The noon time maps taken at 12:30 (Fig. 17) do not feature a distinct yearly signal and the irradiance appears to be more evenly distributed compared to the morning maps. There are, however indications of a weak maxima ($1.3-1.4 \text{ MJ.m}^{-2}.\text{h}^{-1}$) occurring in the central part of the country, very likely due to cloud cover effects.

Generally lower irradiance is displayed in the late afternoon images estimated at 15:30 (Fig. 18). Cloud development is likely to reach maximum intensity at this time, and this process is likely to blur any regional differences. There is however an east-west gradient appearing in January to April, probably a result of lower solar zenith angles in the eastern section of the country at this time.

It is interesting to investigate the spatial distribution of yearly average daily SNIR. To accomplish this, monthly average hourly SNIR for each hour was summed over the day to obtain daily SNIR.

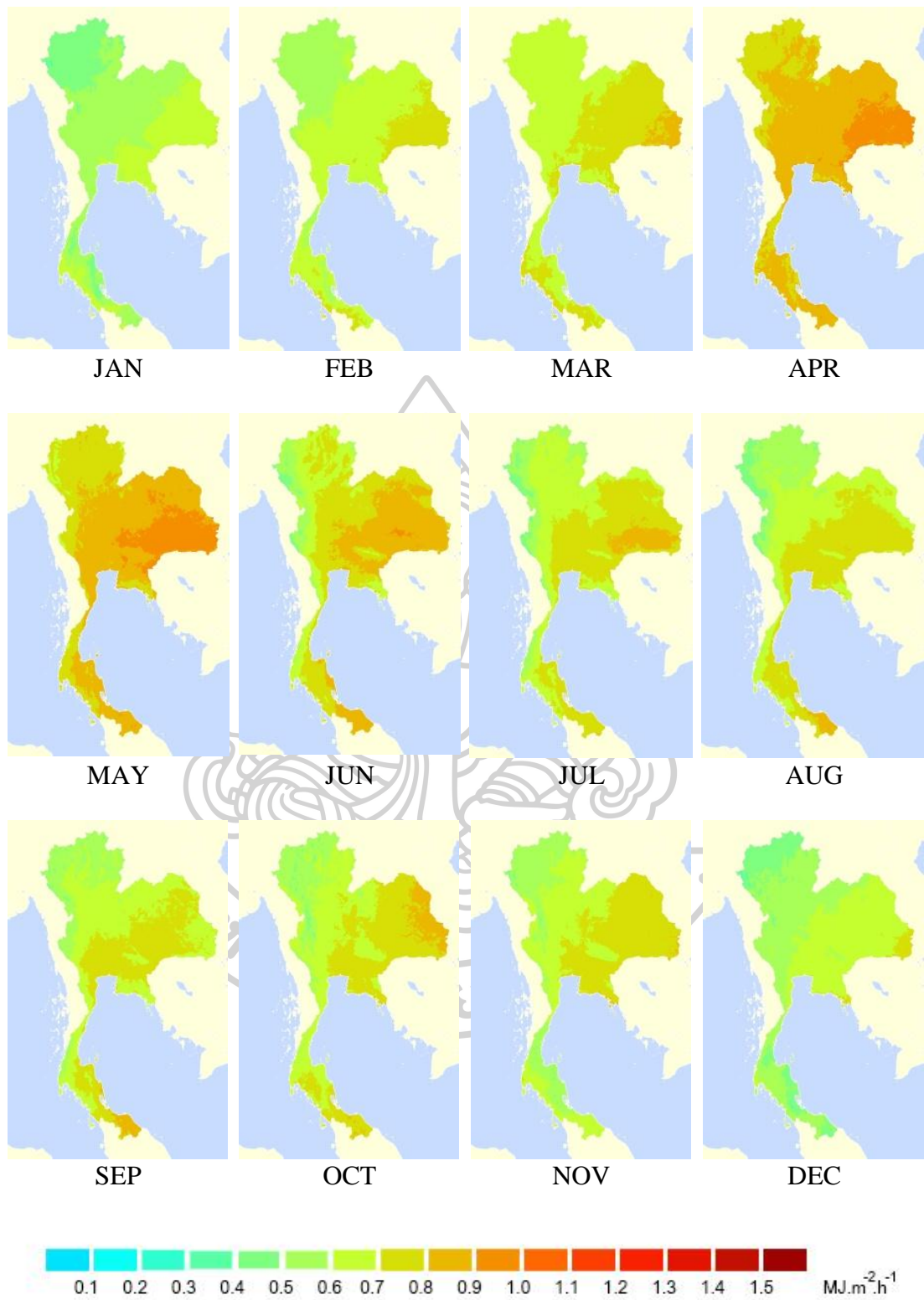


Fig. 16 The monthly average hourly SNIR maps for all months at 9:30 h.

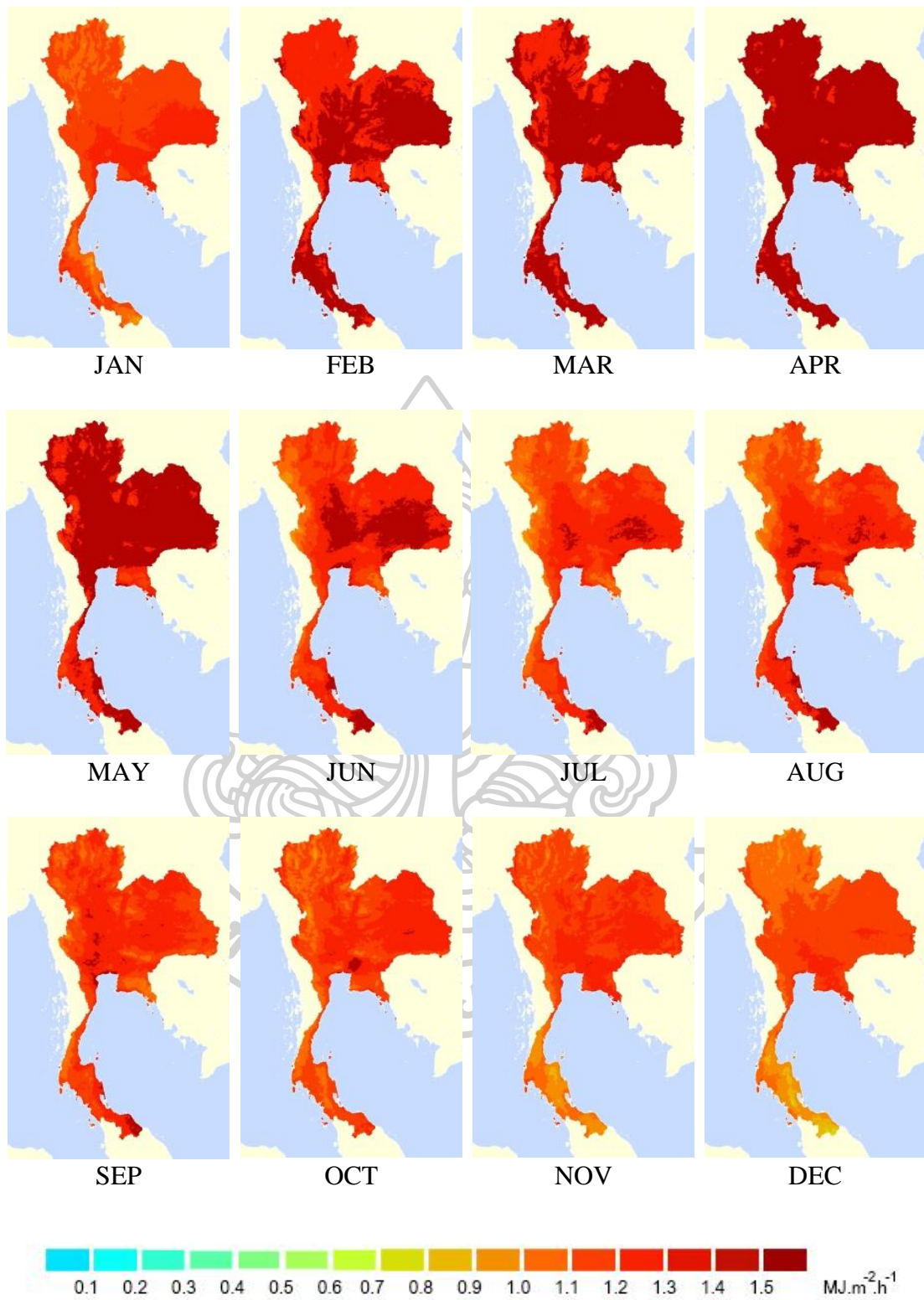


Fig. 17 The monthly average hourly SNIR maps for all months at 12:30 h.

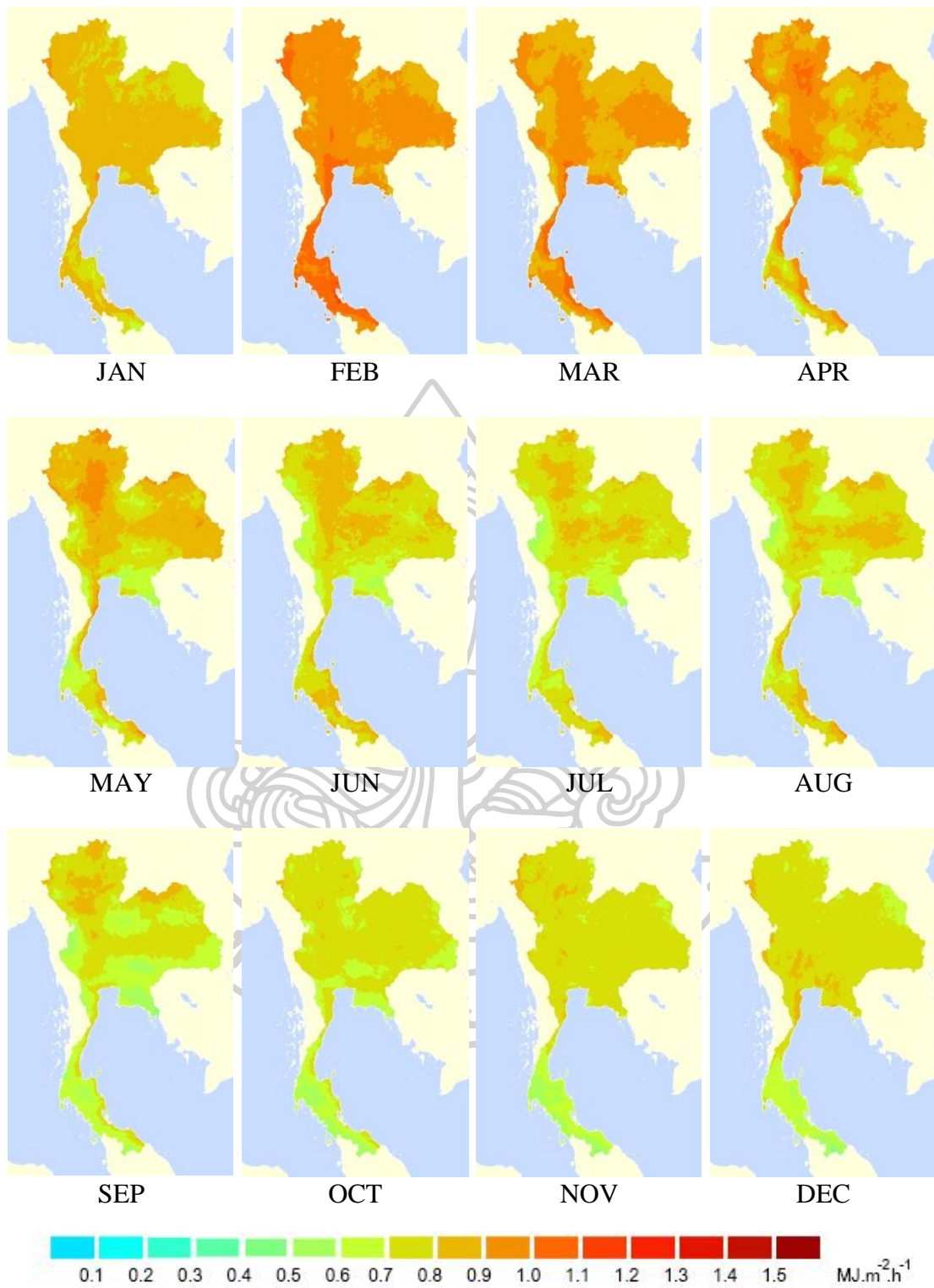
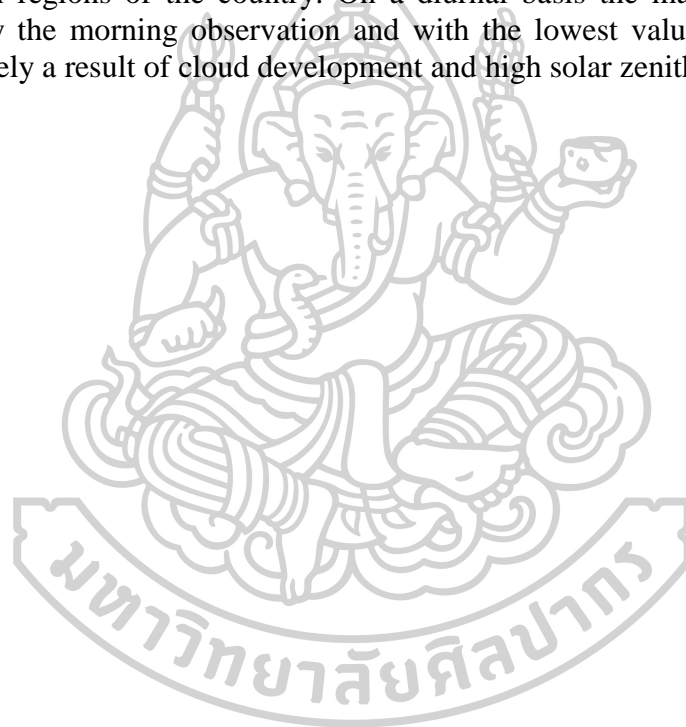


Fig. 18 The monthly average hourly SNIR maps for all months at 15:30 h.

3.4 Conclusions

This study has developed a method to estimate hourly global solar near infrared irradiance at the earth's surface in the Thailand region. The approach combines visible reflectance data from the MTSAT-1R satellite and solar near infrared irradiance measurements from four stations in Thailand. Using a simple radiation budget model, hourly atmospheric reflectance from the four stations are related to a satellite-derived atmospheric reflectance. Surface solar near infrared irradiance in the Thailand region may then be estimated using a simple radiation model which uses a corrected satellite-derived atmospheric reflectance.

Maps of monthly average hourly irradiance are presented at three different times of the day and for all 12 months. They show significant seasonal variability with maxima during mid-year and a tendency for irradiance to be largest in the central and northeastern regions of the country. On a diurnal basis the maxima occur at noon followed by the morning observation and with the lowest values in late afternoon, which is likely a result of cloud development and high solar zenith angle.



Chapter 4

The ratio of solar near infrared radiation to broadband global solar radiation

4.1 Introduction

The amount of solar near infrared radiation (SNIR) incident on the earth's surface SNIR data should be obtained from the measurements. However, the measurements of SNIR are very scarce due to high equipment and operational costs. An alternative to obtain SNIR data is to use modeling approach. In the past decade, various researchers have proposed model to compute SNIR. For example, Escobedo et al. (2011) developed models to estimate SNIR from broadband radiation (BR) under various sky conditions using ground-based measurements at Botucatu in Brazil. Additionally, they also carried out the statistical analysis of hourly and daily SNIR at this site in a later study (Escobedo et al., 2014). Recently, Rossi et al. (2018) was proposed linear regression equation for estimating daily global, daily diffuse and daily direct SNIR as function of daily global, daily diffuse and daily direct BR considering seasonal and cloudy effect. Most of previous models expressed the ratio of SNIR-to-BR as constant values, making their applications being limited. Therefore, semi-empirical SNIR model was an alternative for estimating SNIR. The objective of this work is to develop a more general semi-empirical SNIR model as function of atmospheric constituent affecting SNIR and BR.

4.2 Measurements and data

4.2.1 Ground-based measurements

To formulate the model for calculating global SNIR from global broadband solar radiation (BR) and atmospheric parameters, it is necessary to have global SNIR, global BR and related atmospheric data. In this work, data on global SNIR and global BR were measured at four sites in Thailand namely, Chiang Mai (18.78°N, 98.98°E), Ubon Ratchathani (15.25°N, 104.87°E), Nakhon Pathom (13.82°N, 100.04°E) and Songkla (7.20°N, 100.04°E) and data of these parameters covering the year 2009 – 2013 were collected. At each station, the SNIR and BR are routinely monitored. Global SNIR was measured using a precision spectral pyranometer (Eppley, model PSP) with an RG695 filter which measures a spectral band covering the region 0.695 - 2.80 μm . Kipp&Zonen pyranometer (model cm21) was used to measure a broadband solar radiation. These data from all pyranometers at the four stations were collected in form of voltage signals every second using a Yokogawa datalogger DX2000 model. All voltage signals were converted into near infrared and broadband solar irradiance by dividing sensitivity of the instruments. Then, they were averaged into the hourly data, daily data and monthly average daily data. The hourly data were summed from sunrise to sunset hour for applying in daily model. Similarly, monthly average daily makes on average every day data in each month. All pyranometer were calibrated annually using a traveling pyranometer recently calibrated at the manufacturer.

Aerosol and water vapour were observed from ground-based measurement at four sites in Thailand using Sunphotometer (Cimel, CE318 model). It is the property of our laboratory and part of the AERONET of NASA (Halthore et al., 1997, Holben et al., 1998). Sunphotometer was measured the solar spectral irradiance at wavelengths of 340, 380, 440, 500, 675, 870 and 1020 nm. Then, their data are routinely processed and

annually calibrated by AERONET to provide aerosol optical depth and precipitable water for using in the modeling in this study. The location of the four stations and the instruments are shown in Fig. 19.

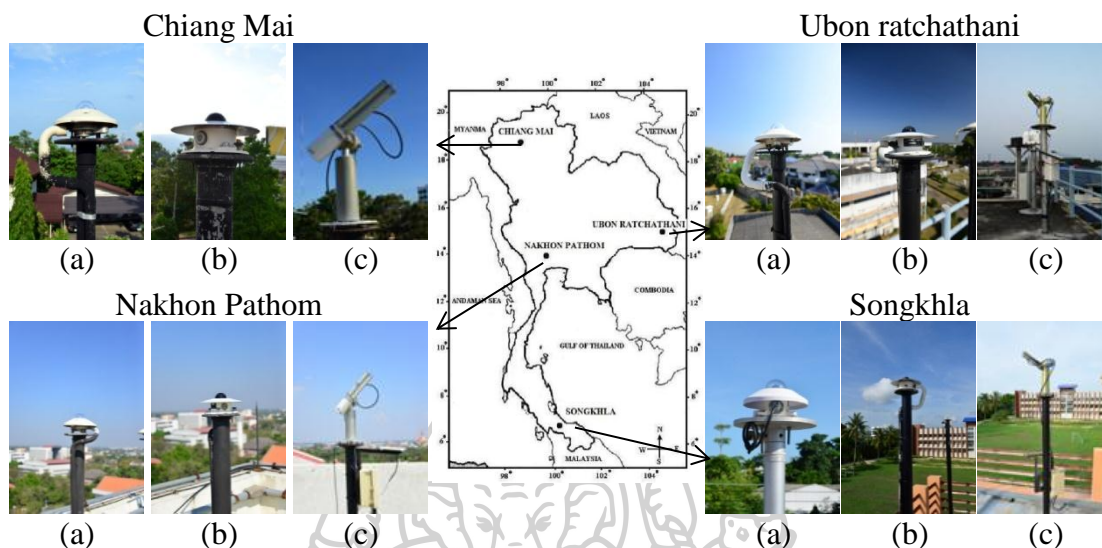


Fig. 19 Installations feature of instruments at 4 sites in Thailand. (a) pyranometer measuring BR, (b) pyranometer measuring SNIR and (c) Sunphotometer.

2.2.2 Satellite data

Cloudiness and ozone data are also required to develop the model of SNIR-to-BR ratios. These parameters were derived from satellite data. Cloudiness is quantified by cloud index (Cano et al., 1986) and it is obtained from the digital data retrieved from the visible channel of the multifunctional transport satellite (MTSAT)-1R satellite encompassing the period 2009-2013. The data are displayed as image covering the entire area of Thailand, with a spatial resolution $3 \text{ km.} \times 3 \text{ km.}$ at each pixel. The satellite images were processed using an Interactive Data Language (IDL) computer program. These images were in satellite projection. Thus, they were transformed to cylindrical projection, being linear in latitude and longitude. Then, the satellite images were navigated using the coastline as a reference. Nine pixels centered at the position of the four solar radiation measuring stations are selected from the images and averaged to represent the gray level of these stations (Fig. 20). Each pixel contains the information in term of digital gray levels varying between 0 and 255. This digital gray level was further converted to pseudo-reflectivity and turn into the earth-atmospheric reflectivity (ρ_{EA}) by calculating with the solar zenith angle of four sites (Janjai et al., 2009). This parameter was related to cloud index(n) as follows:

$$n = \frac{\rho_{EA} - \rho_G}{\rho_c - \rho_{min}} \quad (4.1)$$

where ρ_{EA} , ρ_G and ρ_c are the reflectivity of the earth-atmospheric system, the reflectivity of the ground and the maximum reflectivity of cloud, respectively. The cloud index (n) is an indirect measure of cloudiness through the reflection properties of

the ground, cloud and atmosphere. In the absence of cloud cover, ρ'_{EA} approximates ρ'_G and n is zero. By contrast, in a pixel which is totally covered by cloud, ρ'_c is equal to ρ'_c and n is equal to one. For the case of partly cloudy pixel, the values of n will be in the interval: $0 \leq n \leq 1$.

Total ozone column data from OMI/AURA satellite are also acquired for the study area on a daily basis, encompassing the same period as that of MTSAT-1R data. In this study, the level-3 OMI data with the spatial resolution of 1° latitude \times 1° longitude are used. As these data are daily data, for each day they are assumed to be constant for the whole day.

The data sets consist of ground-based and satellite data encompassing 5 years (2009-2013). They were divided into two datasets, one for the formulation of the model and the other for the model validation. The data period from January 2009 to December, 2012 is used for model development whereas the data period from January to December, 2013 is employed for model validation.

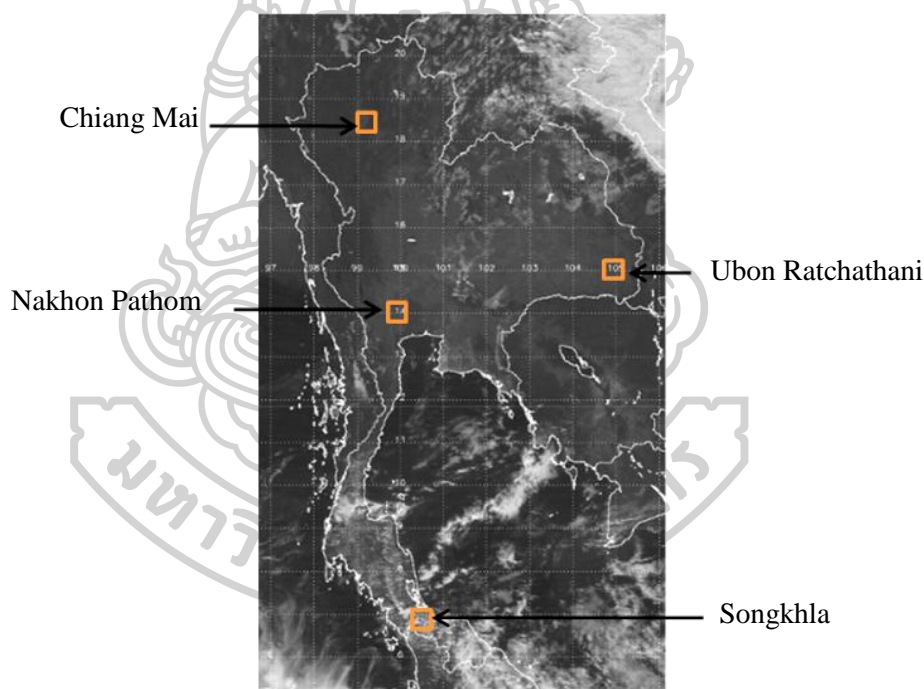


Fig. 20 Example of a satellite image and the position of the pixels selected for calculating cloud index.

4.3 Results and discussions

The models for calculating SNIR proposed in this work were formed into three periods, namely hourly SNIR, daily SNIR and monthly average daily SNIR.

4.3.1 The hourly ratio of SNIR to BR

The models for calculating SNIR in the form of the hourly ratio of SNIR to BR as a function of significantly atmospheric parameter in a semi-empirical formula considers the radiative properties of clouds, aerosols, water vapour, and ozone. There

are the difference in effects of these atmosphere constituents on SNIR and BR. For example, clouds absorb significantly solar radiation in the SNIR band. Aerosols scatter more solar radiation in the short wavelength band than that in the SNIR band. Water vapour also absorbs significantly in the SNIR band. For ozone, it absorbs solar radiation in the visible wavelengths which is part of BR and there is no absorption by ozone in SNIR band. In addition, influence of sun's path, which depends on cosine of zenith angle, also affect to hourly SNIR and hourly BR radiation. With the difference in effects of these atmosphere constituents on SNIR and BR, the model for calculating hourly SNIR in the form of the hourly ratio of SNIR to BR is proposed as follows:

$$\frac{I_{SNIR}}{I_{BR}} = a_0 + a_1 \frac{n}{n_{max}} + a_2 \frac{O_3}{O_{3max}} + a_3 \frac{AOD}{AOD_{max}} + a_4 \frac{w}{w_{max}} \quad (4.2)$$

where I_{SNIR} and I_{BR} are hourly global near infrared irradiation and hourly global broadband solar ($MJ\ m^{-2}\ hr^{-1}$), respectively. $\cos\theta_z$ is cosine of zenith angle (-), n is cloud index(-), O_3 is total ozone column (cm.), AOD is aerosol optical depth at 550 nm.(-), w is precipitable water (cm.), the subscripts "max" refer to maximum value and a_0 , a_1 , a_2 , a_3 and a_4 are empirical coefficients. To obtain the coefficients, Eq.(2) was fitted with the corresponding hourly data collected from the four stations encompassing a period: 2009 – 2012 by using a multi linear regression method (Seber, 1989) and the results are shown in Table 5 All regression coefficients are significant at 95 % with absolute of t-statistic more than ± 2 and $R = 0.51$. A high t-statistic will relate to high correlation and a low probability of the relationship. It determines that all parameters together correlate well with the ratio between SNIR and BR.

Table 5 Values of coefficients of Eq. (4.2) and the corresponding t-statistic.

Coefficients	Values of Coefficient	Standard	t-value
a_0	0.422473	0.006516	64.8382
a_1	-0.042095	0.002328	-18.0815
a_2	0.142213	0.008175	17.3967
a_3	0.135188	0.004354	31.0479
a_4	-0.106771	0.002341	-45.6181

Although, the proposed model was rigorously formulated, it is necessary to validate its performance. To accomplish this, the model was used to calculate SNIR at four stations using input data encompassing the period: January - December, 2013. SNIR calculated from the model was compared to that obtained from the measurements. As these data were not involved in the formulation of the model, they are independent data set. Therefore, these data have merit in the validation. The result is graphically shown in Fig. 21.

From Fig 21, it is observed that most of the calculated SNIR values and measured SNIR values for hourly, daily and monthly average daily are in good agreement, with the discrepancy in terms of root mean square error (RMSD) and mean bias error (MBD) of 2.2 % and 6.7 %, respectively.

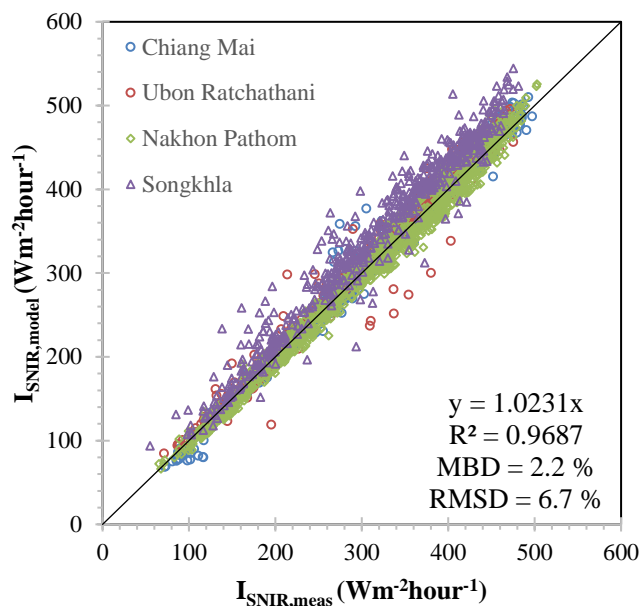


Fig. 21 Comparison between hourly SNIR from the model and that from the measurement.

From Fig. 21, it is observed that most of the calculated SNIR values and measured SNIR values for hourly, daily and monthly average daily are in good agreement, with the discrepancy in terms of root mean square error (RMSD) and mean bias error (MBD) of 2.2 % and 6.7 %, respectively.

The ratio of the proposed model was also compared with that of models available in literatures (Escobedo et al., 2009, 2011), and the results are shown in Table 6. It is observed that the proposed model performance is better than most of the other models. This is likely due to the fact that the proposed model takes cloud, aerosols and water vapour into account, and these atmospheric constituents have important effects of solar radiation in this region, while most of other models do not include these effects. Due to the published models in the past, there are only model for estimating hourly and daily SNIR. Therefore, the proposed monthly average daily model in this work has the advantage of calculating SNIR values to use in many applications.

Table 6 Comparison between hourly SNIR ratio from measurement and those from hourly SNIR ratio model

Model	Type	Ratio	MBD (%)	RMSD (%)
Proposed model	All sky	Eq. (2.2)	1.52	6.85
Escobedo et al. (2009)	$K_T \leq 0.35$ $0.35 < K_T \leq 0.55$ $0.55 < K_T \leq 0.65$ $K_T > 0.65$	0.441 0.461 0.469 0.470	-3.29	9.21
Escobedo et al. (2011)	All sky	0.468	-3.18	8.89

4.3.2 The Daily ratio of SNIR to BR

Numerous SNIR applications were used in form of daily data. Thus, a semi-empirical models for calculating daily SNIR was developed in the form of the daily ratio of SNIR to BR as a function of atmospheric parameters. The model was proposed as follows:

$$\frac{H_{\text{SNIR}}}{H_{\text{BR}}} = b_0 + b_1 \frac{n}{n_{\text{max}}} + b_2 \frac{O_3}{O_{3\text{max}}} + b_3 \frac{\text{AOD}}{\text{AOD}_{\text{max}}} + b_4 \frac{w}{w_{\text{max}}} \quad (4.3)$$

where H_{SNIR} is daily global near infrared irradiation ($\text{MJ m}^{-2} \text{day}^{-1}$), H_{BR} is daily broadband irradiation ($\text{MJ m}^{-2} \text{day}^{-1}$), n is cloud index (-), O_3 is total ozone column (cm.). AOD is aerosol optical depth at 550 nm. (-), w is precipitable water (cm.), the subscripts "max" refer to maximum value and b_0 , b_1 , b_2 , b_3 and b_4 are empirical coefficients. To obtain the coefficients, Eq. (4.3) was fitted with the corresponding daily data collected from the four stations encompassing a period: 2009 - 2012. The value of coefficients is shown in Table 7.

Table 7 Values of coefficients of Eq. (4.3) and the corresponding t-statistic.

Coefficients	Values of Coefficient	Standard	t-value
b_0	0.425382	0.009742	43.6633
b_1	-0.038912	0.003641	-10.6861
b_2	0.149118	0.012176	14.2470
b_3	0.073777	0.005897	12.5106
b_4	-0.105001	0.003641	-28.8348

The model was used to calculate SNIR at four stations using input data encompassing the period: January - December, 2013. SNIR calculated from the model was compared to that obtained from the measurements. As these data were not involved in the formulation of the model, they are independent data set. Therefore, these data have merit in the validation. The result shows in Fig. 22.

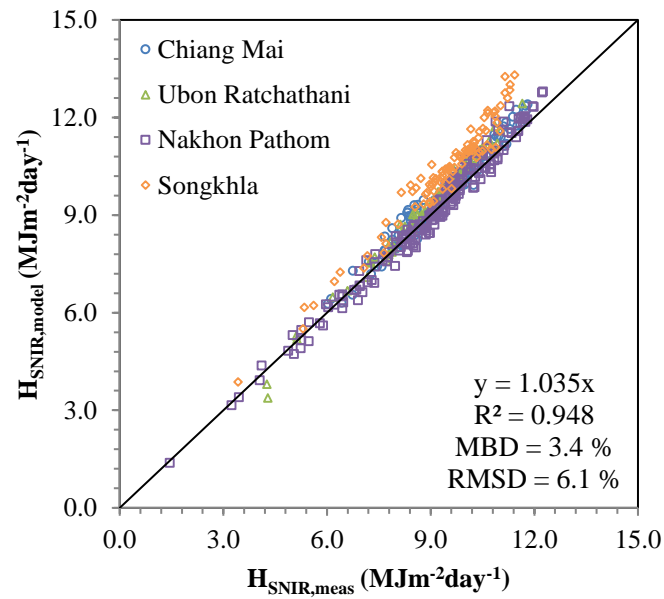


Fig. 22 Comparison between daily SNIR from the model and that from the measurement.

From Fig 22, it is observed that most of the calculated SNIR values and measured SNIR values for hourly, daily and monthly average daily are in good agreement, with the discrepancy in terms of root mean square error (RMSD) and mean bias error (MBD) of 3.4 % and 6.1 %, respectively.

The ratio of the proposed model was also compared with that of models available in literatures (Bolsenga, 1976, Pereira et al., 1982, Escobedo et al., 2009, Escobedo et al., 2011, and Rossi et al., 2018), and the results are shown in Table 8. It is observed that the proposed model performance is better than most of the other models.

Table 8 Comparison between daily SNIR ratio from measurement and those from daily SNIR ratio model

Model	Type	Ratio	MBD (%)	RMSD (%)
Proposed model	All sky	Eq.(4.3)	3.00	5.63
Bolsenga (1967)	Clear sky	0.510	5.95	8.94
Pereira et al. (1982)	Clear sky	0.540	12.19	13.89
Escobedo et al. (2009)	$K_T \leq 0.35$ $0.35 < K_T \leq 0.55$ $0.55 < K_T \leq 0.65$ $K_T > 0.65$	0.440 0.460 0.469 0.475	-3.40	7.86
Escobedo et al. (2011)	All sky	0.469	-2.56	7.14
Rossi et al. (2018)	$K_T \leq 0.35$ $0.35 < K_T \leq 0.55$ $0.55 < K_T \leq 0.65$ $K_T > 0.65$ Summer Autumn Winter Spring Total	0.434 0.450 0.458 0.469 0.488 0.476 0.480 0.451 0.461	-5.46% -3.48	8.90 7.87 7.89

4.3.3 The monthly average daily ratio of SNIR to BR

A semi-empirical model for calculating SNIR in the form of monthly average daily ratio between SNIR and BR as a function of clouds, aerosols, water vapour, and ozone can be written as eq. (4.4).

$$\frac{\overline{H}_{SNIR}}{\overline{H}} = c_0 + c_1 \frac{\overline{n}}{\overline{n}_{max}} + c_2 \frac{\overline{O}_3}{\overline{O}_{3,max}} + c_3 \frac{\overline{AOD}}{\overline{AOD}_{max}} + c_4 \frac{\overline{w}}{\overline{w}_{max}} \quad (4.4)$$

where \overline{H}_{SNIR} and \overline{H}_{BR} are monthly average daily global near infrared irradiation ($MJ m^{-2} month^{-1}$), and monthly average daily global broadband irradiation, respectively. \overline{n} is monthly average cloud index (-), \overline{O}_3 is monthly average total ozone column (cm.). \overline{AOD} is monthly average aerosol optical depth at 550 nm. (-), \overline{w} is monthly average precipitable water (cm.), the subscripts "max" refer to maximum value and c_0 , c_1 , c_2 , c_3 and c_4 are empirical coefficients. The corresponding daily data collected from the four stations encompassing a period: 2009 – 2012 was fitted to obtain the coefficients of Eq. (4.4). The results are shown in Table 9.

Table 9 Values of coefficients of eq. (4.4) and the corresponding t-statistic.

Coefficients	Values of Coefficient	Standard	t-value
c_0	0.373570	0.030390	12.29273
c_1	-0.024634	0.009320	-2.64315
c_2	0.205888	0.039350	5.23222
c_3	0.032981	0.008556	3.85454
c_4	-0.109125	0.011579	-9.42406

The model was used to calculate SNIR at four stations using input data encompassing the period: January - December 2013. SNIR calculated from the model was compared to that obtained from the measurements. As these data were not involved in the formulation of the model, they are independent data set. Therefore, these data have merit in the validation. The result is shown in Fig. 23.

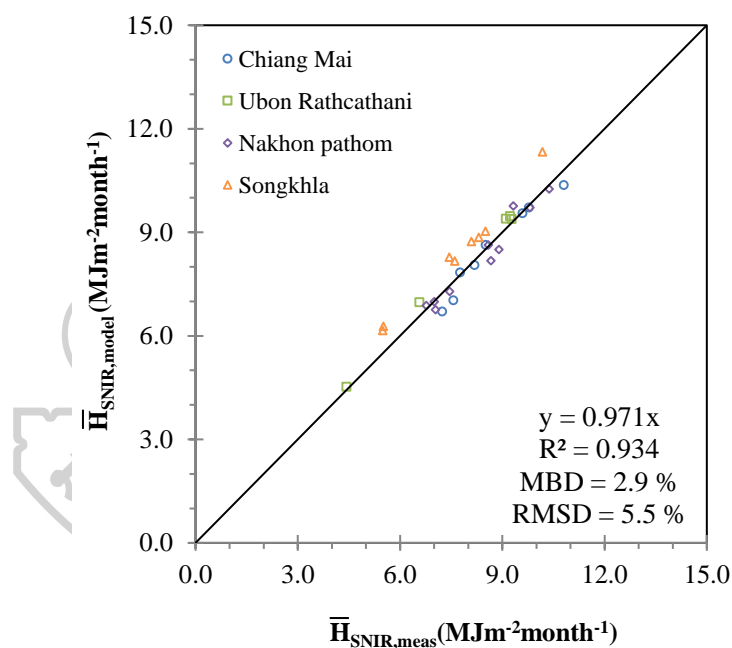
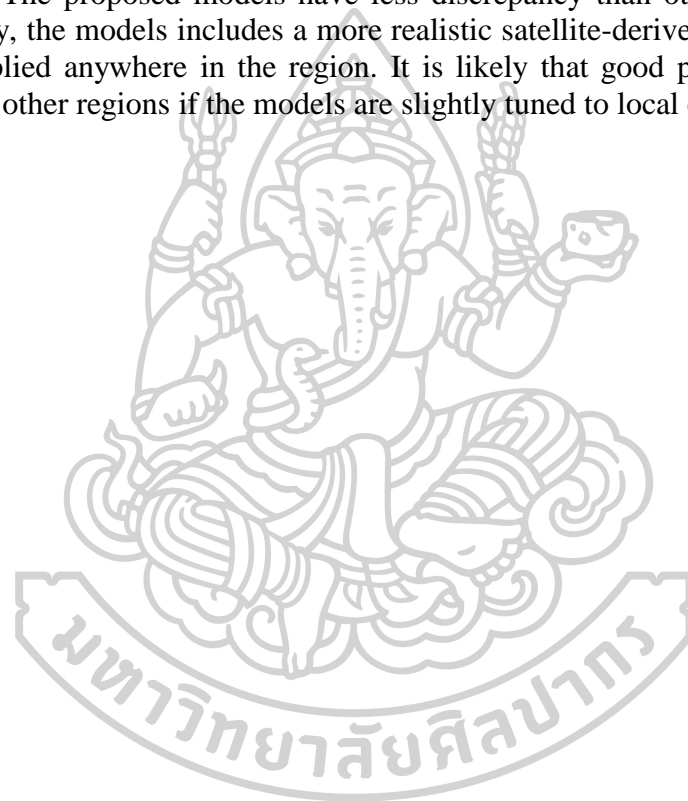


Fig. 23 Comparison between monthly average daily SNIR from the model and that from the measurement.

From Fig 23, it is observed that most of the calculated SNIR values and measured SNIR values for monthly average daily are in good agreement. The ratio of the proposed model is also in good agreement with the discrepancy in terms of root mean square error (RMSD) and mean bias error (MBD) of 2.9 % and 5.5 %, respectively.

4.4 Conclusions

The models for estimating SNIR in the form of ratios between SNIR and BR has been developed. According to the model, the ratio of SNIR-to-BR is expressed as a function of the precipitable water, aerosol optical depth, total ozone column and cloud index. Precipitable water and aerosol optical depth data are obtained from ground-based measurements whereas the values of total ozone column and cloud index were derived from satellite data. All input parameters of the model have significant impact on the predictability of the model. The model is used to estimate SNIR at four sites in the tropical environment of Thailand. Values of SNIR estimated from the model and those obtained from the measurements for the combined data from the four sites are in good agreement. The proposed models have less discrepancy than other existing models. Additionally, the models includes a more realistic satellite-derived cloud index which may be applied anywhere in the region. It is likely that good performances will be achieved in other regions if the models are slightly tuned to local environment.



Chapter 5

The statistical characteristics of solar near infrared radiation in Thailand

5.1 Introduction

The solar near infrared radiation received at the earth's surface is subjected to diurnal, seasonal and annual variations. Moreover, the amount of SNIR incident at the surface under all sky conditions varies with location and atmospheric conditions. Water vapour and clouds are main atmospheric parameters, which absorb significantly solar radiation in near infrared band. There is less solar near infrared radiation received on horizontal plane under overcast sky than that obtained under clear sky due to the effect of clouds (Iqbal, 1983). Therefore, it is necessary to characterize the distributions of solar near infrared radiation for the whole day and over the year. In this chapter, the global and diffuse solar near infrared radiation collected from ground-based meteorological stations, namely Chiang Mai (CM, 18.78°N, 98.98°E), Ubon Ratchathani (UB, 15.25°N, 104.87°E), Nakhon Pathom (NP, 13.82°N, 100.04°E) and Songkhla (SK, 7.20°N, 100.60°E) during the year of 2009-2017 were statistically analyzed. Then, the diurnal and seasonal variations of global and diffuse solar near infrared irradiance were investigated and presented in terms of monthly average hourly and long-term monthly average data. In addition, the statistical distributions of long-term hourly global and diffuse solar near infrared irradiance were also demonstrated.

5.2 Diurnal variation

A. Global solar near infrared radiation

A pyranometer equipped with RG695 filter was used to measure global solar near infrared radiation or global SNIR (0.695 – 2.8 μm) every second. These instantaneous data were averaged to obtain hourly global SNIR in W/m^2 from 5 AM to 7 PM. Then, the global SNIR of each hour was averaged to obtain a long-term monthly average hourly data and presented as the diurnal variation of each month during the year of 2009 - 2017. The diurnal variations of global SNIR for Chiang Mai, Ubon Ratcha Thani, Nakhon Pathom and Songkhla representing the four main regions of Thailand are shown in Fig. 24 - 27, respectively.

From the figures, as expected, the monthly average hourly global SNIR at a given location increased from sunrise to a maximum at noon and decreased to minimum value at the sunset. Thus, the diurnal variations were relatively symmetry around noon time. The maximum value was observed on March around midday of about $400 \text{ w}/\text{m}^2$ for all stations. A standard deviation (SD) shown as error bar in the figure was found to be low in the dry season (November-April) at Chiang Mai, Ubon Ratchathani and Nakhon Pathom. Whereas in the wet season, the standard deviation was higher than the dry season due to the effect of a cloud dynamics influencing by the southwest monsoon in Thailand. For Songkhla station, the standard deviation of global solar near infrared irradiance was found to be high for the whole year because Songkhla station is located

in the southern part of Thailand and has the rainy season lasting for 8 months per year. Therefore, Clouds and rainfall affect highly the fluctuation of global SNIR in this region.

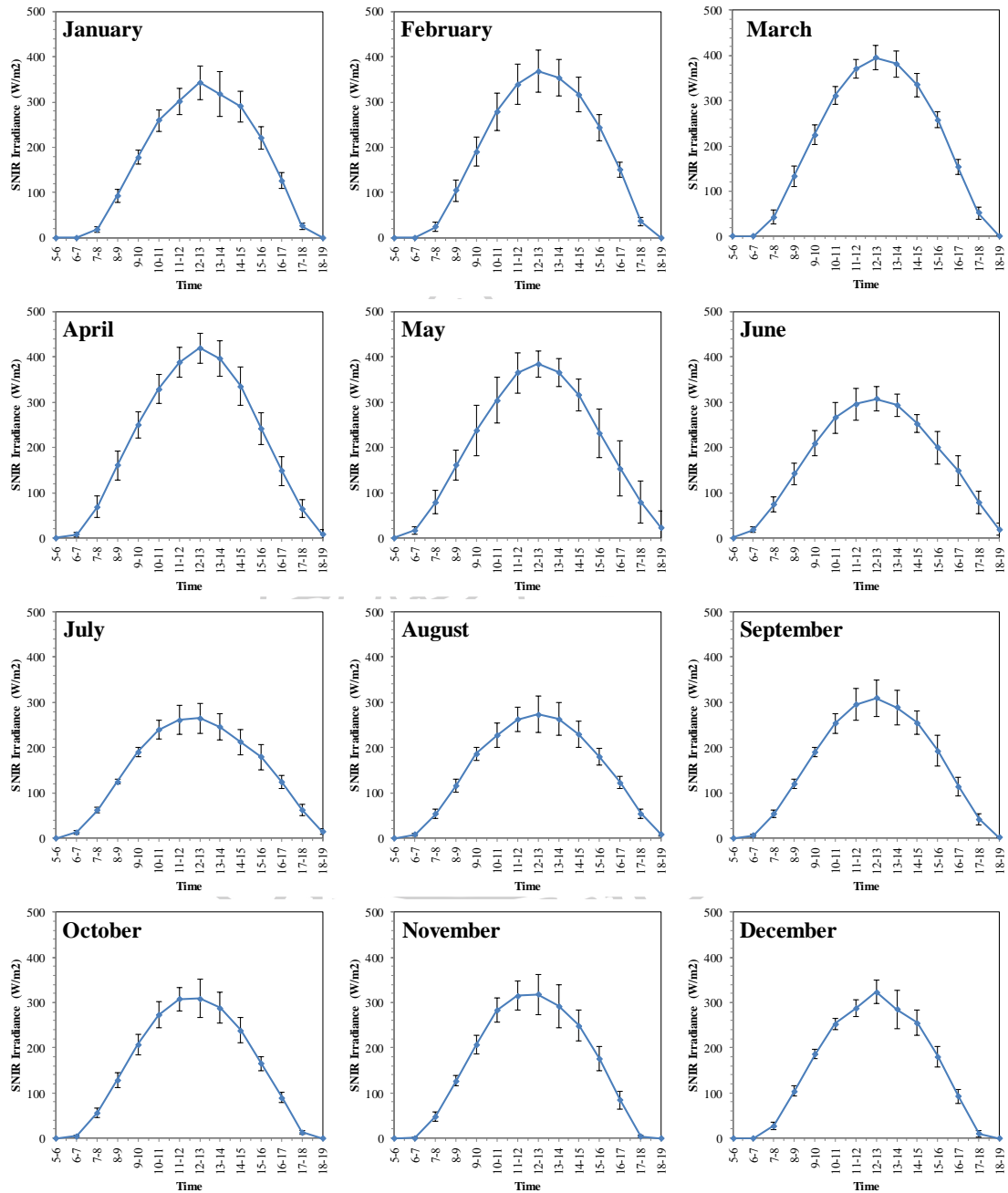


Fig. 24 The variation of monthly average hourly global solar near infrared radiation under all sky condition at Chiang Mai station. [error bar ± 1 standard deviation, SD]

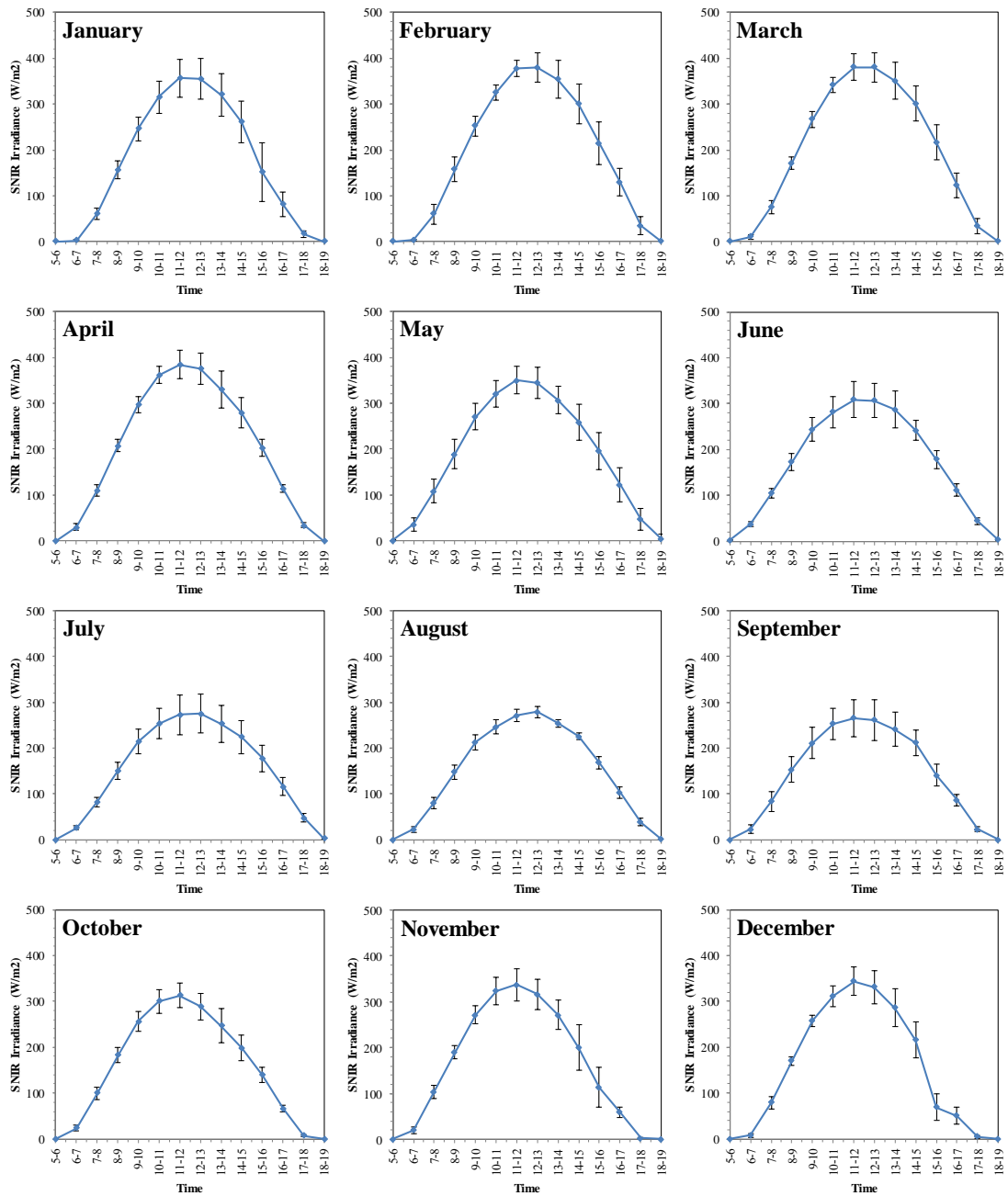


Fig. 25 The variation of monthly average hourly global solar near infrared radiation under all sky condition at Ubon Ratchathani station. [error bar ± 1 standard deviation, SD]

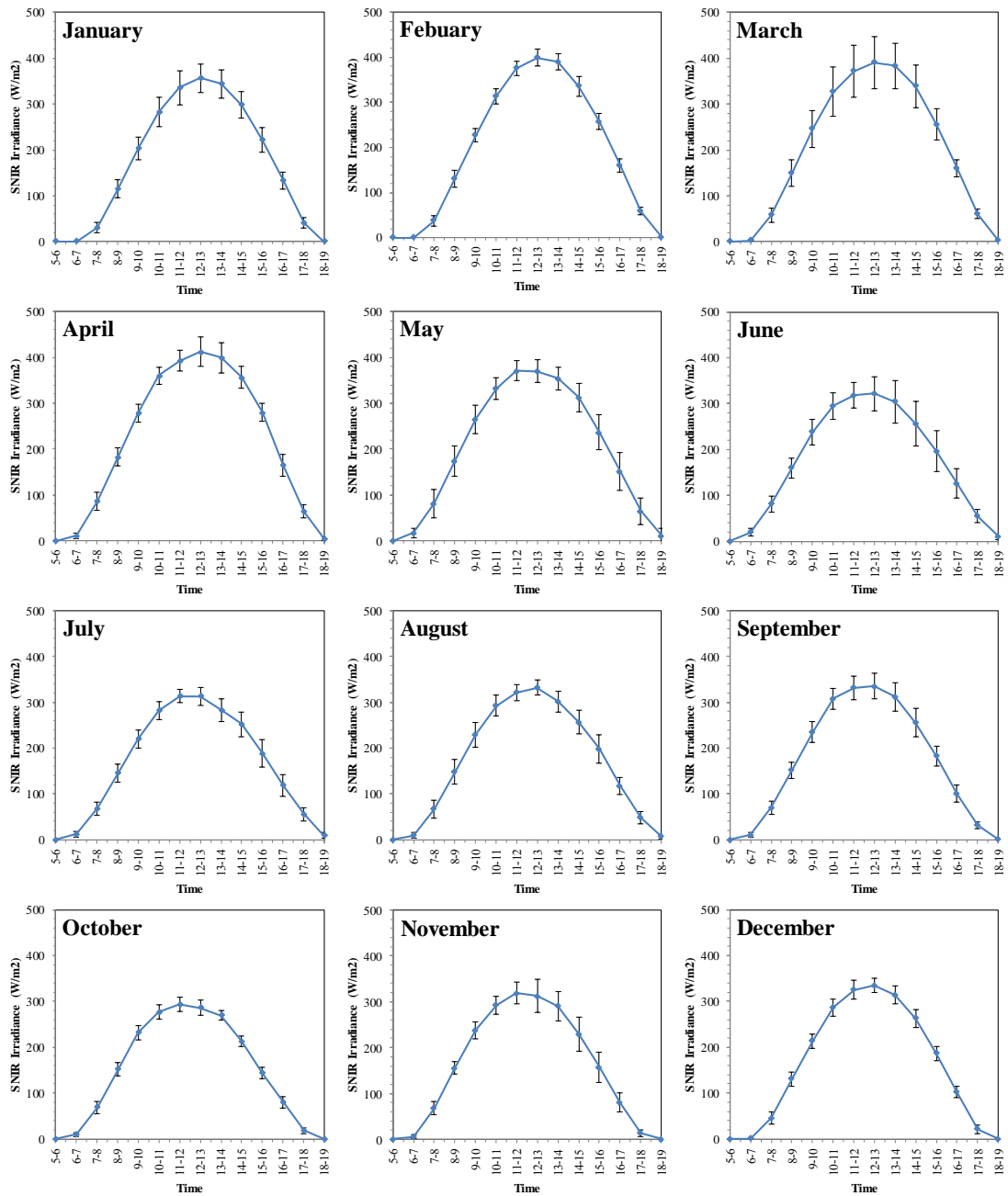


Fig. 26 The variation of monthly average hourly global solar near infrared radiation under all sky condition at Nakhon Pathom station. [error bar ± 1 standard deviation, SD]

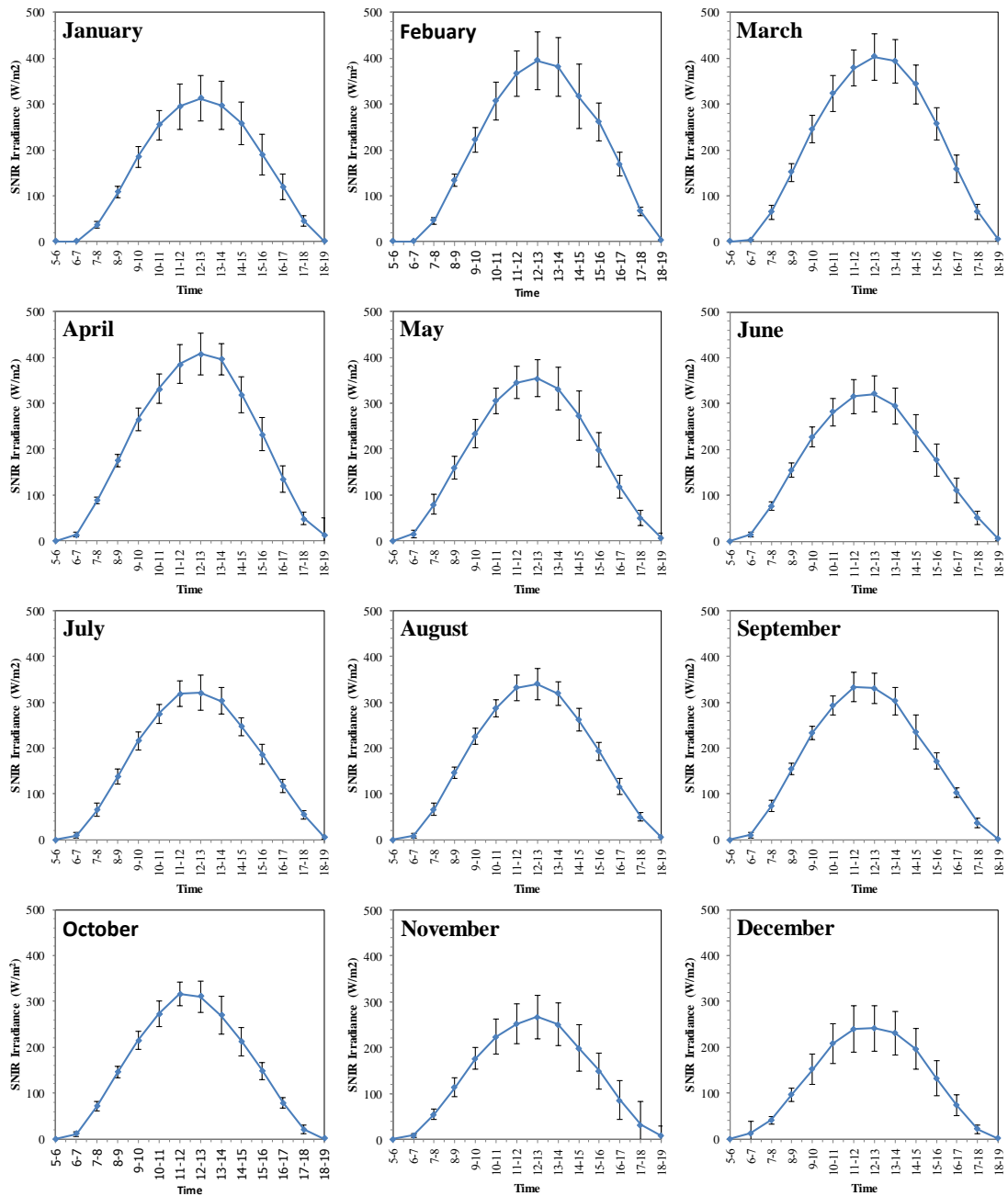


Fig. 27 The variation of monthly average hourly global solar near infrared radiation under all sky condition at Songkhla station. [error bar ± 1 standard deviation, SD]

B. Diffuse solar near infrared radiation

The variation of diffuse solar near infrared radiation incident on the Earth's surface depends on the sun's path, geography and atmospheric constituents at that location. Diffuse solar near infrared radiation is generated by the scattering effect of clouds, water vapour and aerosol. In the case of overcast sky, only diffuse SNIR was incident on the surface due to the scattering of SNIR by clouds. But under clear sky, the SNIR is split into two parts such as direct SNIR and diffuse SNIR, which is scattered by air molecules and aerosol. Therefore, the portion of diffuse radiation under clear sky condition is less than that obtained under overcast sky. In this section, the diffuse SNIR measured by using the pyranometer equipped with RG695 filter installed on a sun tracker together with a shading ball was investigated for four monitoring stations. The diurnal variations of monthly average hourly diffuse SNIR in W/m^2 were presented in Fig. 28 - 31.

The resultant plots showed that the monthly average hourly diffuse SNIR was gradually increased from the morning to the maximum at noon and also gradually decreased to the minimum in the evening. It was also observed that the highest monthly average hourly SNIR was in June for Chiang Mai, in July for Ubon Ratchathani and Nakhon Pathom, while the highest SNIR was occurred in August for Songkhla station. This is because of more clouds and water vapour in the wet season (May-October). The standard deviation (SD) of the diffuse SNIR for these stations varied quite much during the rainy season or between May to October. Whereas, the diffuse SNIR from the sun collected in the dry season (Nov - April) demonstrated the less fluctuation on the SD. However, for Songkhla, it was found that the variation of diffuse SNIR was high throughout the year due to more occurrences of cloud and rain than other regions.

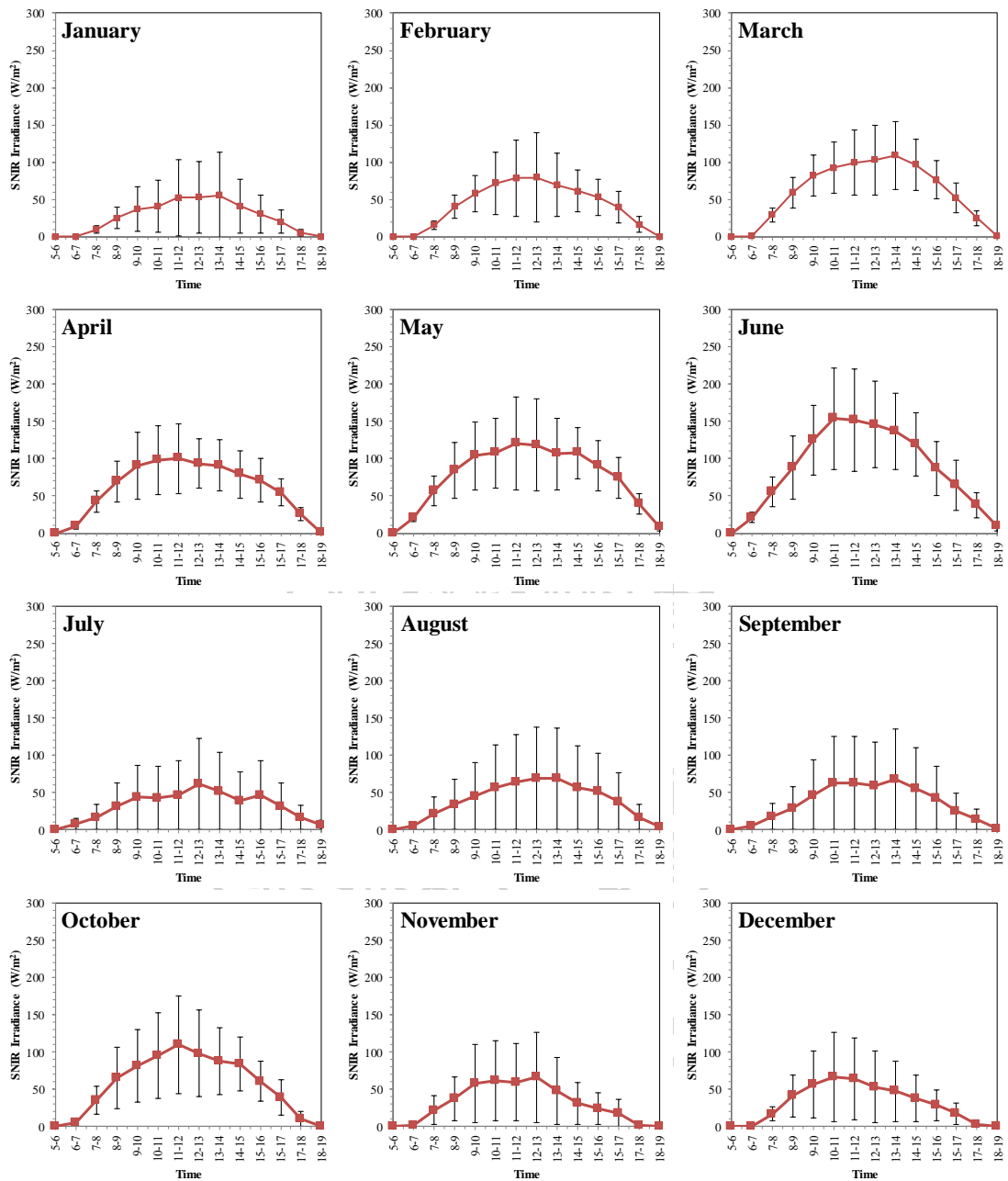


Fig. 28 The variation of monthly average hourly diffuse solar near infrared radiation under all sky condition at Chiang Mai station. [error bar ± 1 standard deviation, SD]

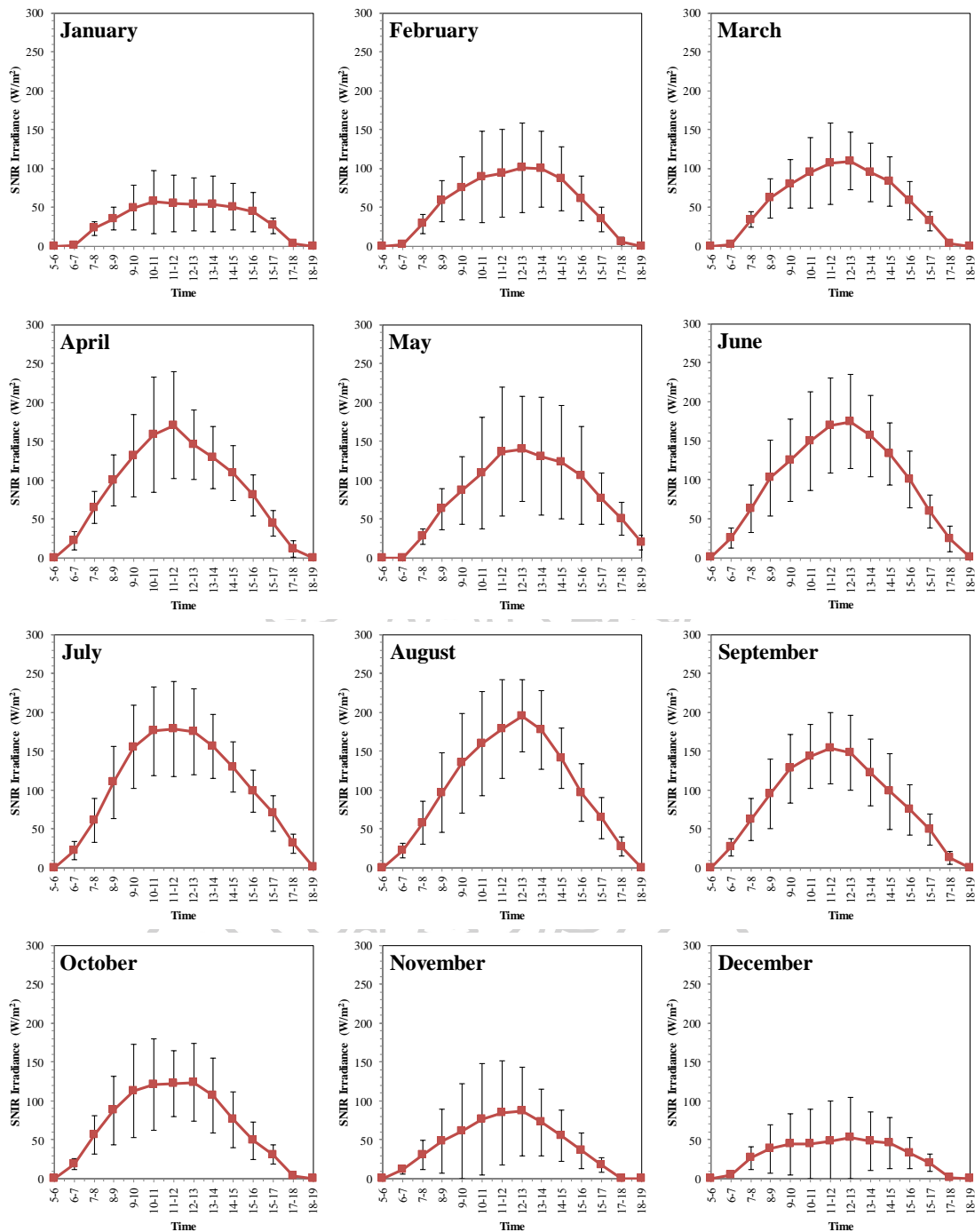


Fig. 29 The variation of monthly average hourly diffuse solar near infrared radiation under all sky condition at Ubon Ratchathani station. [error bar ± 1 standard deviation, SD]

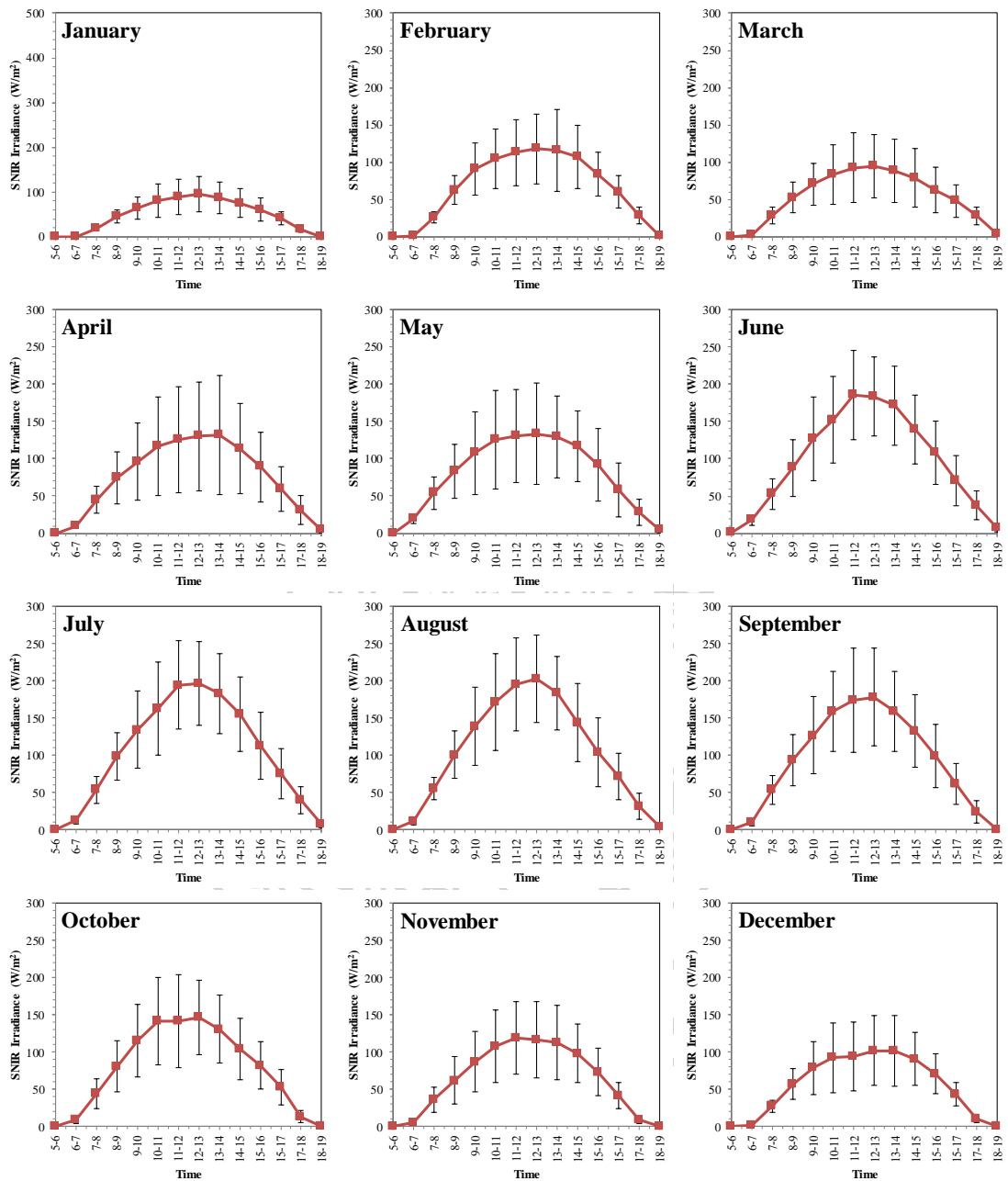


Fig. 30 The variation of monthly average hourly diffuse solar near infrared radiation under all sky condition at Nakhon Pathom station. [error bar ± 1 standard deviation, SD]

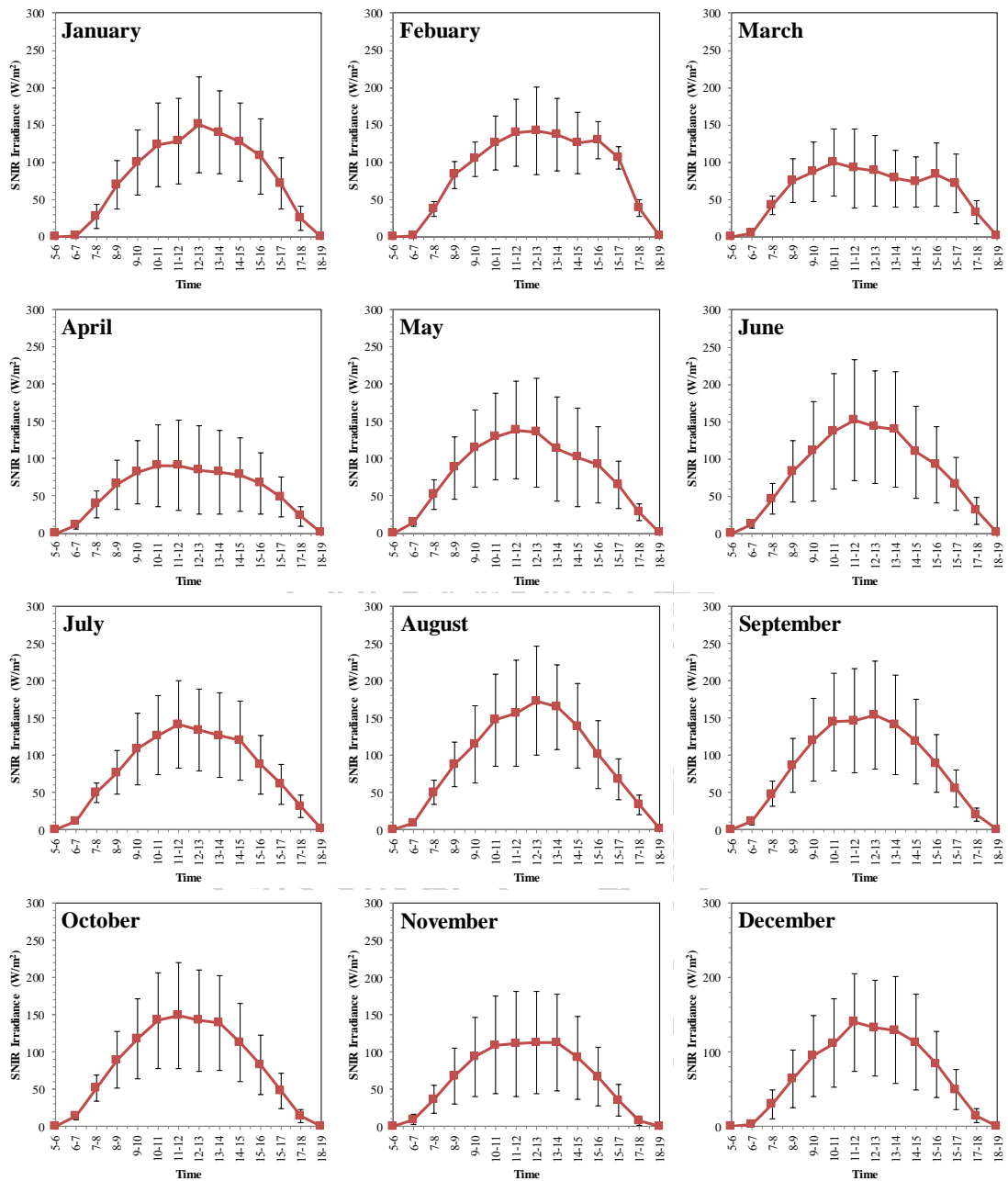


Fig. 31 The variation of monthly average hourly diffuse solar near infrared radiation under all sky condition at Songkhla station. [error bar ± 1 standard deviation, SD]

5.2 Seasonal variation

A. Global solar near infrared radiation

The intensity of solar near infrared radiation (SNIR) varies throughout the year due to the change of solar path length or solar declination. The knowledge of a seasonal variation of SNIR is useful for many solar applications. Therefore, in this section, a daily global solar near infrared irradiance from four ground-based monitoring stations was averaged into a monthly average daily solar near infrared irradiance in a unit of MJ/m²-day. The seasonal evolution of monthly average value of SNIR during January 2009 to December 2017 with the standard error for the four stations were plotted and presented in Fig. 32 – 35.

For the north of Thailand, Chiang Mai station, the amount of monthly average daily global SNIR was the lowest in December with 7.1 MJ/m²-day and gradually increased to the highest value in April with 10.2 MJ/m²-day. The yearly average global SNIR at Chiang Mai was found to be 8.3 MJ/m²-day. For Ubon Ratchathani located in the northeast region, the yearly average value of global SNIR was 8.2 MJ/m²-day. Monthly average global SNIR varied from January to the maximum intensity in September with 6.8 MJ/m²-day. In case of Nakhon Pathom at the central part of Thailand, the variation of global SNIR had a same trend as Ubon Ratchathani that it increased from January to the highest SNIR in April of 10.6 MJ/m²-day and then decreased to the lowest value of 7.3 MJ/m²-day in October. The yearly average of the global SNIR was found to be 8.7 MJ/m²-day. Statistical characteristics of Songkhla station in the southern part of Thailand was quite different from the other due to a small solar incident angle and cloud dynamic affecting the incoming SNIR. Monthly average daily SNIR was a bit changing in each month compared to other stations. The maximum monthly average value was 10 MJ/m²-day in April and the minimum SNIR was in December with 6.0 MJ/m²-day. The average of global SNIR throughout the year of this station was 8.3 MJ/m²-day.

According to the results, we found that the seasonal variation during the year of Chiang Mai, Ubon Ratchathani and Nakhon Pathom showed quite similar variations. The monthly average global SNIR relatively increased to the highest in April because the sun's path slightly drifts into the celestial equator. In addition, rainfall and cloud cover were low in the dry season. Consequently, most areas of Thailand were significantly received high SNIR. Influence of the southwest monsoon covered over Thailand affected to high rainfall and cloud cover, SNIR lightly reduced encompassing May – October representing the wet season. It might also conclude that the monthly average daily SNIR was high in the dry season with the maximum value in April, and vice versa in the wet season. In the period of November – January was covered by the northwest monsoon, which gives clear sky condition in the North, Northeast and Central regions. Additionally, the path of the sun gradually drifts southward of sky celestial equator during that time. Therefore, SNIR on most parts of the country was relatively low during these months. However, for the southern region, there was still a

lot of clouds and rains due to the northeast monsoon passed through the Gulf of Thailand and head to the south. Thus, it led to a slightly decrease of global SNIR.

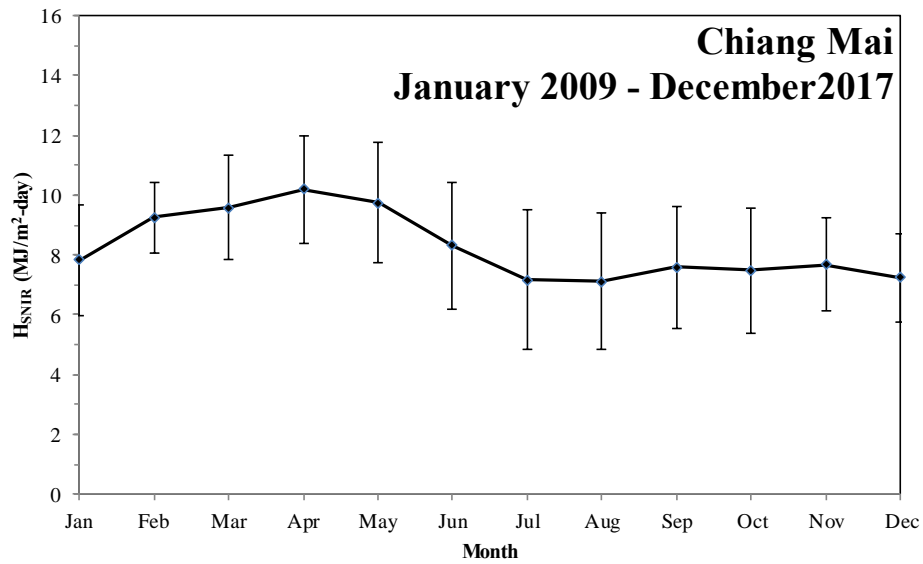


Fig. 32 Variation of global SNIR (H_{SNIR}) during the year at Chiang Mai station.

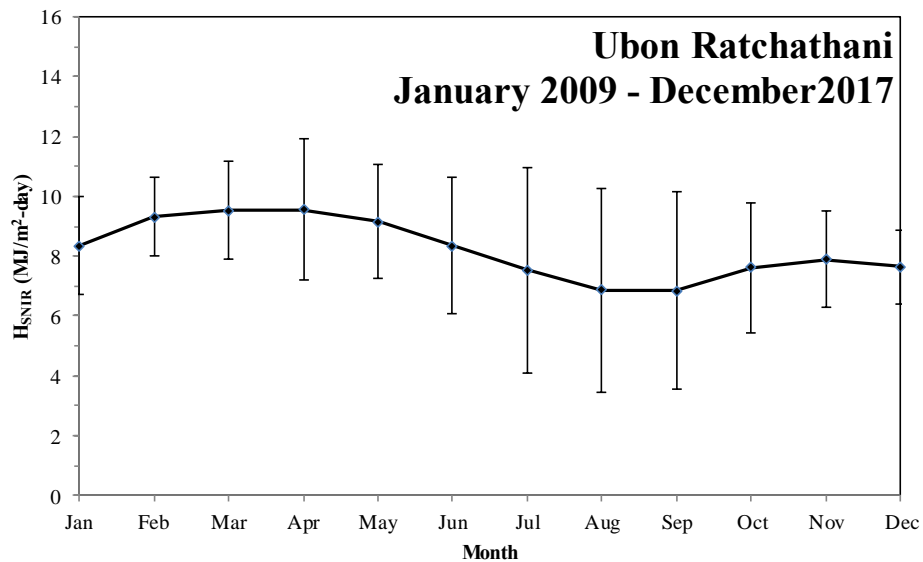


Fig. 33 Variation of global SNIR (\bar{H}_{SNIR}) during the year at Ubon Ratchathani station.

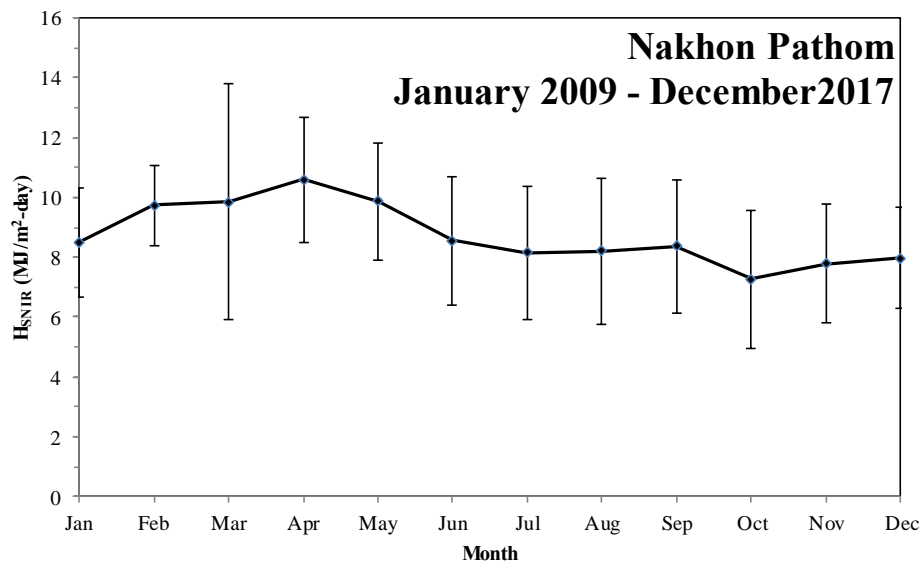


Fig. 34 Variation of global SNIR (\bar{H}_{SNIR}) during the year at Nakhon Pathom station.

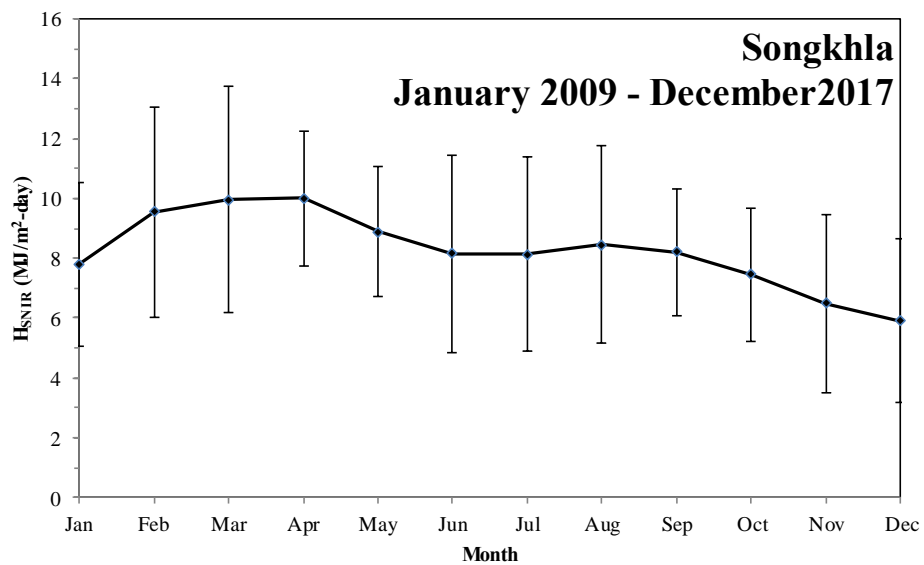


Fig. 35 Variation of global SNIR (\bar{H}_{SNIR}) during the year at Songkhla station.

B. Diffuse solar near infrared radiation

Measured diffuse solar near infrared radiation or diffuse SNIR varies with the season due to a changes in the solar declination and meteorological conditions. In this section, the monthly average daily diffuse SNIR was calculated in the form of energy in MJ/m²-day and analyzed. The seasonal evolution of diffuse SNIR are shown in Fig. 36 - 39.

For Chaing Mai, Ubon Rathcthani and Nakhon Pathom, the amount of diffuse monthly average of daily SNIR was the lowest in January with the values of 1.3, 1.6 and 2.4 MJ/m²-day, respectively. The highest diffuse SNIR was in July with approximately 5.0 MJ/m²-day. The average diffuse SNIR throughout the year were 3.1, 3.4 and 3.7 MJ/m²-day for Chaing Mai, Ubon Ratchathani and Nakhon Pathom stations, respectively.

In case of Songkla station, the variation of diffuse SNIR was different from the others due to longer period of the rainy season, which cloud occurrence has much influence on diffuse SNIR. Monthly average daily diffuse SNIR was a bit changed in each month. Therefore, the amount of diffuse SNIR was relatively high throughout the year with the average of 3.7 MJ/m²-day. The maximum SNIR was 4.4 MJ/m²-day in August and the minimum SNIR was in April (2.7 MJ/m²-day).

From the resultant characteristics, we found that the seasonal variations of monthly average daily diffuse SNIR for Chiang Mai, Ubon Ratchathani and Nakhon Pathom were quite similar patterns. The diffuse SNIR relatively increased to the highest in July because the rainfall and cloud cover were high in rainy season, while diffuse SNIR in the period of November – January was relatively low due to less cloud cover. However, for the southern region, there was still a lot of clouds and rainfall, which led to a slightly increase in diffuse SNIR.

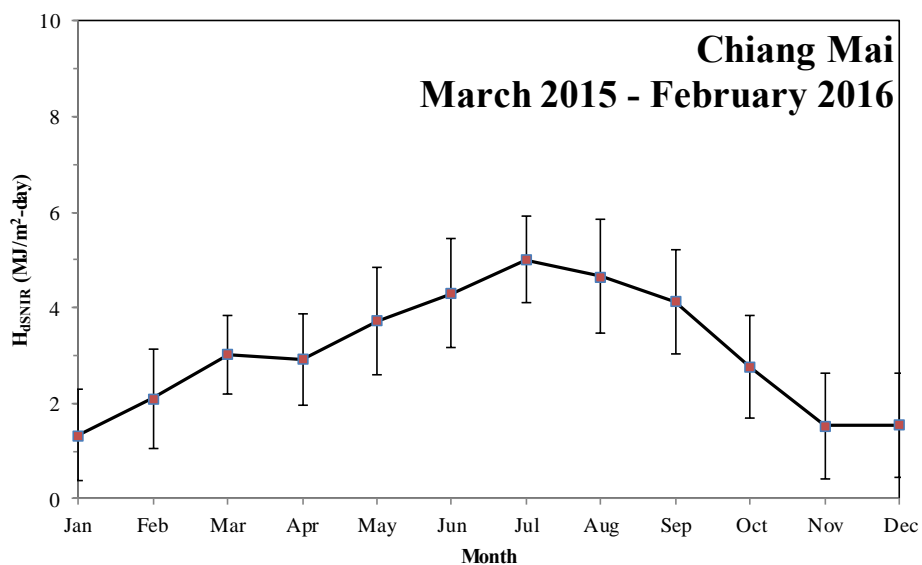


Fig. 36 Variation of diffuse SNIR (\bar{H}_{dSNIR}) during the year at Chiang Mai station.

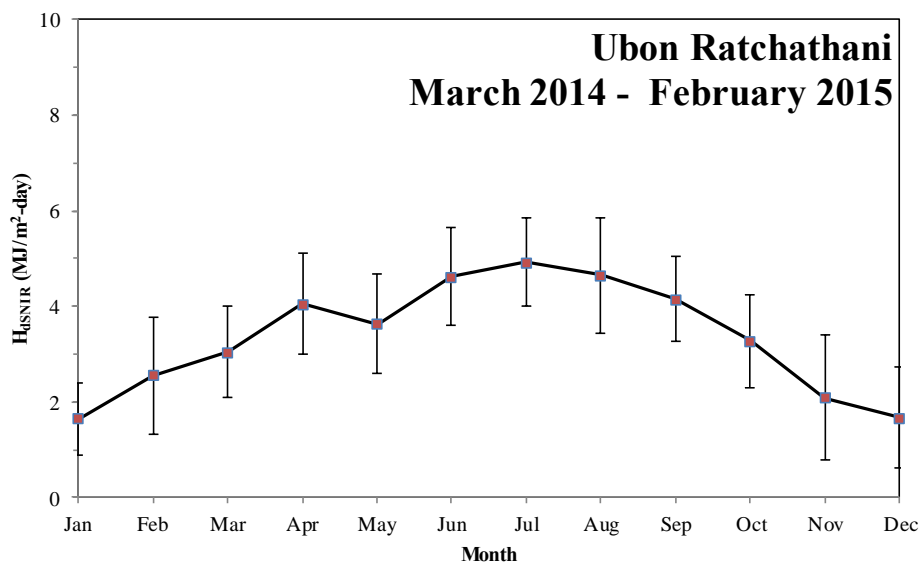


Fig. 37 Variation of diffuse SNIR (\bar{H}_{dSNIR}) during the year at Ubon Ratchathani station.

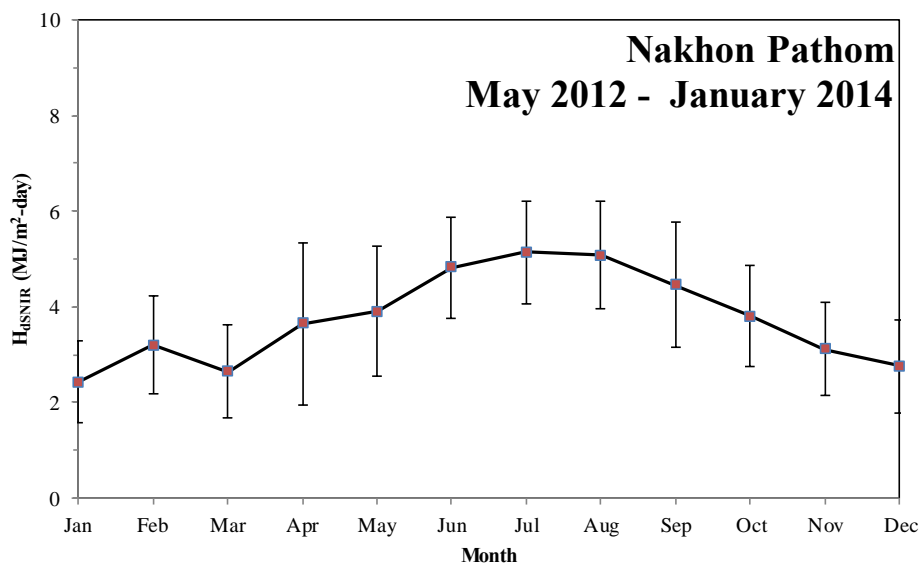


Fig. 38 Variation of diffuse SNIR (\bar{H}_{dSNIR}) during the year at Nakhom Pathom station.

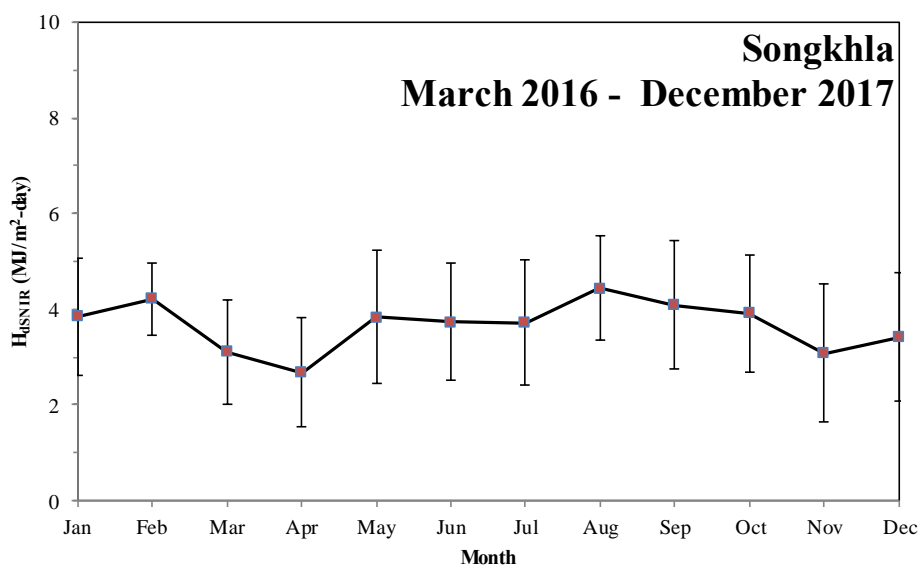


Fig. 39 Variation of diffuse SNIR (\bar{H}_{dSNIR}) during the year at Songkhla station.

5.3 Distributions of hourly solar near infrared radiation

A. Global solar near infrared radiation

In case of clear sky condition, the global solar near infrared radiation changes and its diurnal variation is demonstrated by gradually increasing from the morning until the highest at noon and gradually decreasing continuously until the evening. However, under cloudy sky conditions, SNIR was disturbed by the effect of clouds and causes the infrared radiation intensity from the sun to be lower than it should have received. Therefore, the solar infrared radiation under cloudy sky conditions, which were most frequent sky conditions, was important for the further utilization.

In this section, the measured hourly SNIR data from four stations during the year of 2009 to 2017 was analyzed as a percentage of the global SNIR and presented as a histogram. These histograms showed the frequency distributions of hourly global SNIR in various ranges and months for the whole year. The results are shown in Fig. 40 – 43.

From these resulting figures, most of hourly global SNIR for each month was in the range of 0 – 100 W/m² with the frequency varied between about 38 – 55%. The highest value of SNIR, higher than 400 W/m², was found in April, which are 19.9%, 16.9%, 18.7% and 22.4% for Chiang Mai, Ubon Ratchathani, Nakhon Pathom and Songkhla station, respectively.

In addition, the amount of hourly global SNIR from each station for all months during the year 2009 - 2017 was also investigated and then demonstrated in Fig 44. The histogram showed the similar frequency distribution to the distribution of each month. The maximum frequency of hourly SNIR was in the range of 0-100 W/m² within 40.4 % - 45.5 % for all stations. The maximum hourly SNIR being higher than 400 W/m² has the frequency distribution between 5.1% - 8.0% and the highest frequency occurred at Nakhon Pathom station located in the central part of Thailand.

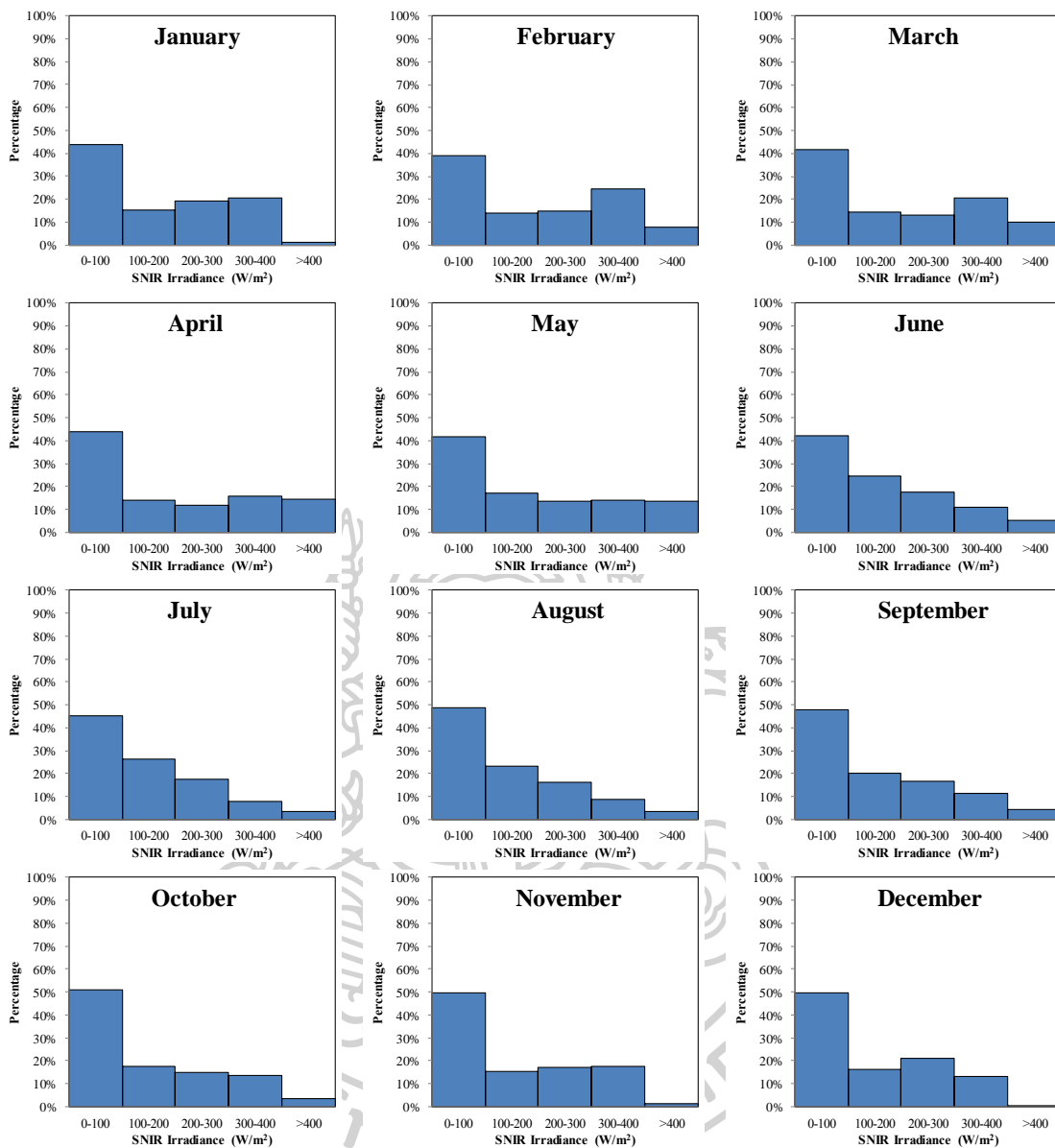


Fig. 40 The statistical distributions of hourly global SNIR for each month at Chiang Mai station.

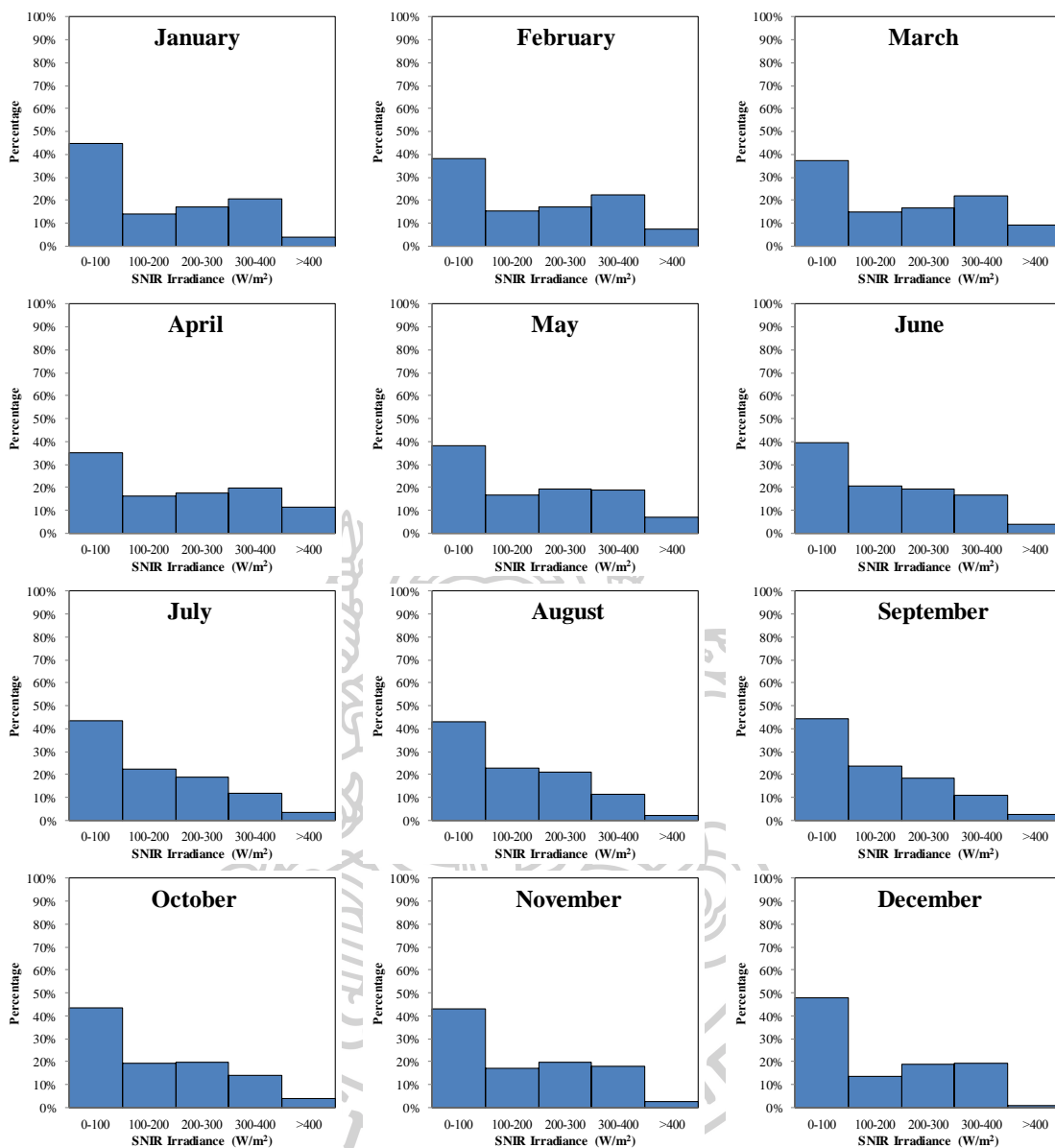


Fig. 41 The statistical distributions of hourly global SNIR for each month at Ubon Rathchani station.

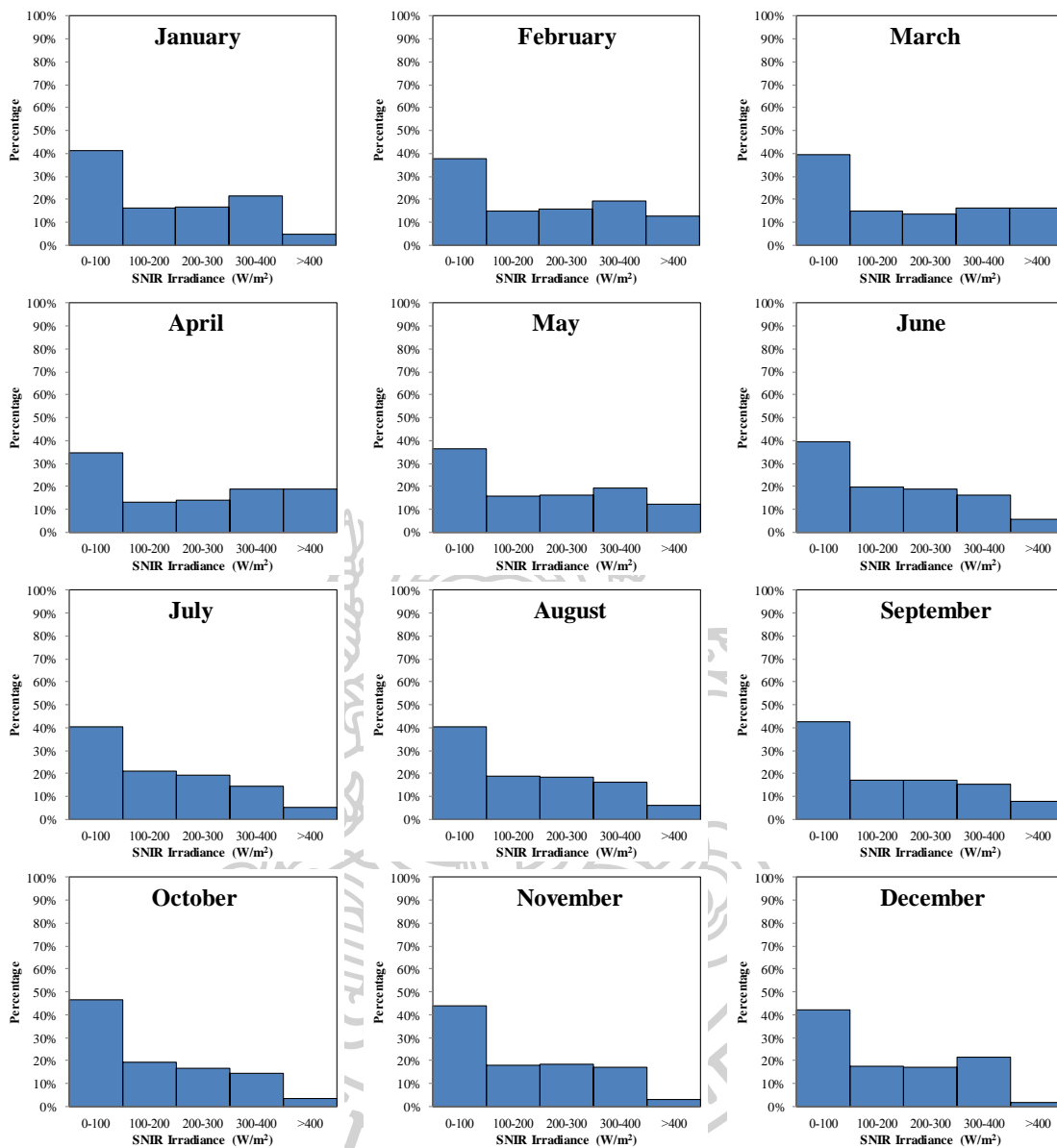


Fig. 42 The statistical distributions of hourly global SNIR for each month at Nakhon Pathom station.

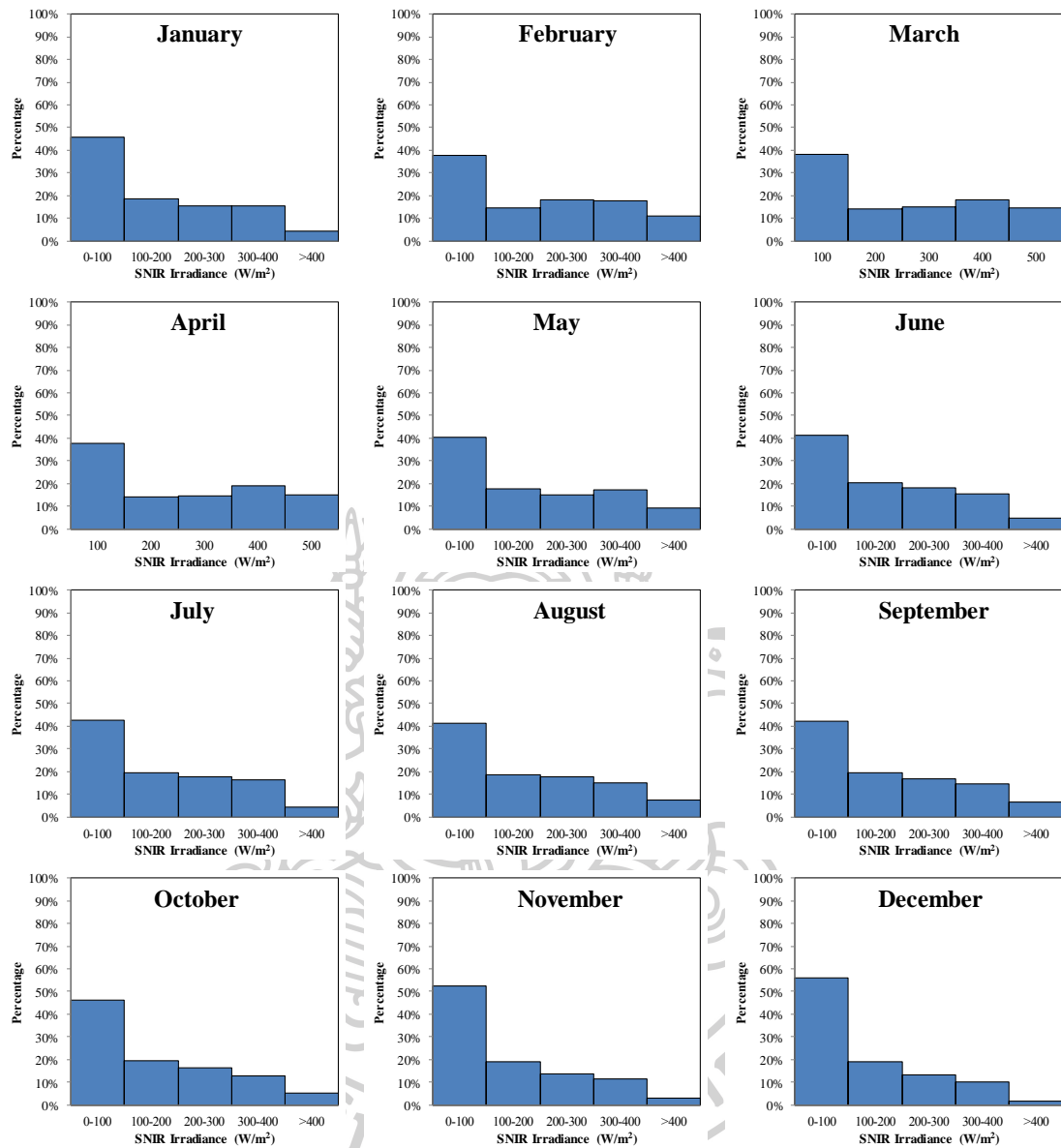


Fig. 43 The statistical distributions of hourly global SNIR for each month at Songkhla station.

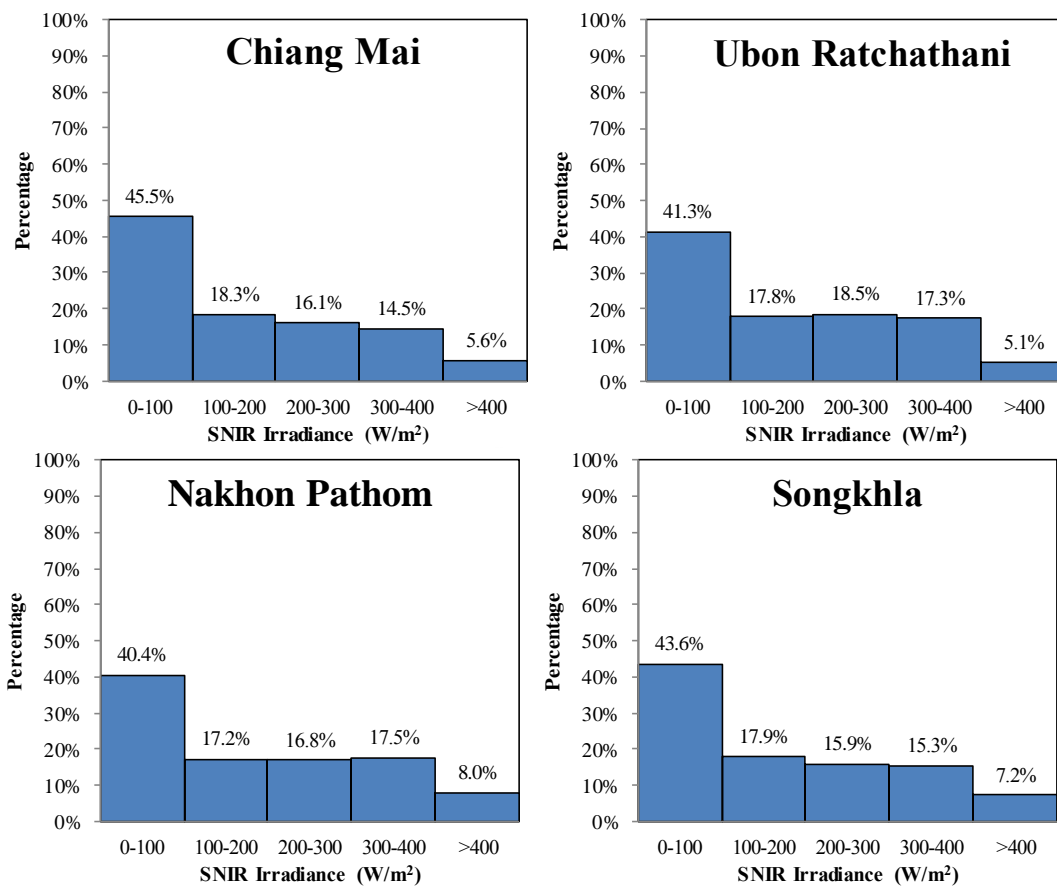
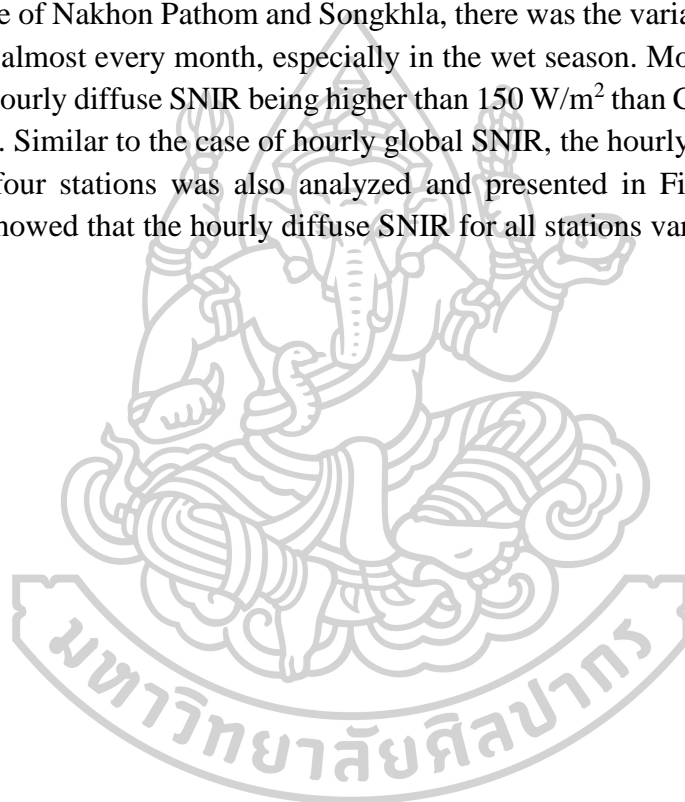


Fig. 44 The statistical distributions of hourly global SNIR for all month at Chiang Mai, Ubon Ratchathani, Nakhon Pathom and Songkhla station.

B. Diffuse solar near infrared radiation

In general sky conditions, diffuse SNIR was scattered by clouds, which can attenuate diffuse SNIR. Therefore, it is necessary to investigate the distribution of hourly diffuse SNIR. In this section, measured hourly diffuse solar near infrared radiation data during 2009 - 2012 was analyzed as a percentage of the irradiance intensity range. The distributions of the diffuse SNIR for four stations are shown in Fig. 45 – 48.

From the histogram of Chiang Mai station and Ubon Ratchathani, the most of hourly diffuse SNIR was in the range less than 50 W/m^2 in dry season and showed small variations of frequency for all ranges in the wet season, caused by clouds and rains. In case of Nakhon Pathom and Songkhla, there was the variation of diffuse SNIR distribution almost every month, especially in the wet season. Moreover, both stations have more hourly diffuse SNIR being higher than 150 W/m^2 than Chiang Mai and Ubon Rathathani. Similar to the case of hourly global SNIR, the hourly diffuse SNIR for all months of four stations was also analyzed and presented in Fig. 49. The resulting histogram showed that the hourly diffuse SNIR for all stations varied in every range.



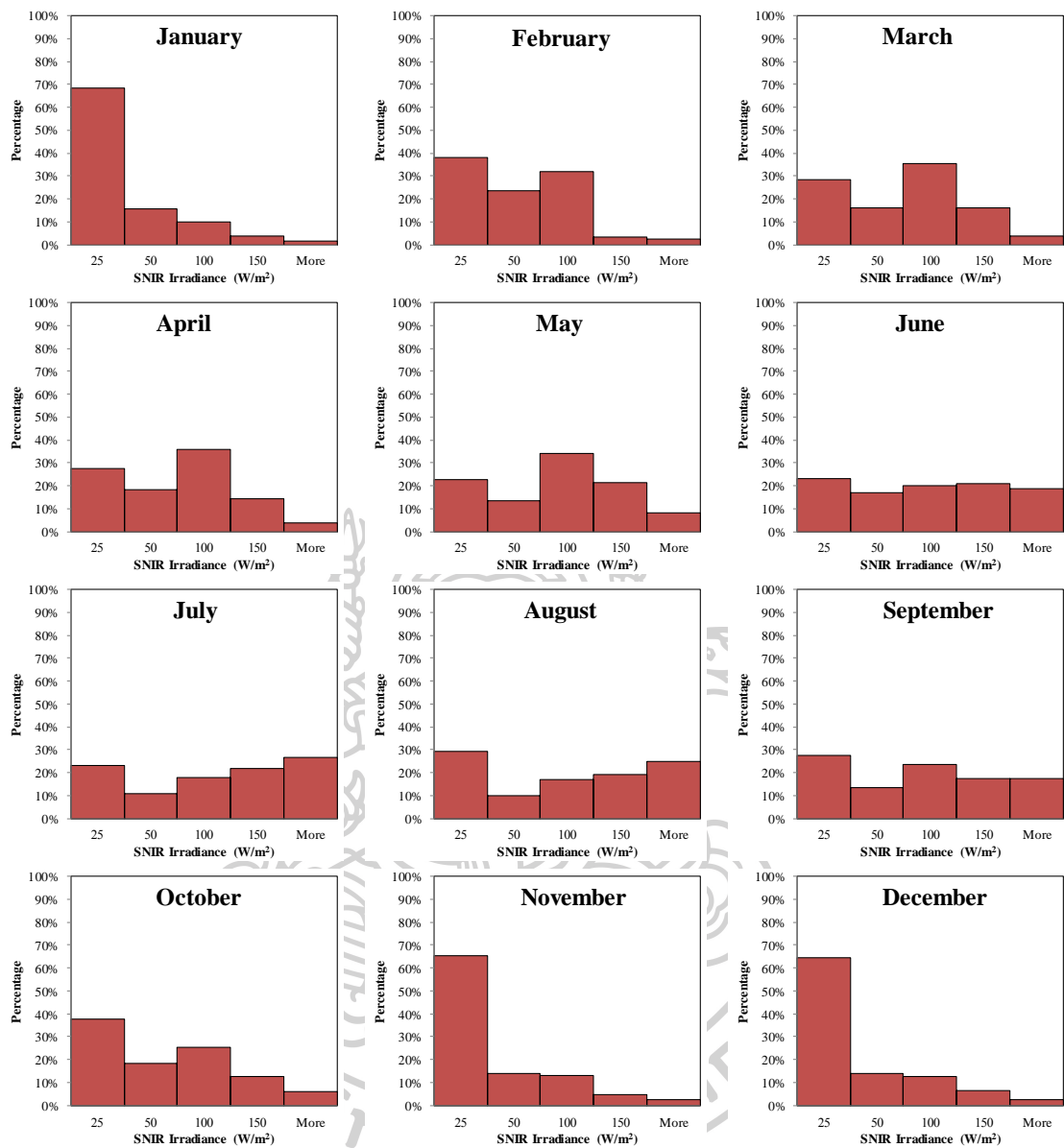


Fig. 45 The statistical distribution of hourly diffuse SNIR for each month at Chiang Mai station.

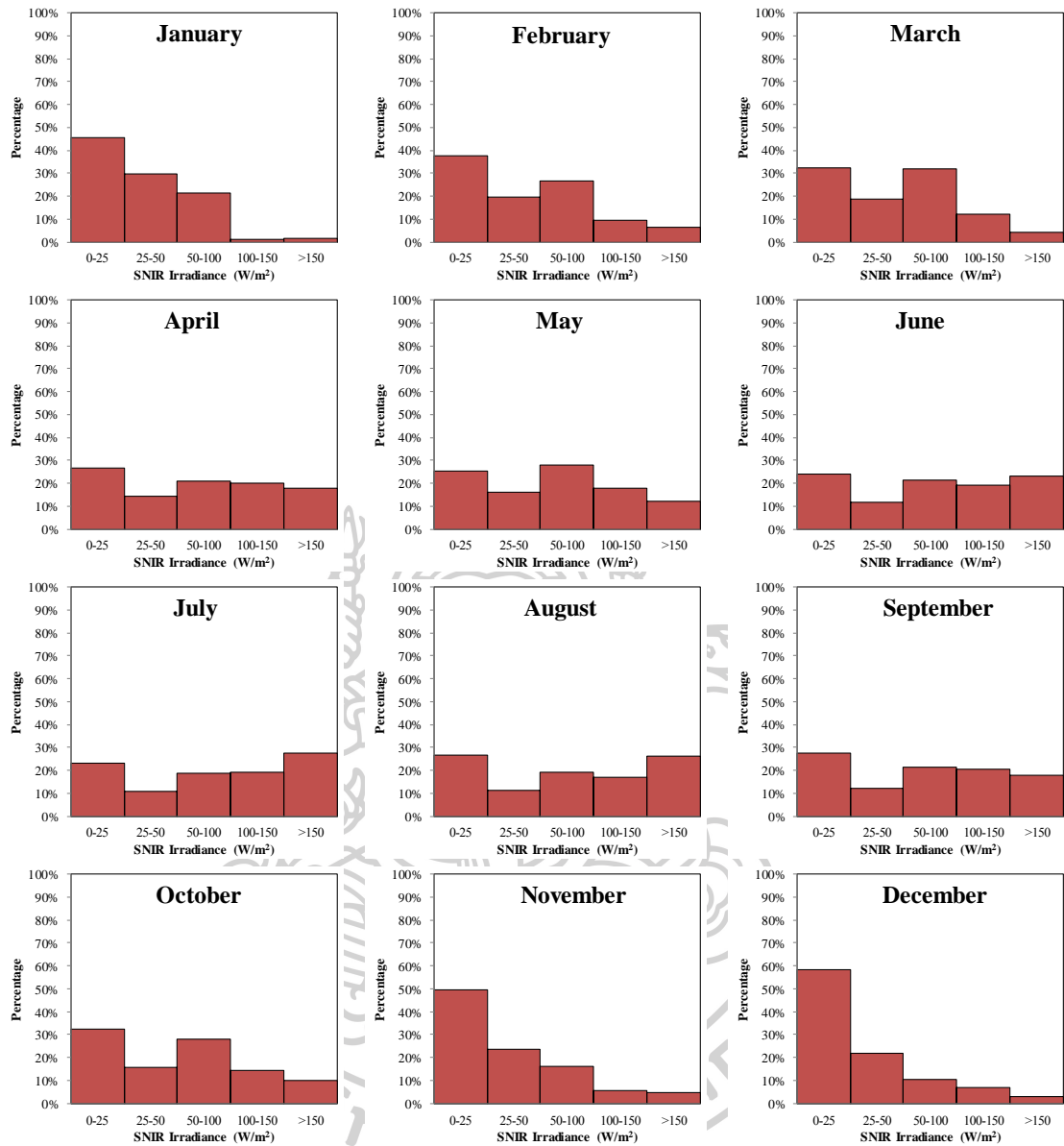


Fig. 46 The statistical distribution of hourly diffuse SNIR for each month at Ubon Raththani station.

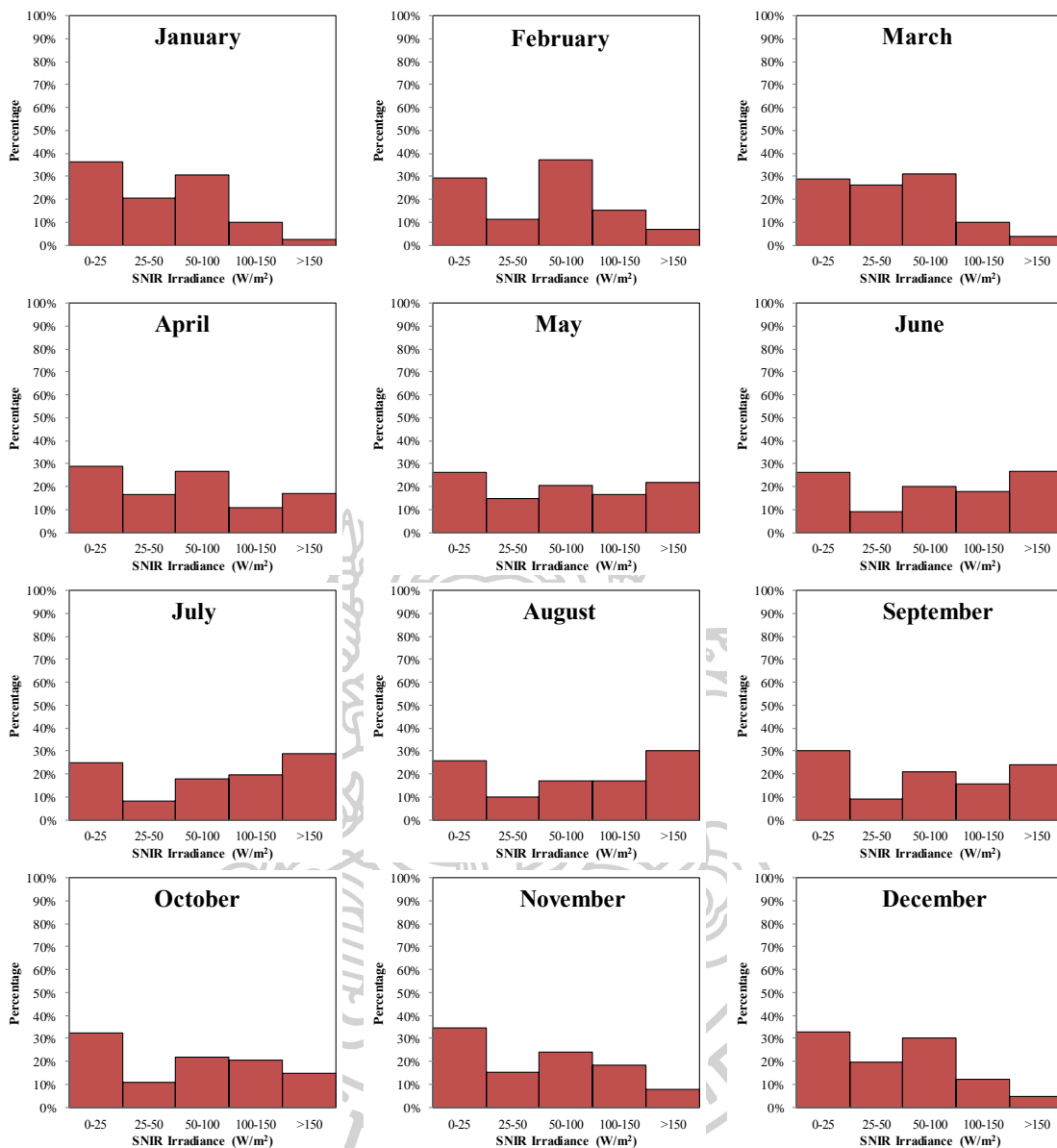


Fig. 47 The statistical distribution of hourly diffuse SNIR for each month at Nakhon Pathom station.

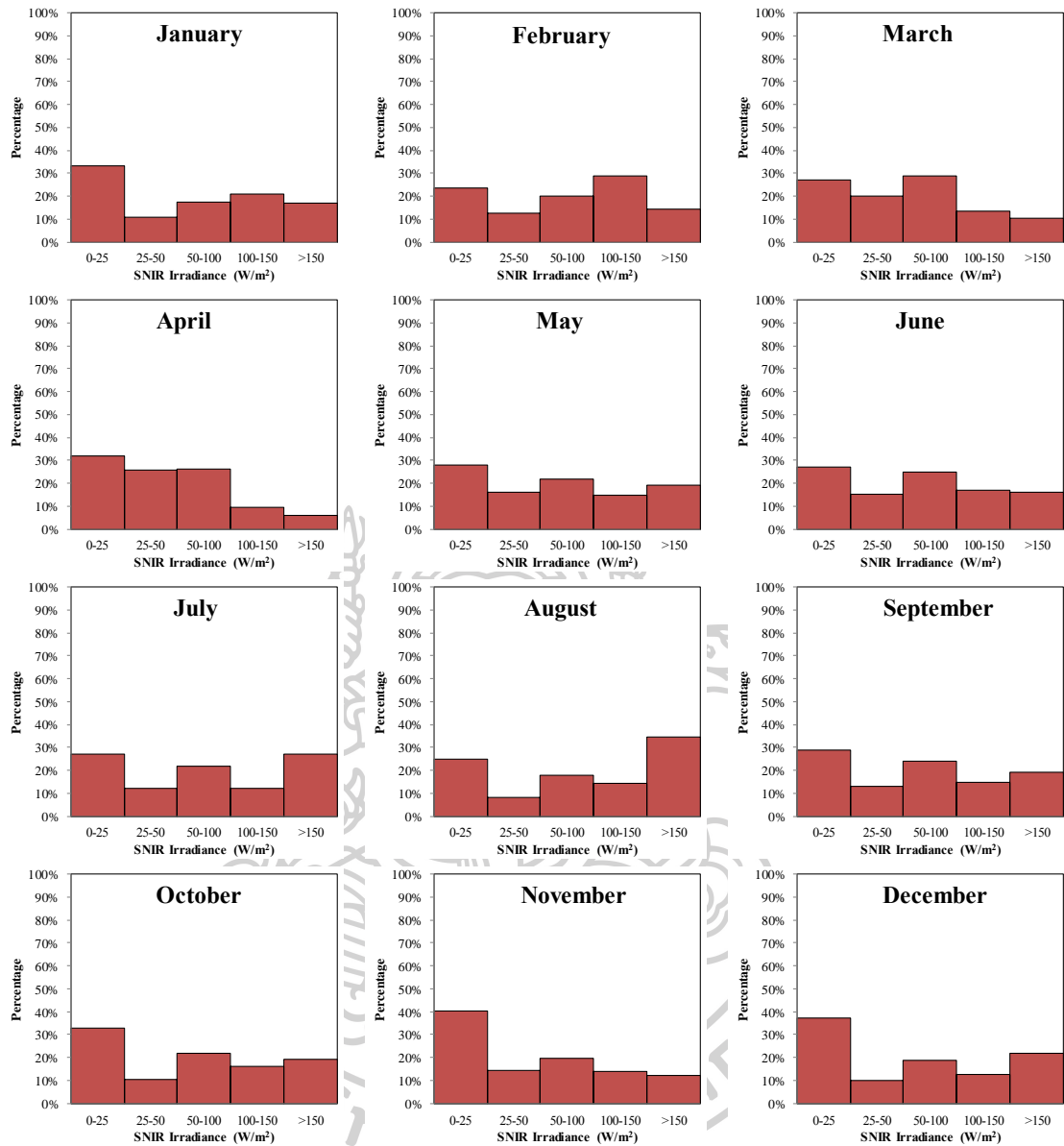


Fig. 48 The statistical distribution of hourly diffuse SNIR for each month at Songkhla station.

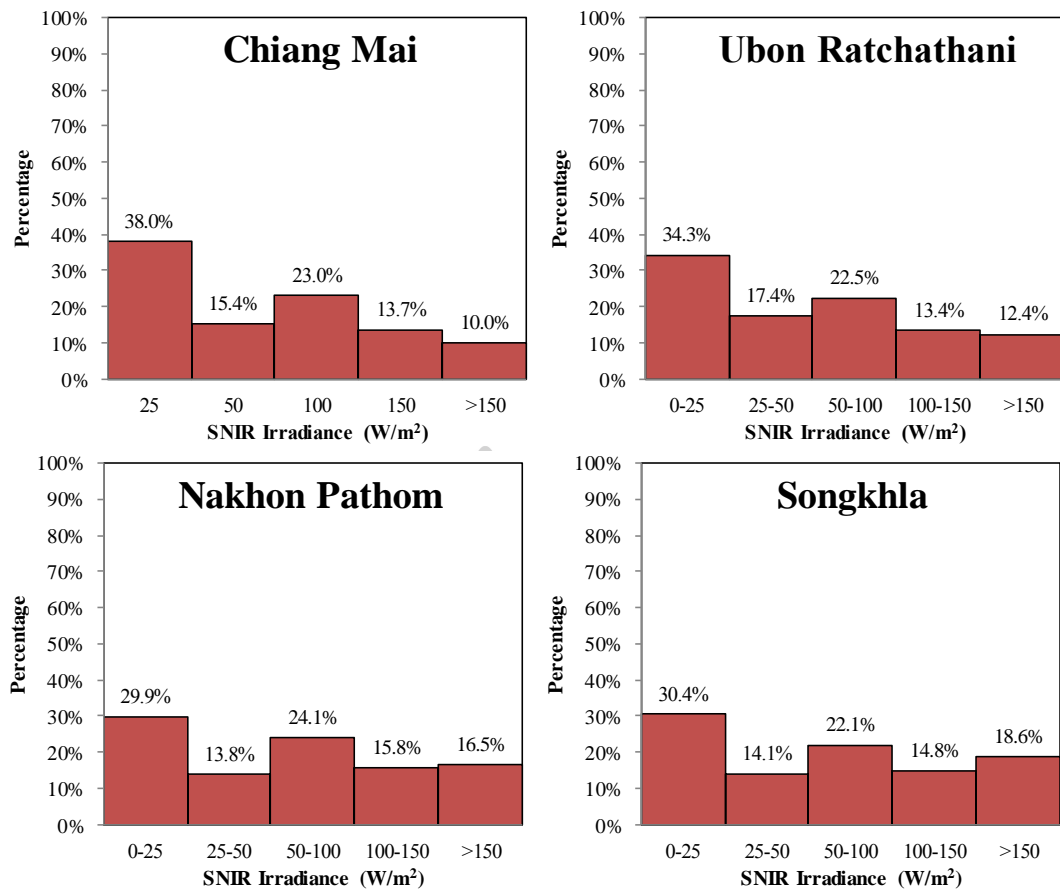


Fig. 49 The statistical distributions of hourly diffuse SNIR for all month at Chiang Mai, Ubon Ratchathani, Nakhon Pathom and Songkhla station.



5.4 Distributions of daily solar near infrared radiation

A. Global solar near infrared radiation

Daily solar near infrared radiation was important for many applications as mentioned before. Thus, in this section, daily solar near infrared radiation was obtained by summing hourly solar near infrared irradiance over day and the distribution of these data for four stations during the year of 2009 to 2017 were analyzed as a percentage of the global SNIR and presented as a histogram. These histograms showed the frequency distributions of daily global SNIR in various ranges and months for the whole year. The results are shown in Fig. 50 - 53.

From these figures, most of daily global SNIR during the rainy season were in the range of 6 - 9 MJ/m²-day while in the dry season were in the range of 9 - 12 MJ/m²-day. The highest value of SNIR, which was higher than 12 MJ/m²-day was found in April, which had the percentage of 7.0%, 7.0%, 29.5% and 13.5% for Chiang Mai, Ubon Ratchathani, Nakhon Pathom and Songkhla station, respectively.

Furthermore, the amount of daily global SNIR from each station for all months during the year 2009 - 2017 was also investigated as shown in Fig 54. The histograms showed the similar pattern as the distribution of each month. The maximum frequency of daily SNIR was in the range of 6-9 MJ/m²-day with 42.8% and 44.6% for Chiang Mai and Ubon Ratchathani stations, respectively, while Nakhon Pathom and Songkhla have the maximum frequency in the range of 9 - 12 MJ/m²-day with 41.0% and 40.9%, respectively. The maximum daily SNIR being higher than 12 MJ/m²-day has the frequency distribution between 1.5% - 4.7% and the highest frequency occurs at Nakhon Pathom station located in the central part of Thailand.



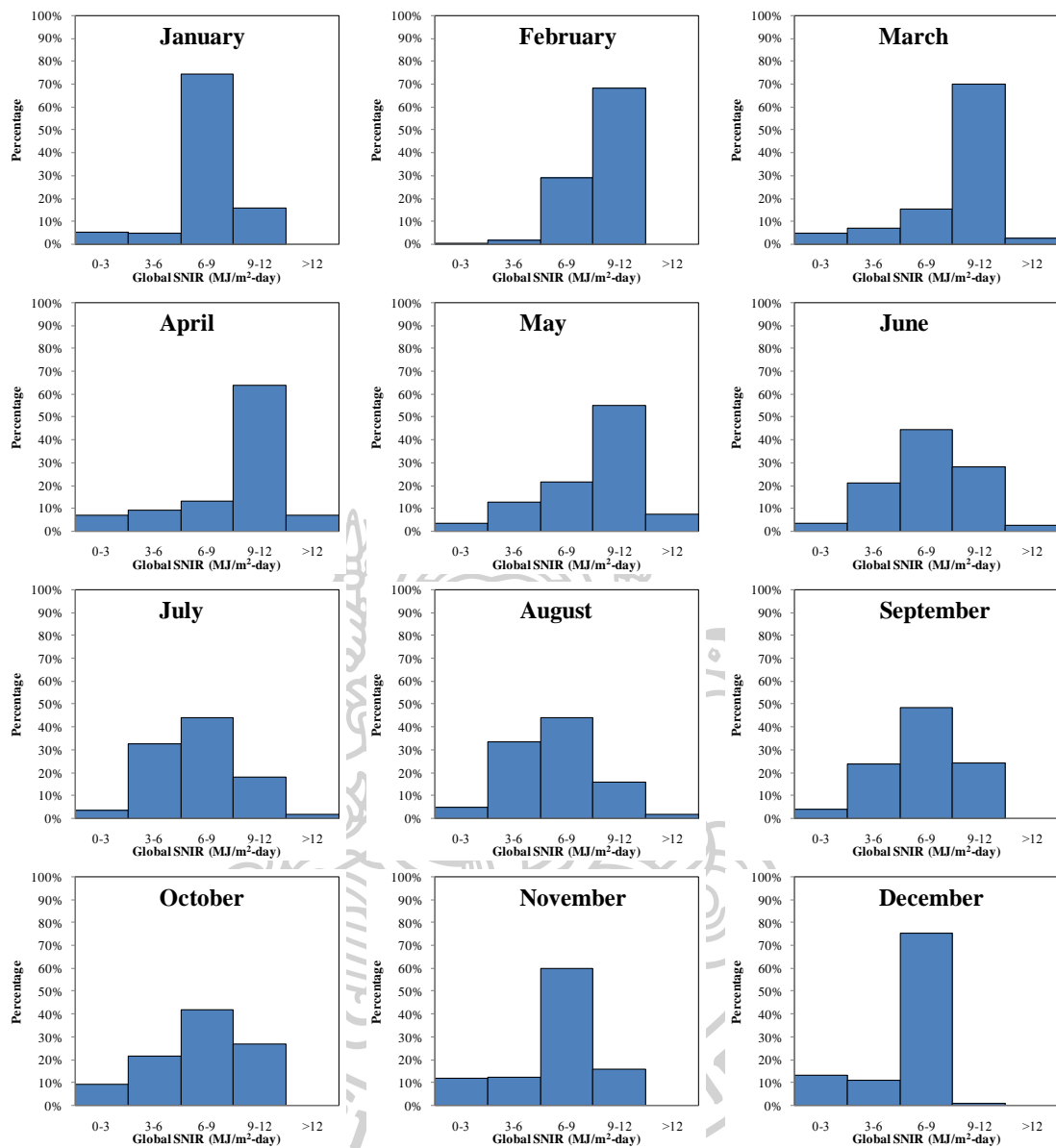


Fig. 50 The statistical distributions of daily global SNIR for each month at Chiang Mai station.

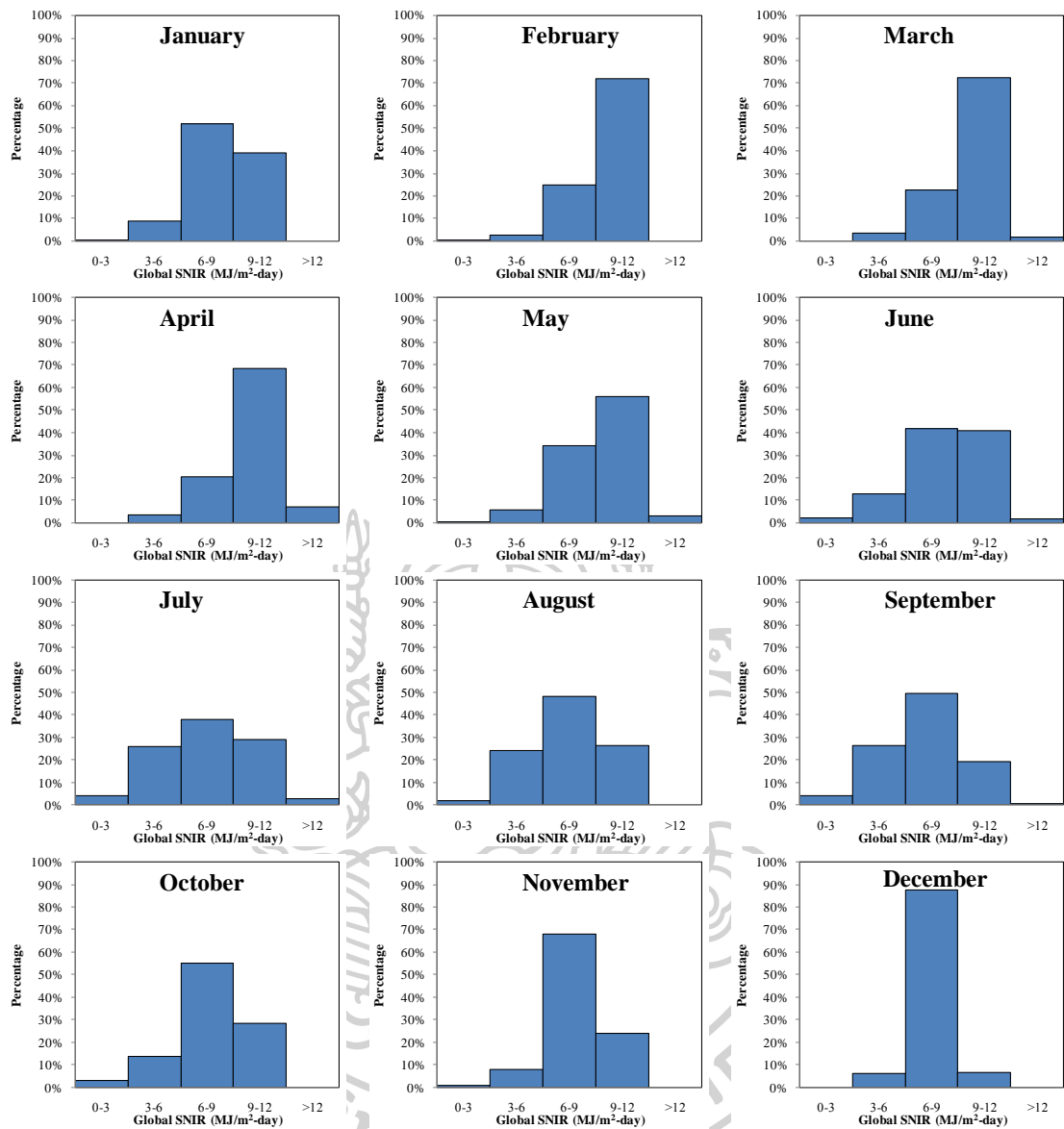


Fig. 51 The statistical distributions of daily global SNIR for each month at Ubon Rathethani station.

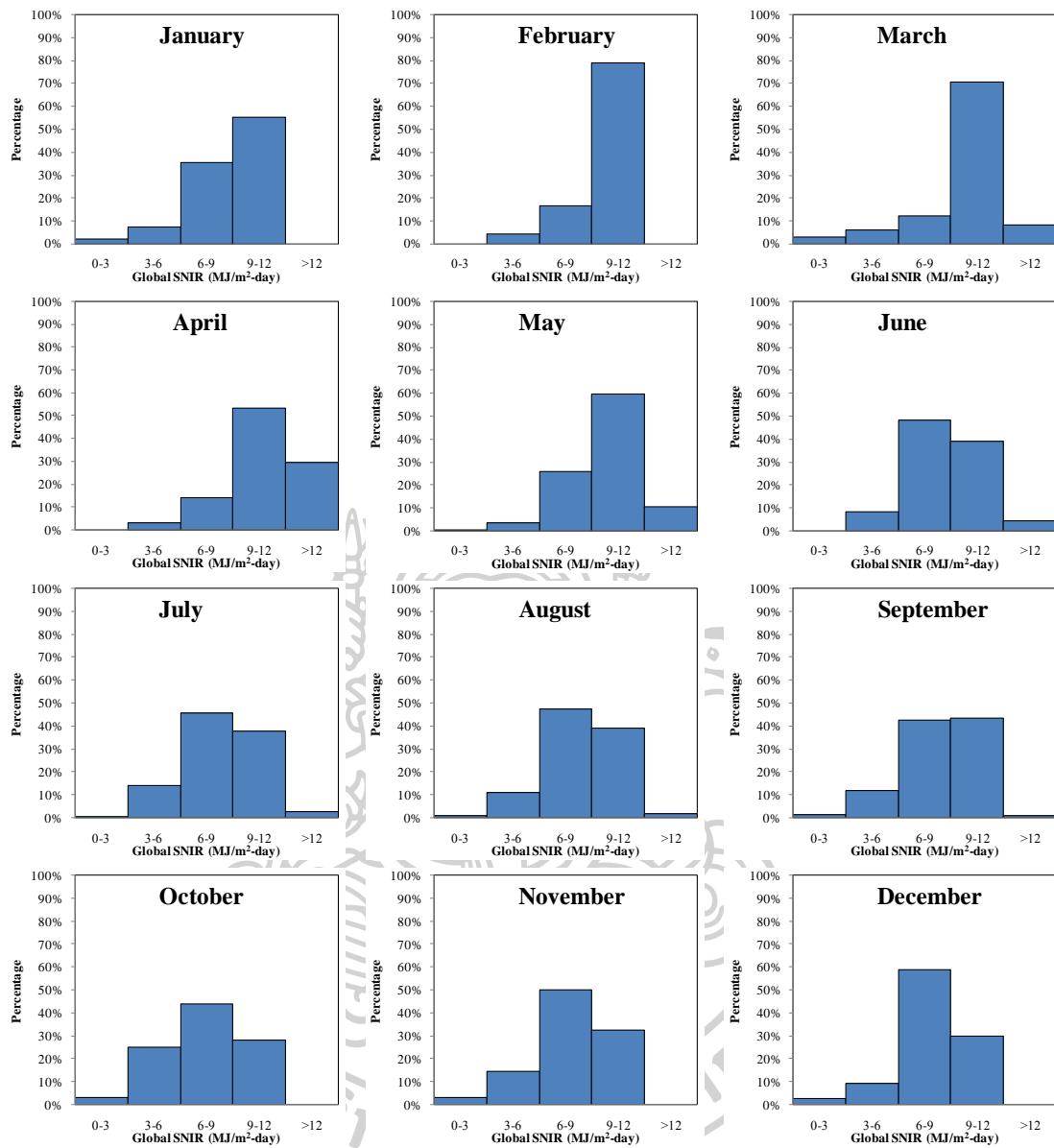


Fig. 52 The statistical distributions of daily global SNIR for each month at Nakhon Pathom station.

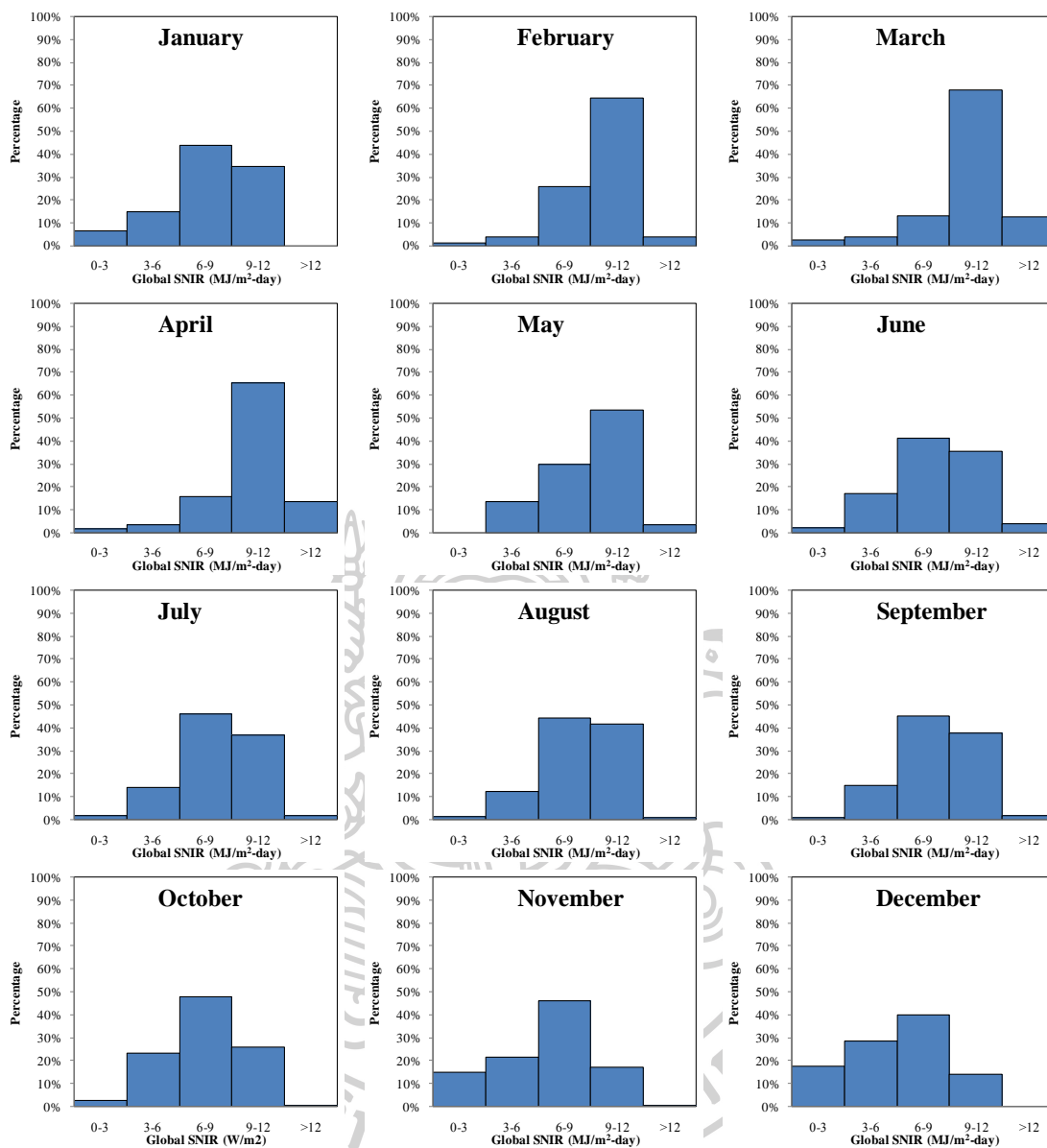


Fig. 53 The statistical distributions of daily global SNIR for each month at Songkhla station.

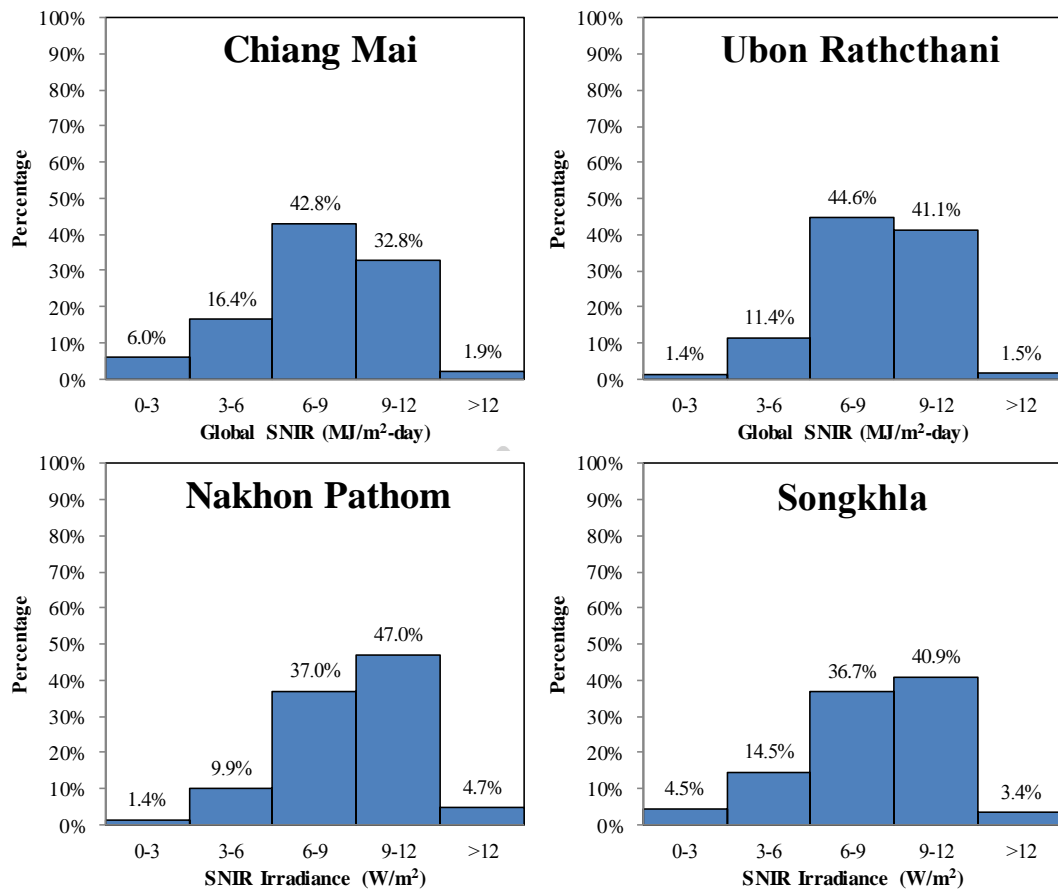


Fig. 54 The statistical distributions of daily global SNIR for all month at Chiang Mai, Ubon Ratchathani, Nakhon Pathom and Songkhla station.



B. Diffuse solar near infrared radiation

Diffuse SNIR was mainly scattered by clouds and affected to the attenuation of diffuse SNIR. Therefore, as same as the global SNIR, the distribution of daily diffuse SNIR was necessarily investigated. In this section, measured hourly diffuse solar near infrared radiation data during 2009 - 2012 was summed in form of daily diffuse SNIR and analyzed as a percentage of the radiation intensity range. The distributions of the diffuse SNIR for four stations are shown in Fig. 55 – 58.

From the resulting histogram of Chiang Mai, Ubon Ratchathani and Nakhon Pathom station in the dry season, the most of daily diffuse SNIR was in the range less than 2 MJ/m²-day. However, in the wet season, the most of daily diffuse SNIR was found in the range more than 4 MJ/m²-day. Moreover, the results showed large variations of frequency for all ranges over year. In case of Songkhla station, the most of daily diffuse SNIR frequency was in the range more than 4 MJ/m²-day, whereas in March and April had the most of daily diffuse SNIR in the range of 3 - 4 MJ/m²-day due to less cloud cover than other month. Moreover, Nakhon Pathom and Songkhla station had more daily diffuse SNIR being higher than 4 MJ/m²-day than Chiang Mai and Ubon Rathcathani. Daily global SNIR for all months of four stations was also analyzed as shown in Fig. 59. The resulting histogram presented that the daily diffuse SNIR for all stations varied in every range. The most frequency was found in range more than 4 MJ/m²-day with 30.7%, 37.1%, 47.3% and 48.9% for Chiang Mai, Ubon Ratchathani, Nakhon Pathom and Songkhla, respectively.



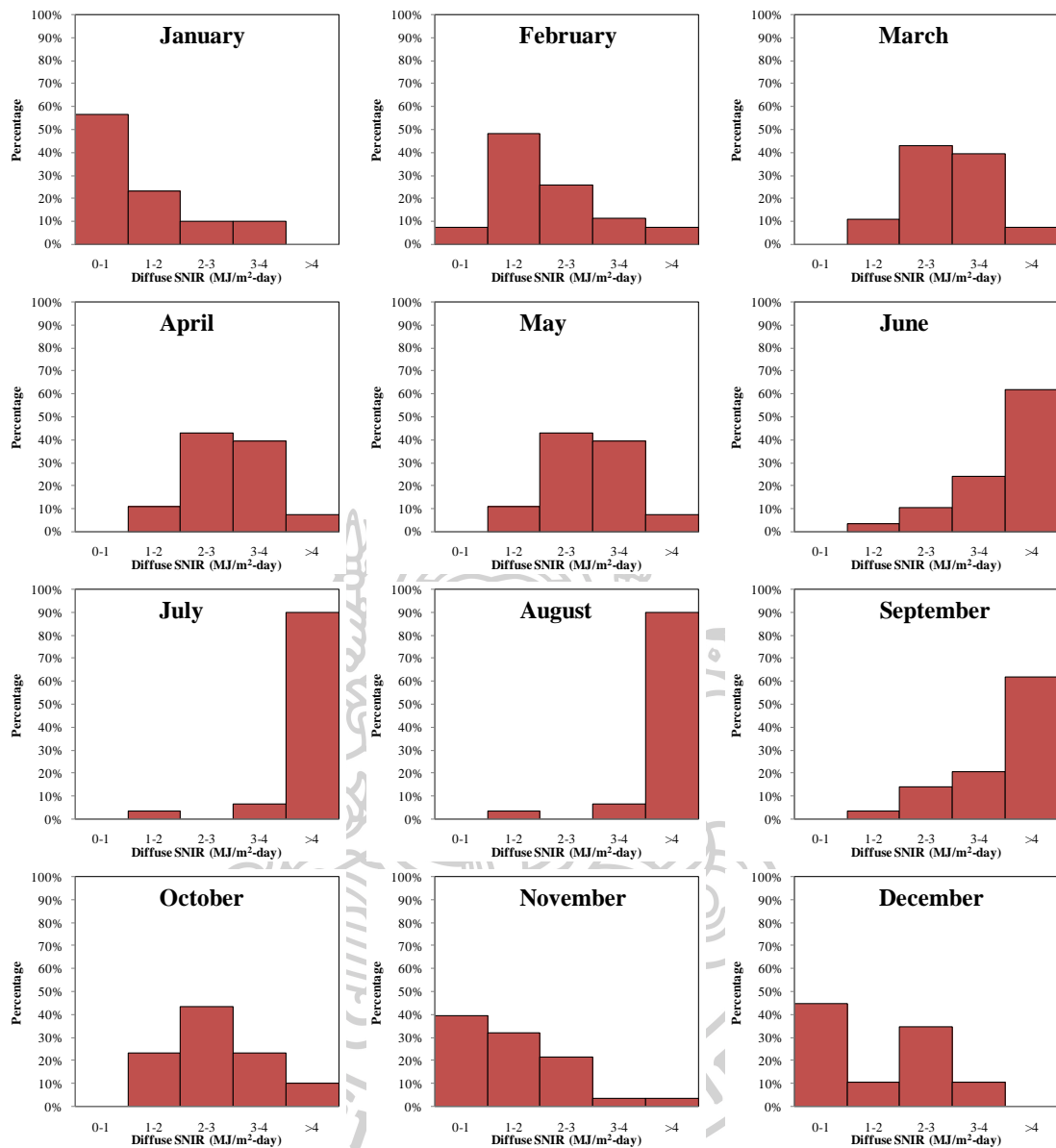


Fig. 55 The statistical distribution of daily diffuse SNIR for each month at Chiang Mai station.

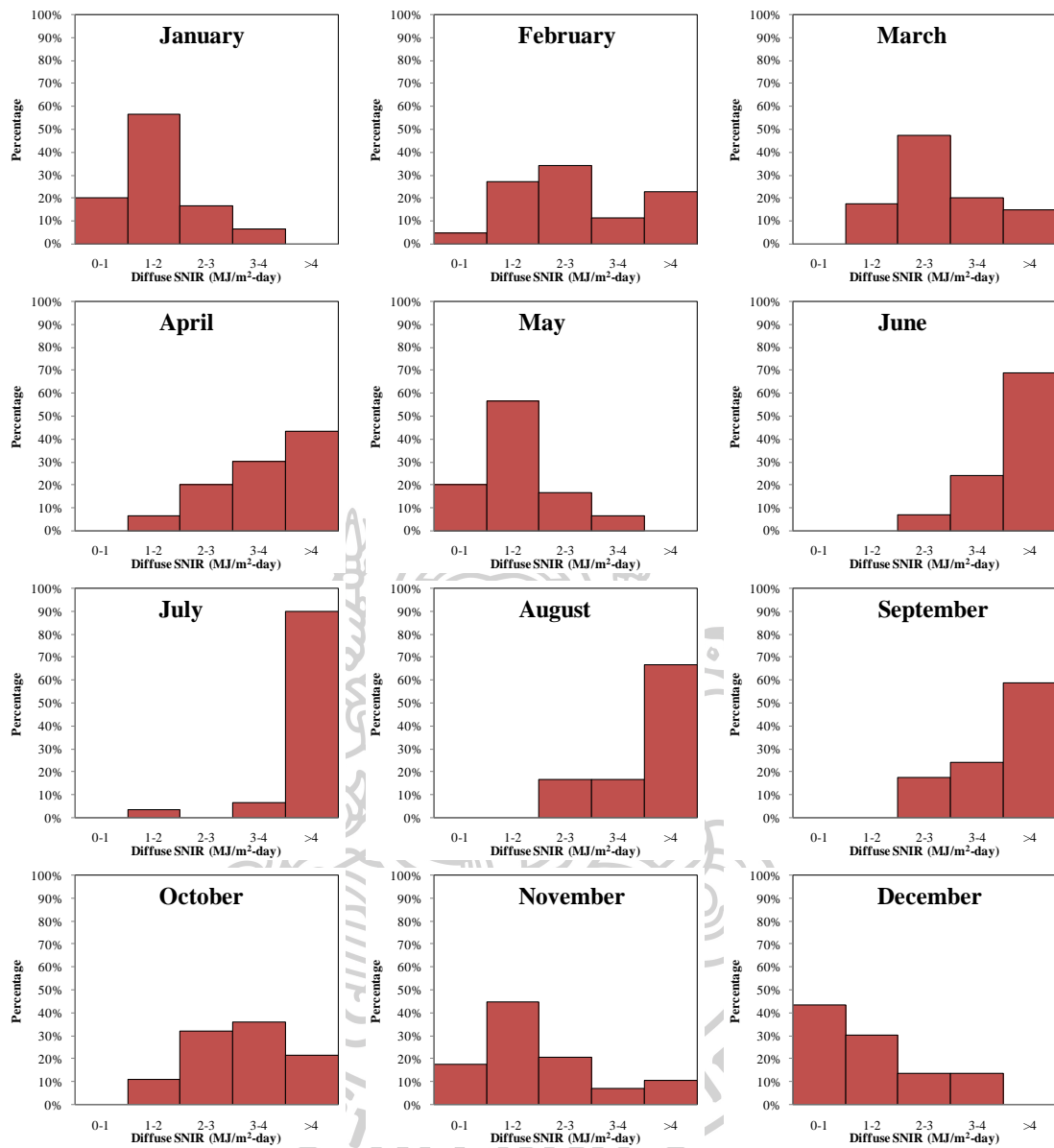


Fig. 56 The statistical distribution of daily diffuse SNIR for each month at Ubon Ratchathani station.

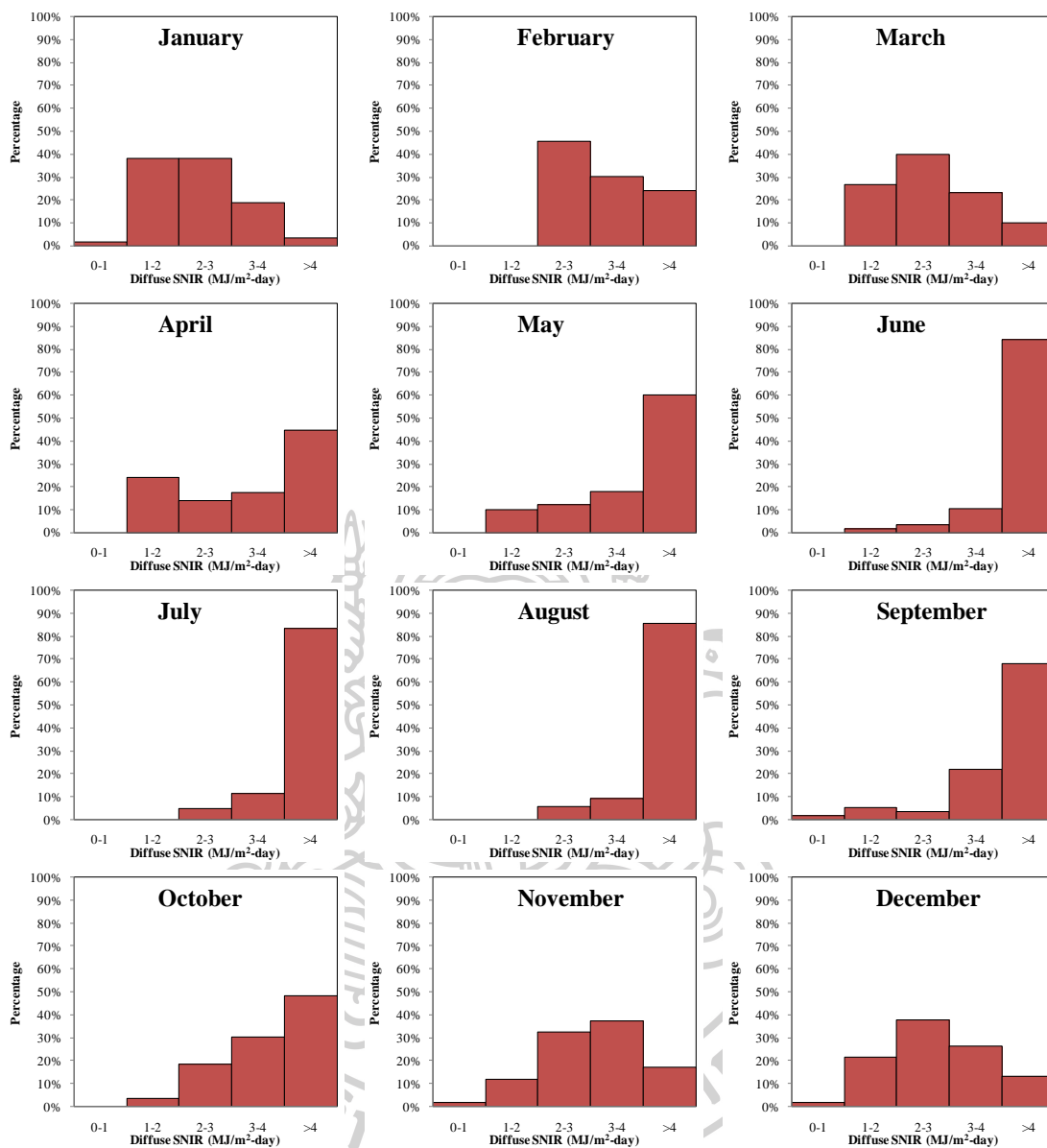


Fig. 57 The statistical distribution of daily diffuse SNIR for each month at Nakhon Pathom station.

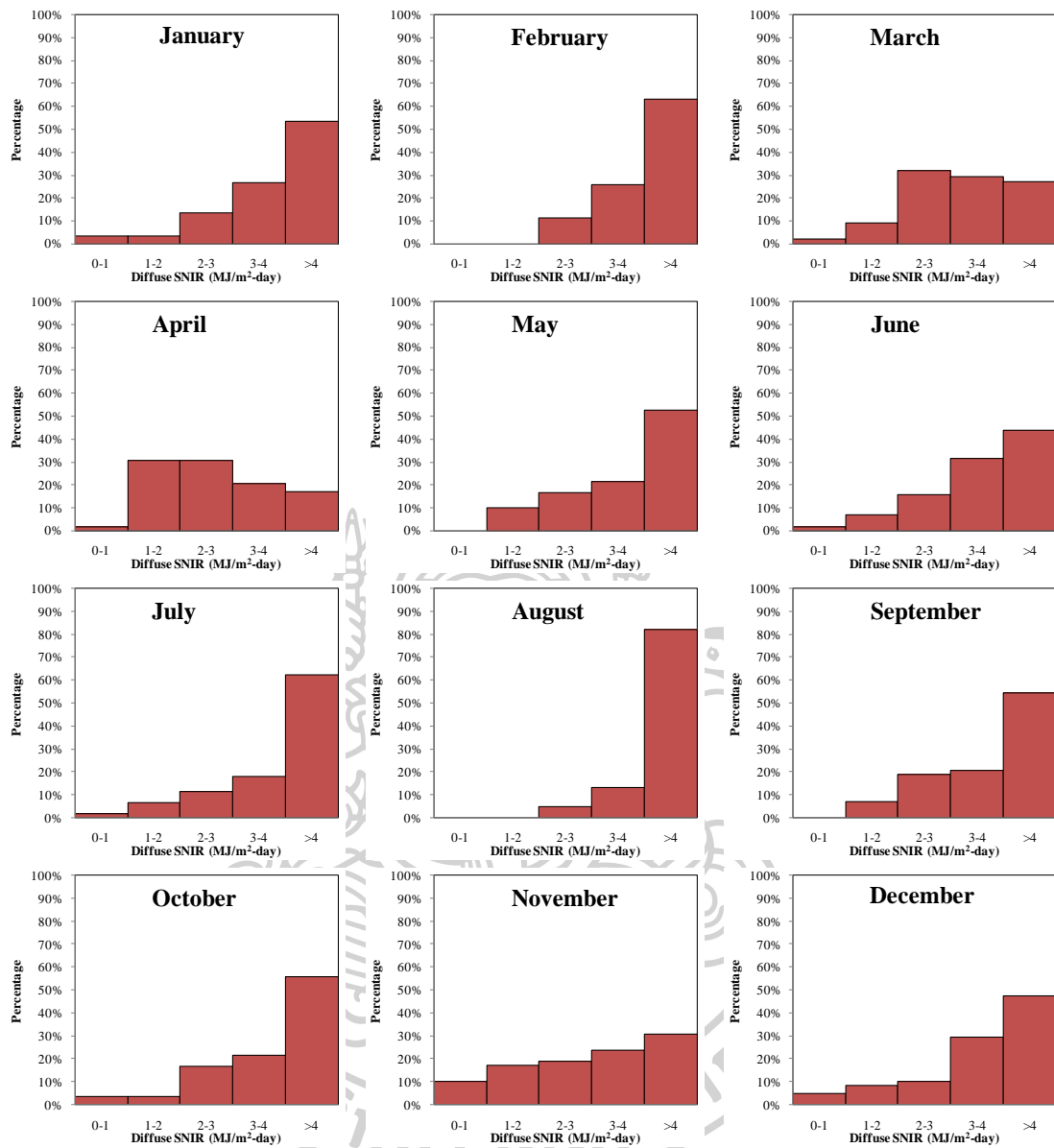


Fig. 58 The statistical distribution of daily diffuse SNIR for each month at Songkhla station.

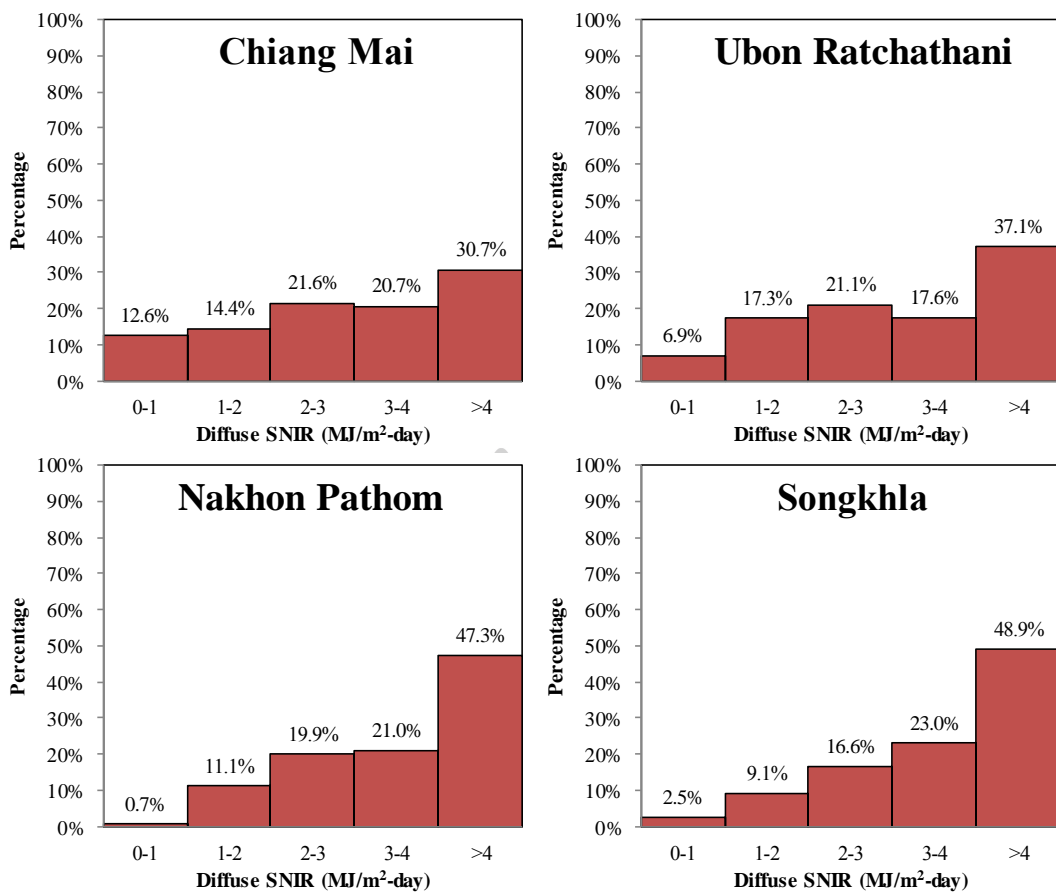


Fig. 59 The statistical distributions of daily diffuse SNIR for all month at Chiang Mai, Ubon Ratchathani, Nakhon Pathom and Songkhla station.



Chapter 6

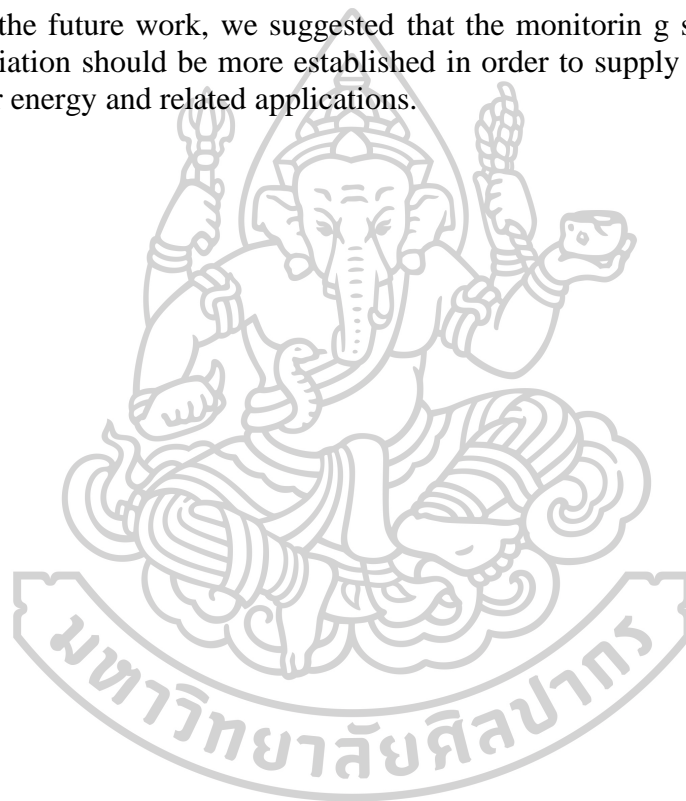
Conclusions

Solar near infrared radiation (SNIR) lies between $0.7 - 3.0 \mu\text{m}$ and its energy is about 52% of the total energy emitted from the sun. The SNIR passes through the atmosphere consists of the portion that directly incident on the surface is called direct SNIR and the rest, which is scattered from the atmospheric constituents and clouds is called a diffuse SNIR. The sum of direct and diffuse SNIR is called a global SNIR. SNIR is used in many applications for example, in remote satellite technique for estimating atmospheric water vapour and in deriving some properties of clouds. In order to utilize the SNIR, we need to know the information of SNIR data acquiring by measurement. However, the monitoring station for measuring SNIR is still not sufficient. Moreover, the SNIR component is less investigated in comparison with other solar radiation segments. Therefore, in this work, the various models for estimating global and diffuse SNIR by using ground-based and satellite based data was proposed. This can be summarized as follows:

- 1) A semi-empirical model for estimating diffuse solar near infrared irradiance has been developed for Thailand. Diffuse SNIR was influenced primarily by the optical path length and to a lesser degree, by cloud cover depletion and water vapour absorption. The earth-atmospheric reflectivity from satellite data was used as a surrogate for cloud index, while relative humidity and air temperature data from surface stations were used to estimate precipitable water. Diffuse SNIR was best modelled using the above three variables as independent terms in an exponential relationship. This semi-empirical model is in reasonable agreement with independent diffuse SNIR data, giving a root mean square difference and mean bias difference of 16.7% and 1.5%, respectively. Then the proposed model was used to provide the long-term diffuse SNIR maps for Thailand.
- 2) Parameterized model for estimating hourly global SNIR at the earth's surface in Thailand was proposed. The approach combines visible reflectance data from the MTSAT-1R satellite and solar near infrared irradiance measurements from four stations in Thailand. Using a simple radiation budget model, hourly atmospheric reflectance from the four stations are related to a satellite-derived atmospheric reflectance. Surface SNIR in the Thailand region may then be estimated using a simple radiation model which uses a corrected satellite-derived atmospheric reflectance. Maps of monthly average hourly irradiance are presented at three different times of the day and for all 12 months.
- 3) The models for estimating hourly, daily, and monthly average daily global SNIR in form of ratios between SNIR and BR has been developed. According to the model, the ratio of SNIR-to-BR is expressed as a function of the precipitable water, aerosol optical depth, total ozone column and cloud index. Global SNIR estimated from the model and those obtained from the measurements are in good agreement.

- 4) Statistical characteristics of global and diffuse solar near infrared radiation in Chiang Mai, Ubon Ratchathani, Nakhon Pathom and Songkhla station was analyzed. The diurnal variation increased from the morning until the highest at noon and gradually decreased at the evening. The highest global SNIR of Chiang Mai, Ubon Ratchathani, Nakhon Pathom stations and Songkhla station was in the dry season and lower in the wet season. Diffuse SNIR in Chiang Mai, Ubon Ratchathani, Nakhon Pathom and Songkhla station was high in the wet season and low in the dry season. The distribution of hourly and daily global and diffuse SNIR at Chiang Mai, Nakhon Pathom, Ubon Ratchathani and Songkhla stations had the similar trend. Most frequencies decrease when SNIR increases.

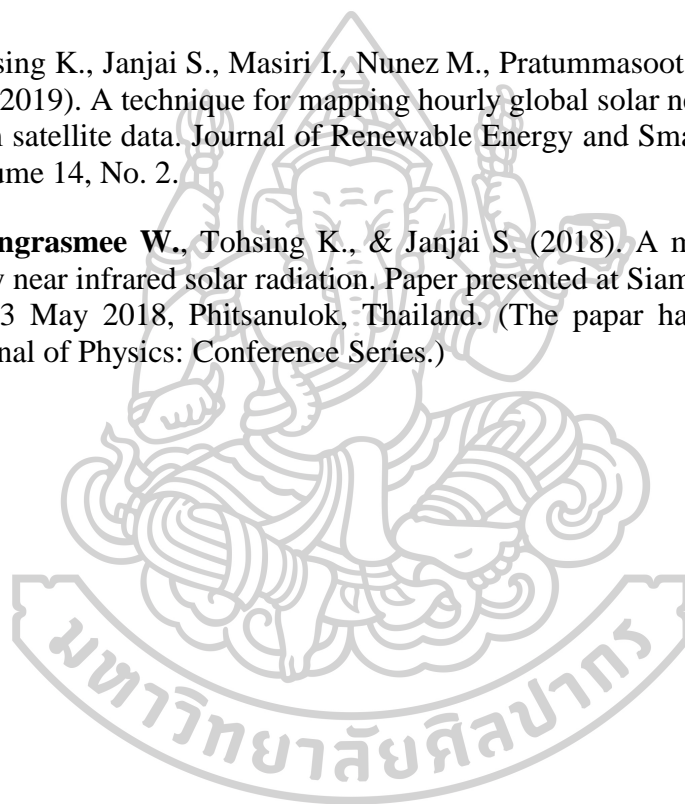
For the future work, we suggested that the monitoring station for solar near infrared radiation should be more established in order to supply efficiently the SNIR data to solar energy and related applications.



Appendix 1 Publications

Parts of this thesis have been published international journals and conference proceeding as follows:

1. Charuchittipan, D., Choosri, P., Janjai, S., Buntoung, S., Nunez, M., & **Thongrasmee, W.** (2018). A semi-empirical model for estimating diffuse solar near infrared radiation in Thailand using ground-and satellite-based data for mapping applications. *International Journal of Renewable energy*, Volume 117, 175-183, (impact factor 4.9).
2. Tohsing K., Janjai S., Masiri I., Nunez M., Pratummasoot N. & **Thongrasmee W.** (2019). A technique for mapping hourly global solar near infrared radiation from satellite data. *Journal of Renewable Energy and Smart Grid Technology*. Volume 14, No. 2.
3. **Thongrasmee W.**, Tohsing K., & Janjai S. (2018). A model for calculating daily near infrared solar radiation. Paper presented at Siam physics conference, 21-23 May 2018, Phitsanulok, Thailand. (The papar has been published in *Journal of Physics: Conference Series*.)



Appendix 2 Nomenclature

AOD	aerosol optical depth at 500 nm (-)
$\overline{\text{AOD}}$	monthly average daily aerosol optical depth at 500 nm (-)
H_{BR}	daily global broadband radiation (MJ/m ² day)
$\overline{H_{\text{BR}}}$	monthly average daily global broadband radiation (MJ/m ² day)
H_{dSNIR}	daily diffuse solar near infrared radiation (MJ/m ² day)
$\overline{H_{\text{dSNIR}}}$	monthly average daily diffuse solar near infrared radiation (MJ/m ² day)
H_{SNIR}	daily global solar near infrared radiation (MJ/m ² day)
$\overline{H_{\text{SNIR}}}$	monthly average daily global solar near infrared radiation (MJ/m ² day)
I_{0SNIR}	Extraterrestrial global solar near infrared radiation (MJ/m ² h)
I_{BR}	hourly global broadband radiation (MJ/m ² h)
$\overline{I_{\text{d0SNIR}}}$	Extraterrestrial diffuse solar near infrared radiation (MJ/m ² h)
$\overline{I_{\text{dSNIR}}}$	monthly average hourly diffuse solar near infrared radiation (MJ/m ² h)
$\overline{I_{\text{dSNIR,mod}}}$	calculated monthly average hourly diffuse solar near infrared radiation (MJ/m ² h)
$\overline{I_{\text{dSNIR,meas}}}$	measured monthly average hourly diffuse solar near infrared radiation (MJ/m ² h)
I_{SNIR}	hourly global solar near infrared radiation (W/m ² h)
$\overline{I_{\text{SNIR}}}$	hourly average hourly global solar near infrared radiation (W/m ² h)
$k_{\text{a}\lambda}$	absorption coefficient for mixed gases in the atmosphere (-)
$k_{\text{w}\lambda}$	absorption coefficient for water vapour in the atmosphere (-)
m	air mass (-)
_{max}	subscript “max” refer to maximum value
n	cloud index (-)
\overline{n}	monthly average daily cloud index (-)
N	total number of data
O_3	ozone optical depth (dobson)
$\overline{O_3}$	monthly average daily ozone optical depth (dobson)
p_s	saturated vapour pressure (mbar)
rh	relative humidity pressure (decimal)
R^2	level of confidence

SE	standard error
T	temperature (K)
VIS	visibility (km)
w	precipitable water (cm)
\overline{w}	monthly average daily precipitable water (cm)
α'_{aer}	gases absorption in satellite band
α'_A	atmospheric absorption in satellite band (-)
α'_{gas}	gases absorption in satellite band
α'_{SNIR}	atmospheric absorption in solar near infrared band (-)
α'_w	water vapour absorption in satellite band
ρ'_{aer}	the scattering contribution by aerosol depletion
ρ'_A	atmospheric reflectivity in satellite band (-)
ρ'_c	maximum reflectivity of cloud in satellite band (-)
ρ'_{EA}	earth-atmospheric reflectivity in satellite band (-)
ρ'_{GSNIR}	Surface reflectivity in solar near infrared band (-)
ρ'_G	Surface reflectivity in satellite band (-)
ρ'_{min}	Minimum reflectivity of cloud in satellite band (-)
ρ'_{SNIR}	atmospheric reflectivity in solar near infrared band (-)
τ'_{gas}	gases transmittance in satellite band
τ'_{wr}	water vapour transmittance in satellite band
τ'_{SNIR}	atmospheric transmission in solar near infrared band
ω_0	aerosol single scattering albedo
θ_Z	solar zenith angle (degree)

REFERENCES

- Bolsenga, S. (1967). Near infrared radiation in Northern Greenland. *Journal of Applied Meteorology*, 6(2), 449-451.
- Cano, D., Monget, J.-M., Albuissou, M., Guillard, H., Regas, N., & Wald, L. (1986). A method for the determination of the global solar radiation from meteorological satellite data. *Solar Energy*, 37(1), 31-39.
- Charuchittipan, D., Choosri, P., Janjai, S., Buntoung, S., Nunez, M., & Thongrasmee, W. (2018). A semi-empirical model for estimating diffuse solar near infrared radiation in Thailand using ground-and satellite-based data for mapping applications. *Renewable energy*, 117, 175-183.
- Choosri, P., Janjai, S., Nunez, M., Buntoung, S., & Charuchittipan, D. (2017). Mapping diffuse photosynthetically active radiation from satellite data in Thailand. *Advances in Space Research*, 60(11), 2345-2354.
- Cole, R. (1976). Direct solar radiation data as input into mathematical models describing the thermal performance of buildings—II. Development of relationships. *Building Environment*, 11(3), 181-186.
- Dougherty, C. (2011). *Introduction to econometrics*: Oxford University Press.
- Escobedo, J., Gomes, E. N., Oliveira, A. P., & Soares, J. (2009). Modeling hourly and daily fractions of UV, PAR and NIR to global solar radiation under various sky conditions at Botucatu, Brazil. *Applied Energy*, 86(3), 299-309.
- Escobedo, J., Gomes, E. N., Oliveira, A. P., & Soares, J. (2011). Ratios of UV, PAR and NIR components to global solar radiation measured at Botucatu site in Brazil. *Renewable energy*, 36(1), 169-178.
- Escobedo, J. F., Dal Pai, A., de Oliveira, A., Soares, J., & Dal Pai, E. (2014). Diurnal and annual evolution of UV, PAR and NIR irradiations in Botucatu/Brazil. *Energy Procedia*, 57, 1130-1139.
- Exell, R. (1984). Mapping Solar Radiation by Meteorological Satellite. *International Energy Journal*, 6(1).
- Gates, D., Murcray, D., Shaw, C., & Hevbold, R. (1958). Near infrared measurements by balloon to an altitude of 10,000 feet. *Optical Society of America*, 43, 1010-1016.
- Gautier, C., Diak, G., & Masse, S. (1980). A simple physical model to estimate incident solar radiation at the surface from GOES satellite data. *Applied Meteorology*, 19(8), 1005-1012.
- Haar, T. V., Raschke, E., Bandeen, W., & Pasternak, M. (1973). Measurements of solar energy reflected by the earth and atmosphere from meteorological satellites. *Solar energy*, 14(2), 175-184.
- Halthore, R. N., Eck, T. F., Holben, B. N., & Markham, B. L. J. J. o. G. R. A. (1997). Sun photometric measurements of atmospheric water vapor column abundance in the 940-nm band. *102(D4)*, 4343-4352.
- Holben, B. N., Eck, T. F., Slutsker, I., Tanre, D., Buis, J., Setzer, A., . . . Nakajima, T. (1998). AERONET—A federated instrument network and data archive for aerosol characterization. *Remote Sensing of Environment*, 66(1), 1-16.
- Iqbal, M. (1983). *An introduction to solar radiation*. New York: Academic Press.

- Janjai, S., Buntung, S., Wattan, R., & Masiri, I. (2010). Mapping solar ultraviolet radiation from satellite data in a tropical environment. *Remote Sensing of Environment*, 114(3), 682-691.
- Janjai, S., Laksanaboonsong, J., Nunez, M., & Thongsathitya, A. (2005). Development of a method for generating operational solar radiation maps from satellite data for a tropical environment. *Solar Energy*, 78(6), 739-751.
- Janjai, S., Pankaew, P., & Laksanaboonsong, J. (2009). A model for calculating hourly global solar radiation from satellite data in the tropics. *Applied Energy*, 86(9), 1450-1457.
- JMA. (2009). Conversion table of satellite data. from Japanese Meteorological Agency
- Leckner, B. (1978). The spectral distribution of solar radiation at the earth's surface—elements of a model. *Solar Energy*, 20(2), 143-150.
- Li, J., & Heap, A. D. (2008). A review of spatial interpolation methods for environmental scientists.
- Liu, X., Newchurch, M., Loughman, R., & Bhartia, P. (2004). Errors resulting from assuming opaque Lambertian clouds in TOMS ozone retrieval. *Journal of Quantitative Spectroscopy Radiative Transfer*, 85(3-4), 337-365.
- Liu, Y., Key, J. R., Ackerman, S. A., Mace, G. G., & Zhang, Q. (2012). Arctic cloud macrophysical characteristics from CloudSat and CALIPSO. *Remote Sensing of Environment*, 124, 159-173.
- Martins, F. R., Pereira, E. B., & Abreu, S. (2007). Satellite-derived solar resource maps for Brazil under SWERA project. *Solar Energy*, 81(4), 517-528.
- Masiri, I., Nunez, M., & Weller, E. (2008). A 10-year climatology of solar radiation for the Great Barrier Reef: implications for recent mass coral bleaching events. *International Journal of Remote Sensing*, 29(15), 4443-4462.
- Mayer, B., & Kylling, A. (2005). The libRadtran software package for radiative transfer calculations—description and examples of use. *Atmospheric Chemistry Physics*, 5(7), 1855-1877.
- Moody, E. G., King, M. D., Schaaf, C. B., Hall, D. K., & Platnick, S. (2007). Northern Hemisphere five-year average (2000–2004) spectral albedos of surfaces in the presence of snow: Statistics computed from Terra MODIS land products. *Remote Sensing of Environment*, 111(2-3), 337-345.
- Muneer, T. (2007). *Solar radiation and daylight models*: Routledge.
- Nunez, M. (1993). The development of a satellite-based insolation model for the tropical western Pacific Ocean. *International Journal of Climatology*, 13(6), 607-627.
- Pereira, A. R., Machado, E. C., & de Camargo, M. B. P. (1982). Solar radiation regime in three cassava (*Manihot esculenta* Crantz) canopies. *Agricultural Meteorology*, 26(1), 1-10.
- Petty, G. W. (2006). *A first course in atmospheric radiation*: Sundog Pub.
- Pinker, R., & Laszlo, I. (1992). Modeling surface solar irradiance for satellite applications on a global scale. *Journal of Applied Meteorology*, 31(2), 194-211.
- Polo, J., Zarzalejo, L. F., & Ramirez, L. (2008). Solar radiation derived from satellite images. In *Modeling solar radiation at the earth's surface* (pp. 449-462): Springer.

- Rossi, T. J., Escobedo, J. F., dos Santos, C. M., Rossi, L. R., da Silva, M. B. P., & Dal Pai, E. (2018). Global, diffuse and direct solar radiation of the infrared spectrum in Botucatu/SP/Brazil. *Renewable Sustainable Energy Reviews*, 82, 448-459.
- Schillings, C., Mannstein, H., & Meyer, R. (2004). Operational method for deriving high resolution direct normal irradiance from satellite data. *Solar Energy*, 76(4), 475-484.
- Seber, G. A. F. (1989). *Nonlinear regression / G. A. F. Seber and C. J. Wild*. New York :: John Wiley.
- Stephens, G. (1994). *Remote sensing of the lower atmosphere: an introduction*. Oxford: Oxford University Press Inc.
- Tanre, D., Deroo, C., Dehaut, P., Herman, M., Morcrette, J., Perbos, J., & Deschamps, P. (1986). Simulation of the satellite signal in the solar spectrum: User's Guide. Lille: LOA.
- Tarpley, J. (1979). Estimating incident solar radiation at the surface from geostationary satellite data. *Journal of Applied Meteorology*, 18(9), 1172-1181.
- Thongrasmee, W., Tohsing, K., & Janjai, S. (2018). *A model for calculating daily near infrared solar radiation*. Paper presented at the Journal of Physics: Conference Series.
- Tohsing, K., Janjai, S., Masiri, I., Nunez, M., Pratummasoot, N., & Thongrasmee, W. (2019). A technique for mapping hourly global solar near infrared radiation from satellite data. *Journal of Renewable Energy and Smart Grid Technology*, 14(2).
- Weiss, A., & Norman, J. (1985). Partitioning solar radiation into direct and diffuse, visible and near-infrared components. *Agricultural Forest meteorology*, 34(2-3), 205-213.





VITA

NAME Warangkana Thongrasmee

DATE OF BIRTH 19 May 1990

PLACE OF BIRTH Bangkok

INSTITUTIONS ATTENDED Bachelor of Science (Physics) Silpakorn University, Nakhon Pathom Thailand.
Master of Science (Physics) Silpakorn University, Nakhon Pathom Thailand.

HOME ADDRESS 296 Sukhothai road, Dusit, Bangkok 10300

PUBLICATION

- 1.) Charuchittipan, D., Choosri, P., Janjai, S., Buntoung, S., Nunez, M., & Thongrasmee, W. (2018). A semi-empirical model for estimating diffuse solar near infrared radiation in Thailand using ground-and satellite-based data for mapping applications. *Renewable energy*, 117, 175-183
- 2.) Tohsing, K., Janjai, S., Masiri, I., Nunez, M., Pratummasoot, N., & Thongrasmee, W. (2019). A technique for mapping hourly global solar near infrared radiation from satellite data. *Journal of Renewable Energy and Smart Grid Technology*, 14(2)
- 3.) Thongrasmee, W., Tohsing, K., & Janjai, S. (2018). A model for calculating daily near infrared solar radiation. Paper presented at Siam physics conference, 21-23 May 2018, Phitsanulok, Thailand. (The paper has been published in *Journal of Physics: Conference Series*.)